STATISTICAL AND REALISTIC NUMERICAL MODEL INVESTIGATIONS OF ANTHROPOGENIC AND CLIMATIC FACTORS THAT INFLUENCE HYPOXIC AREA VARIABILITY IN THE GULF OF MEXICO

A Dissertation

by

YANG FENG

Submitted to the Office of Graduate Studies of
Texas A&M University
in partial fulfillment of the requirements for the degree of

DOCTOR OF PHILOSOPHY

May 2012

Major Subject: Oceanography

STATISTICAL AND REALISTIC NUMERICAL MODEL INVESTIGATIONS OF ANTHROPOGENIC AND CLIMATIC FACTORS THAT INFLUENCE HYPOXIC AREA VARIABILITY IN THE GULF OF MEXICO

A Dissertation

by

YANG FENG

Submitted to the Office of Graduate Studies of
Texas A&M University
in partial fulfillment of the requirements for the degree of

DOCTOR OF PHILOSOPHY

Approved by:

Co-Chairs of Committee,	Steven DiMarco
	George Jackson
Committee Members,	Robert Hetland
	Thomas Bianchi
	Piers Chapman
	Steven Davis
Head of Department,	Piers Chapman

May 2012

Major Subject: Oceanography

ABSTRACT

Statistical and Realistic Numerical Model Investigations of
Anthropogenic and Climatic Factors that Influence Hypoxic Area Variability in the
Gulf of Mexico. (May 2012)
Yang Feng, B. S., Ocean University of China;
M.S., Ocean University of China
Co–Chairs of Advisory Committee: Dr. Steven DiMarco
Dr. George A. Jackson

The hypoxic area in the Gulf of Mexico is the second largest in the world, which has received extensive scientific study and management interest. Previous modeling studies have concluded that the increased hypoxic area in the Gulf of Mexico was caused by the increased anthropogenic nitrogen loading of the Mississippi River; however, the nitrogen-area relationship is complicated by many other factors, such as wind, river discharge, and the ratio of Mississippi to Atchafalaya River flow. These factors are related to large-scale climate variability, and thus will not be affected by regional nitrogen reduction efforts.

In the research presented here, both statistical (regression) and numerical models are used to study the influence of anthropogenic and climate factors on the hypoxic area variability in the Gulf of Mexico. The numerical model is a three-dimensional, coupled hydrological-biogeochemical model (ROMS-Fennel). Results include: (1) the west wind duration during the summer explain 55% of the hypoxic area variability since 1993. Combined wind duration and nitrogen loading explain over 70% of the variability, and combined wind duration and river discharge explain over 85% of the variability. (2) The numerical model captures the temporal variability, but over-estimates the bottom oxygen concentrations. The model shows that the simulated

hypoxic area is in agreement with the observations from the year 1991, as long as hypoxia is defined as oxygen concentrations below 3 mg/L rather than below 2 mg/L. (3) The first three modes from an Empirical Orthogonal Function (EOF) analysis of the numerical model output results explain 62%, 8.1% and 4.9% of the variability of the hypoxic area. The Principle Component time series is cross-correlated with wind, dissolved inorganic nitrogen concentration and river discharge. (4) Scenario experiments with the same nitrogen loading, but different duration of upwelling favorable wind, indicate that the upwelling favorable wind is important for hypoxic area development. However, a long duration of upwelling wind decreases the area. (5) Scenario experiments with the same nitrogen loading, but different discharges, indicate that increasing river discharge by 50% increases the area by 42%. Additionally, scenario experiments with the same river discharge, but different nitrogen concentrations, indicate that reducing the nitrogen concentration by 50% decreases the area by 75%. (6) Scenario experiments with the same nitrogen loading, but different flow diversions, indicate that if the Atchafalaya River discharges increased to 66.7%, the total hypoxic area increases the hypoxic area by 30%, and most of the hypoxic area moved from east to west Louisiana shelf. Additionally, if the Atchafalaya River discharge decreased to zero, the total hypoxic area increases by 13%. (7) Scenario experiments with the same nitrogen loading, but different nitrogen forms, indicate that if all the nitrogen was in the inorganic forms, the hypoxic area increases by 15%. These results have multiple implications for understanding the mechanisms that control the oxygen dynamics, reevaluating management strategies, and improving the observational methods.

To my beloved husband Tiezheng Jia, my mother, Likun Yu, and my father, Weili Feng

ACKNOWLEDGMENTS

I would like to take this opportunity to thank Dr. Steven DiMarco for providing me financial support during my five year Ph.D. study. I also thank him a lot for giving me complete freedom in choosing my research topic and backing up me all the time.

Next, I would like to thank Dr. George Jackson for devoting a lot of time and energy in helping me improve my research. I also thank him for making a lot of effort in teaching me how to do scientific research and write scientific papers. I was highly influenced by his passion for science.

I would like to extend my gratitude to Dr. Rob Hetland and Dr. Katja Fennel for providing all kinds of technical support on the ROMS modeling work. Thanks to Dr. Tom Bianchi for contributing insightful ideas for this research. Thanks to Dr. Piers Chapman and Dr. Steven Davis for improving the writing quality of this dissertation.

TABLE OF CONTENTS

CHAPTER Page

LIST OF TABLES

LIST OF FIGURES

FIGURE Page

FIGURE Page

CHAPTER I

INTRODUCTION

Oxygen is essential for the survival of many animals on land and in the ocean. Oxygen helps break down the organic material to provide energy for life. In aquatic environments, such as oceans, rivers and lakes, the concentration of oxygen dissolved in the water has to be above a minimum value to support the normal metabolism of marine organisms. Different organisms have different requirements for this minimum dissolved oxygen (DO) concentration. Generally, most nekton suffer from stress when DO is less than 3 mg/L; behavior of most of the less-mobile benthos may become abnormal when DO is less than 2 mg/L (*Rabalais and Turner*, 2001; *Diaz et al.*, 1999; *Diaz and Rosenberg*, 1995).

Hypoxia in the aquatic environment is defined to be the DO concentration that is low enough to impact the normal function of living organisms. The DO level used to define hypoxia varies (*Tyson and Pearson*, 1991). However, the most commonly used definition is DO $<$ 2 mg/L (2 ppm, 1.4 ml/L, or 62 μM). *Diaz and Rosenberg* (1995) define hypoxia to be the situation where DO $<$ 2 ml/L (2.8 mg/L, 2.8 ppm or 91.4 μM). In some situations, the DO can be depleted to extremely low levels (even to zero), i.e., anoxia. Hypoxic or anoxic conditions have been widely observed in estuaries, e.g., Chesapeake Bay (*Newcombe and Horne*, 1938); semi-closed seas, e.g. Northern Adriatic, Baltic, Kattegat, and Black Seas (*Justic*, 1988; *Baden et al.*, 1990; *Zaitsev*, 1992; *Karlson et al.*, 2002); or even open coastal systems, e.g. Gulf of Mexico, East China Sea, and the Pacific Ocean off the coast of Oregon (*Rabalais*

This dissertation follows the style of *Journal of Geophysical Research*.

et al., 2001; *Grantham et al.*, 2004; *Wei et al.*, 2006; *Chen et al.*, 2007). Hypoxia can alter behavior, physiology and reproduction of benthic fauna, and cause habitat compression or loss for many demersal and pelagic fishes (*Caddy*, 1993; *Nissling and Vallin*, 1996; *Rabalais and Turner*, 2001; *Cheng et al.*, 2002; *Eby and Crowder*, 2002; *Kodama et al.*, 2002; *Gray et al.*, 2002; *Wu et al.*, 2003; *Baird et al.*, 2004; *Breitburg et al.*, 2009). It has been listed as a major global environmental problem along with overfishing, habitat loss, and harmful algal blooms (*Diaz and Rosenberg*, 2008).

The two primary factors that cause the development and maintenance of oceanic hypoxia are the strength of the stratification of the water column, which inhibits low oxygen sub-pycnocline water exchange with oxygen-rich surface water, and the microbial decomposition of organic matter in the sub-pycnocline layer, which consumes oxygen during the decay process.

Hypoxia can be either naturally or anthropogenically induced. Naturally-induced hypoxia generally occurs in regions where upwelling is intense. There, nutrients are brought to the ocean surface and stimulate phytoplankton growth. Subsequent sinking of phytoplankton increases the supply of organic material to mid-water or to the bottom where microbial processes deplete oxygen. When combined with relatively slow-moving circulation and oxygen-poor source waters, a large area of oxygen minimum zone (OMZ) results. OMZs are widely found at depths of about 200–1000 m in the eastern Pacific Ocean, the southeast Atlantic off West Africa, and in the northern Indian Ocean. They have existed over geological time-scales (over thousands of years). The DO level used to define OMZs varies, ranging from 0.28 - 2.8 mg/L, which equals to 0.2 - 2 ml/L, 0.9 - 91.4 μM. (*Kamykowski and Zentara*, 1990; *Helly and Levin*, 2004; *Karstensen et al.*, 2008; *Fuenzalida et al.*, 2009; *Paulmier and Ruiz-Pino*, 2009; *Ulloa and Pantoja*, 2009).

Anthropogenically-induced hypoxia is caused by nutrient over-loading that leads

to the excess growth of the phytoplankton or by direct organic material input. The principal factor that drives the increased addition of nutrients and organic matter has been attributed to increased populations and increased living standards, which result in the expansion of agricultural and industrial activities and the acceleration of urbanization (*Conley et al.*, 2009; *Nixon*, 1995). Anthropogenically-induced hypoxia began in the 19th century and has worsened in the last 50 years (*Diaz and Rosenberg*, 1995; *Diaz*, 2001; *Diaz and Rosenberg*, 2008). It is found at depths as shallow as 1–2 m in estuaries to as deep as 600–700 m in coastal seas and usually occurs in summer when stratification of the water column is most intense. Regions of anthropogenically-induced hypoxia have been called "dead zones" because the movement of organisms away from them or the mortality of benthic fauna that cannot move has been observed.

Hypoxia in the northern Gulf of Mexico has been defined as DO concentration < 2 mg/L, the threshold at which most demersal fish, crabs and shrimps are detrimentally impacted (*Renaud*, 1986; *Rabalais et al.*, 2002a). Hypoxic water off Louisiana is distributed on the shelf in regions with bottom depths between 7–60 m from the Mississippi River Bird's Foot delta in the east to the Texas/Louisiana border in the west. Hypoxia occurs as early as late February and can last until early October, but is most severe, continuous and widely distributed during June–August (*Rabalais et al.*, 2001).

The hypoxia in the Gulf of Mexico is considered to be the anthropogenic-induced type. The Mississippi River system is the largest in the North America and among the top ten largest in the world, draining over 40% of the continental United States. It delivers large amounts of freshwater, nutrients, and sediment to the northern Gulf of Mexico every year (*Milliman and Meade*, 1983). The nutrient concentrations of the Mississippi River have changed dramatically since the mid-20th century due to human activities (*Rabalais et al.*, 2007a; *Turner and Rabalais*, 1994; *Rabalais et al.*, 1996).

The primary changes include an increase in mean annual nitrogen concentrations, decreasing silicate concentrations, and varying concentrations of phosphorus (*Turner and Rabalais*, 1991, 2003). The increased nitrate loading enhances primary production and the subsequent settling of the resulting organic material (*Justic et al.*, 2002; *Scavia et al.*, 2003; *Turner et al.*, 2006). This has occurred with concomitant loss of riparian wetlands.

In addition to the nitrogen-stimulated high primary production, the physical environment of the Texas–Louisiana shelf also favors the formation of large hypoxic regions. The wind over the northern Gulf of Mexico has a strong seasonal pattern. During much of the year (September–May), the wind is strong and downwelling favorable (blowing from east to west). However, in summer (June–August), the wind decreases and becomes upwelling favorable, i.e. from west to east (*Cochrane and Kelly*, 1986; *Cho et al.*, 1998; *Nowlin et al.*, 1998, 2005). The freshwater introduced by the Mississippi River intensifies the stratification of the Louisiana shelf under the weak and upwelling-favorable wind condition, facilitating hypoxia formation by inhibiting the supply of atmospheric oxygen to subpycnocline waters (*Wiseman et al.*, 1997; *Hetland and DiMarco*, 2008).

Hypoxia in the northern Gulf of Mexico was first reported in the early 1970s (*Ward et al.*, 1979). Annual shelf-wide surveys to estimate the areal extent of hypoxia started in 1985. Observations show that the hypoxic area has increased in the past 26 years. The average hypoxic area was about 7200 km^2 from 1985 to 1990, 14,600 km^2 from 1991 to 2000, and 16,000 km^2 from 2001 to 2009. In some years, the hypoxic area can be over 20,000 km^2 (1999, 2001, 2002, 2007 and 2008). The areal extent has become the largest in the western Atlantic Ocean and second largest in the world (*Rabalais et al.*, 2007b).

Although the reason for the rapid areal expansion of hypoxia has been known

to result from increased nitrogen loading since the 1950s, there is still debate on the relative importance of the processes that control the spatial and temporal variability of the DO concentration in bottom waters. *Wiseman et al.* (1997) used observational data to identify a secondary-pycnocline in summer and to reveal the relationship between the intensified stratification and bottom DO concentrations. Others (*Aller*, 1998; *Bianchi and Allison*, 2009; *Bianchi et al.*, 2009) suggested that organic material transport to the shelf by fluid and mobile muds might also introduce important oxygen-consuming material. *Krug* (2007) and *Krug and Merrifield* (2007) proposed that hypoxic condition change was caused by the Atchafalaya River capturing the flow of the Mississippi River. *Donner and Scavia* (2007) examined how climate change induced precipitation affects the nitrate loading of the Mississippi River and hypoxic area growth. *Hetland and DiMarco* (2008) concluded that the processes controlling hypoxia were different on different regions of the Louisiana shelf, while *DiMarco et al.* (2010) revealed that the spatial variability of the hypoxic area is influenced by the local topography.

The *Mississippi River/Gulf of Mexico Watershed Nutrient Task Force* (2001) established the goal of reducing the size of the hypoxic area to a five-year running mean of 5,000 km^2 by 2015 through voluntary reduction of nitrogen-based fertilizer inputs. The *Mississippi River/Gulf of Mexico Watershed Nutrient Task Force* (2008) reassessed the 2001 plan and confirmed that 5,000 km^2 remained a reasonable goal but would be difficult to reach by 2015, and recommended that accelerated nitrogen reductions were needed to achieve the goal. However, predicting the nitrogen—area relationship is complicated by non-nutrient factors, especially the natural climate variability. First, total nitrogen loading is equal to the nitrogen concentration multiplied by freshwater discharge. Much of variation in nutrient loading is driven by changes in flow. Unlike the nitrogen concentrations, the freshwater discharge is less

regulated by the action plans, but rather by precipitation that is highly influenced by the weather activities. Separating the role of nitrogen concentration from the freshwater discharge and estimating their individual contributions to hypoxic area are important as regards determining the effect of action plans (*Greene et al.*, 2009; *Donner and Scavia*, 2007; *U.S. Enviromental Protection Agency*, 1998, 2004, 2007). Second, the wind is the primary driver of the low-frequency circulation on the Texas–Louisiana shelf. Changes in wind direction alter the horizontal distribution of the river plume, and therefore, the vertical stratification. The relationship between the hypoxic area and wind direction has been explored in other regions, including the Chesapeake Bay and west Long Island Sound (*Scully*, 2010a,b; *Wilson et al.*, 2008). Wind direction could also play an important role in the Gulf of Mexico.

Besides the above natural climate variability, there is also great scientific and management interest in understanding the roles of other sources of oxygen-consuming materials and the relative roles of the Mississippi and Atchafalaya River plumes, and in documenting the high spatial and temporal variability of the bottom DO concentrations. The best tools to understand the variability of hypoxic area and to investigate the dynamic relationship between hypoxic area variability and different factors are statistical and numerical models.

Bottom water oxygen concentrations have been modeled for many years. *Breed et al.* (2004) and *Green et al.* (2006, 2008) focused on the relationship between nutrient loading and biological processes, such as primary production and organic matter sinking, that result in hypoxia. *Bierman et al.* (1994) and *Rowe* (2001) calculated the relative importance of multiple processes, including physical mixing and advection, biological respiration, and primary production, that control the DO dynamics. *Justic et al.* (1996, 2002) studied the relationship between the anthropogenic nutrient loading and intensified hypoxia events since the 1950s at one location. The above

models were used to understand mechanisms only and could not be used to calculate the hypoxic area directly. In addition, because these models emphasized the biogeochemical processes, they did not represent the influence of ocean physics conditions mechanistically. Some models have been used to estimate the hypoxic area directly by emphasizing factors and forcing that can control the areal extent. *Turner et al.* (2006) explained the change in hypoxic area using a multiple linear regression model, with May Mississippi River nitrogen loading and Julian year as predictors. The relationship to Julian year was later interpreted as a proxy for carbon stored in the sediments (*Turner et al.*, 2008). *Greene et al.* (2009) separated the role of several individual nutrient concentration and river discharge, and used a multiple linear regression model to explain the hypoxic area variability. An important conclusion of both *Turner et al.* (2008) and *Greene et al.* (2009) was that the relationship between the Gulf hypoxic area and nitrogen loading changed in the early 1990s. *Scavia et al.* (2003) reproduced the hypoxic area by using a one-dimensional Streeter-Phelps dissolved oxygen model, driven by the May-June total nitrogen loading from the Mississippi and Atchafalaya Rivers. The model was modified to study the role of phosphate (*Scavia and Donnelly*, 2007) and to incorporate an additional parameter to account for the system change in the 1990s (*Liu et al.*, 2010). The models of *Scavia et al.* (2003); *Scavia and Donnelly* (2007) and *Liu et al.* (2010) were only one-dimensional, predicting the length of the hypoxic zone along the shelf. They used linear regressions between the observed hypoxic area and its length to calculate the area of hypoxia. *Donner and Scavia* (2007) studied how precipitation influences the total nitrate load of the Mississippi River and hypoxic areal extent in the northern Gulf of Mexico by using multiple linear regressions. They emphasized the role of natural climate controlled river discharge on the hypoxic area variability.

The *Hetland and DiMarco* (2008) model was the first attempt at determining

oxygen dynamics on the Louisiana shelf using a coupled hydrodynamic circulation and oxygen model. i.e., Regional Ocean Modeling System (ROMS) and a simple parameterization of oxygen dynamics to predict the hypoxic region. The model has been improved by coupling it with a nitrogen-based model (*Fasham et al.*, 1990; *Fennel et al.*, 2006, 2008) to study the nitrogen-dynamics on the Texas-Louisiana shelf *Fennel et al.* (2011).

Statistical models are relatively easy to operate to find possible relationships between different causal factors and the areal extent of hypoxia. Numerical models provide insight into the mechanisms that drive these relationships. In this dissertation, I use both statistical analysis and a coupled physical-biogeochemical numerical model to study the mechanisms controlling or affecting the areal extent of hypoxia in the northern Gulf of Mexico, including both the nutrient and non-nutrient factors. For the statistical analysis, I made regression analyses between the hypoxic area and multiple factors, including the freshwater discharge, the nitrate loading and the duration of upwelling favorable wind. For the numerical model, I used the model of *Fennel et al.* (2011) with an expanded oxygen component to study the oxygen dynamics and hypoxic extent. The model is three-dimensional, has realistic topography, and is forced by freshwater, nitrogen loading and freshwater discharge.

The external forcings and internal processes that drive oxygen concentration changes are shown in Figure 1. The *Fennel et al.* (2011) model includes six nitrogen components: NO_3^-, NH_4^+, phytoplankton, zooplankton, small and large detritus. The NO_3^- and NH_4^+ are taken up by the phytoplankton during primary production. The phytoplankton is consumed by zooplankton and converts to the detritus pool on death. Small detritus converts to large detritus through coagulation. Both small and large detritus are returned to NH_4^+ through remineralization. Part of the phytoplankton, small and large detritus pools sink to the sediment and participate in

biogeochemical processes there. The model assumes that part of the organic matter in the sediment remineralizes to NH_4^+ and is released to the water column, while another part is denitrified to N_2 and lost from the system. The lost nitrogen is replenished by nitrogen from the rivers. The model assumes that the riverine nitrogen is in both the organic and inorganic form. The organic nitrogen enters the model domain as small detritus.

The oxygen is a variable independent to nitrogen. The oxygen is produced during primary production and consumed by zooplankton metabolism, small and large detritus remineralization and denitrification of organic material. The oxygen is also influenced through exchange with the atmosphere.

In addition to the internal biogeochemical processes, the oxygen concentration is also influenced by horizontal advection and vertical mixing. The advection is determined by the magnitute of the currents and vertical mixing is determined by the strength of the pycnocline. They are driven by the combined effects of wind and freshwater discharge. Although the wind magnitude controls the strength of vertical mixing, the wind speed is low during summer every year except in hurricane years, and does not drive the interannual variability of hypoxic areas. Since I am interested in hypoxic area during non-hurricane years, I excluded the wind magnitude as a study variable in the research.

The objectives of this dissertation include:

1. To identify and compare factors that influence the hypoxic area over the Louisiana shelf. The factors that are focused on in this research include: the anthropogenic nitrogen loading, the large-scale climate controlled river discharge, and the duration of westerly winds in summer.

2. To hindcast the hypoxic area from 1985 - 2009 using a multiple variable statis-

tical model and a coupled physical-biogeochemical numerical model.

3. To identify the variability of the hypoxic area on a daily to monthly time scales.

4. To investigate how the duration of west wind influences oxygen concentrations using the numerical model.

5. To run numerical simulations to isolate factors that control and influence the areal extent of hypoxia by differentiating between tightly coupled system forcings, including: the freshwater discharge and nutrient concentration; the ratio of Mississippi to Atchafalaya River runoff; the nitrogen type of nutrient in dissolved inorganic form and organic form.

6. To compare DO dynamics controlled by different processes, including advection, mixing and biological respiration.

This dissertation is organized into five chapters.

Chapter I provides an introduction to hypoxia over the Louisiana shelf and previous modeling activities.

In chapter II, I test the influence of wind duration, the Mississippi River discharge, and nitrate loading on the hypoxic area in the northern Gulf of Mexico region by using a variety of linear regression (statistical) models.

In chapter III, I use a coupled physical-biogeochemical model (ROMS-Fennel) with the expanded oxygen component to study hypoxia on the Louisiana shelf. I compare the simulated oxygen field with the available observations; examine the application of the model to DO simulation; and use EOF analysis to identify typical patterns of hypoxia.

In chapter IV, I examine the variability of the hypoxic area in five hypothetical scenarios with the same total nitrogen loading but different physical or nutrient type

forcings. The tested physical forcings include wind, freshwater discharge, and the ratio of Mississippi and Atchafalya River flow. For the nutrient type scenario, I use single dissolved inorganic nitrogen (DIN) and combined DIN and particulate organic nitrogen (PON).

Chapter V provides the conclusions of this study.

Results from this dissertation study are expected to help us better understand the physical and biological mechanisms that control or affect hypoxic area, provide useful advice for current management strategies and action plans, and enhance prediction efforts for management.

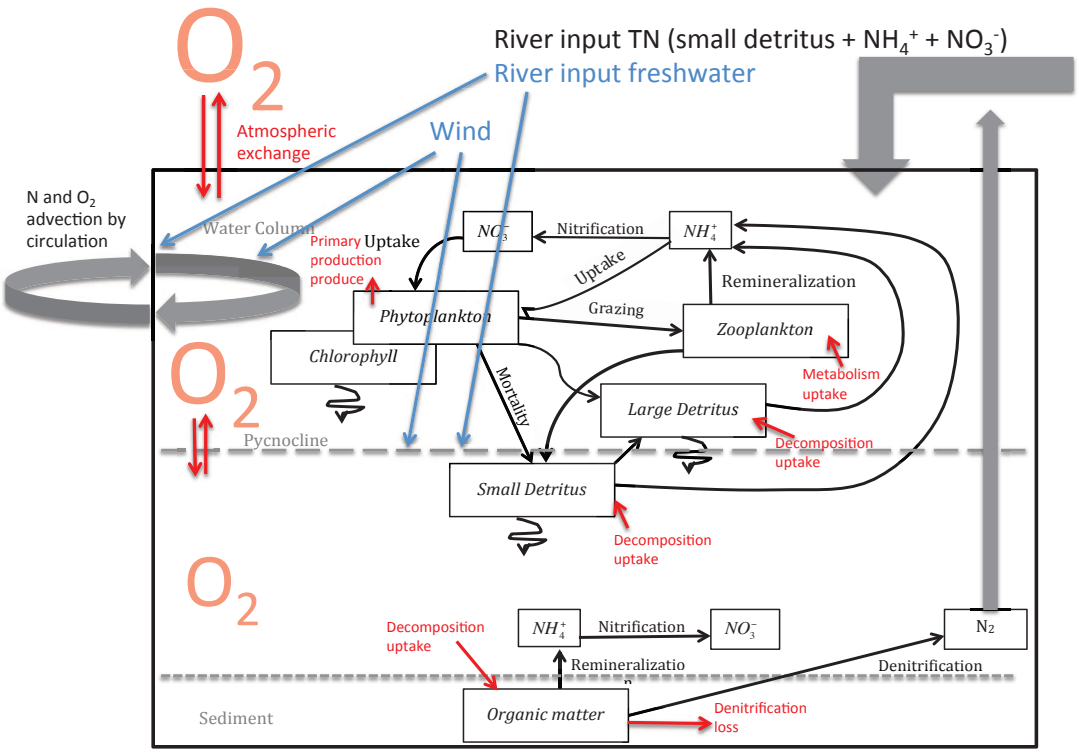

Fig. 1: The conceptual model of processes that change the nitrogen and oxygen concentration. The nitrogen components and processes that change the concentration of nitrogen components are in black. The oxygen components and processes that change the oxygen concentration are in red. The system receives nitrogen from the river, and losses nitrogen from denitrification. Oxygen may be exchanged between the atmosphere and ocean. Both the oxygen and nitrogen components may be advected from one place to another by the currents. The strength of the currents and pycnocline are determined by the wind and freshwater (blue).

CHAPTER II

A STATISTICAL STUDY ON THE RELATIVE ROLE OF WIND FORCING AND RIVERINE NUTRIENT INPUT ON THE EXTENT OF HYPOXIA IN THE NORTHERN GULF OF MEXICO

A. Introduction

The Mississippi River is the largest river system in North America. It delivers large amounts of freshwater (about 380 km^3/year) and nitrogen (about 1.3×10^{11} mol/year) to the Louisiana shelf in the spring, causing a large hypoxic area in the summer and resulting in harm to the ecosystem (*Dagg and Breed*, 2003; *Rabalais et al.*, 2002a).

The hypoxic region of the northern Gulf of Mexico has been surveyed annually in late July since 1985. The reported hypoxic areas range from 40 km^2 to 22,000 km^2 and average more than 13,600 km^2 (*Dale et al.*, 2010). Both statistical and mechanistic models have been used to explore factors affecting the areal extent. Several authors show that the variation in the hypoxic area is related primarily to the variation of nutrient supply or stream flow from the Mississippi and Atchafalaya Rivers. *Wiseman et al.* (1997) found a high correlation between hypoxic area in July and the average Mississippi River stream flow for the previous 11 months (using data from 1985 - 1988, 1990 - 1994). *Turner et al.* (2006) explained the change in hypoxic area using a multiple linear regression model, with the May Mississippi River nitrogen loading and Julian year as predictors. The relationship to Julian year was interpreted in that study as a proxy for carbon stored in the sediments (*Turner et al.*, 2008). *Greene et al.* (2009) used a multiple linear regression model to predict the area using nitrate and phosphate concentrations and river discharge. An important conclusion of both *Turner et al.* (2008) and *Greene et al.* (2009) was that the relation-

ship between the Gulf hypoxic area and nitrogen loading changed in the early 1990's. *Scavia et al.* (2003) reproduced the hypoxic area by using a one-dimensional Streeter-Phelps dissolved oxygen model, driven by the May-June total nitrogen loading from the Mississippi and Atchafalaya Rivers. *Liu et al.* (2010) improved this model by incorporating an additional parameter to account for a system change in 1993. The above models serve as the basis for the present hypoxia management strategy of the U. S. Environmental Protection Agency. Action Plans in 2001 and 2008 call for reductions in nutrient additions throughout the Mississippi River watershed to achieve the goal of reducing the 5-year running average hypoxic area to 5000 km^2 [*Mississippi River/Gulf Mexico Watershed Nutrient Task Force* 2001; 2008].

Observations have shown that the hypoxic area can vary greatly over both daily and seasonal time scales (*Rabalais et al.*, 1999, 2007b; *Bianchi et al.*, 2010). Such variability can result from non-river factors, such as the topography and the wind strength and direction (*Hetland and DiMarco*, 2008; *DiMarco et al.*, 2010). Furthermore, the reported hypoxic area can differ substantially from predictions made using the *Turner et al.* and *Scavia et al.* models. In 2009, the observed area was about 8,000 km^2; the predictions from these two models were 25,000 km^2 and 22,000 km^2, respectively. The reason for the nearly three-fold difference has been hypothesized to be the long duration of the west wind preceding the observations (Rabalais 2009, unpublished, `http://www.gulfhypoxia.net/`, Feng et al, 2010 unpublished).

The wind is the primary driver of the low-frequency circulation on the Texas-Louisiana shelf (*Nowlin et al.*, 2005; *Cho et al.*, 1998). It has a strong seasonal variation, typically being strong and downcoast (from east to west) during the non-summer season; and being weak and upcoast during the summer (*Cochrane and Kelly*, 1986). The change in wind direction alters the horizontal distribution of the river plume and, therefore, the vertical stratification. The relationship between the

Gulf hypoxic area and the average east-west wind speed has been examined in a recent study *(Forrest et al, 2011)*. The correlation was weak ($r^2 = 0.16$), but statistically significant. The relationship between the hypoxic area and the wind has also been explored in other regions, including the Chesapeake Bay and the west Long Island Sound (*Scully*, 2010a,b; *Wilson et al.*, 2008). These studies in other regions used the duration of a directional wind, not average wind speed, as a predictive variable. In this study, we test the influence of wind duration, the Mississippi River discharge, and nitrate loading on the hypoxic area in the northern Gulf of Mexico region by using a variety of linear regression models.

B. Methods

Since 1985, there has been an annual survey in late July to determine the areal extent of hypoxia on the Texas-Louisiana shelf between the Mississippi River bird foot delta and the Texas border (*Rabalais et al.*, 2001). The data have been the basis for both analyses of shelf hypoxia and policy discussions (*Rabalais et al.*, 2002b, 2007b). We focus on observations since 1993, the year in which the relationship between hypoxic area and riverine nitrogen loading changed (*Greene et al.*, 2009). In addition, we have excluded three years of data due to the influence of strong storms prior to the cruises: 2003 (Tropical Storm Bill and Hurricane Claudette), 2005 (Hurricane Dennis), and 2010 (Hurricane Alex and Tropical Depression Bonnie). The extreme weather conditions in the above three years disrupted the stability of the water column and mixed high oxygen surface water with low oxygen bottom water. The resulting hypoxic area distributions were patchy during the hurricane years rather than the usual continuous distributions (hypoxic area images: `http://www.gulfhypoxia.net/`).

We use multiple data sets in our analysis. The regional wind data are from the North America Regional Reanalysis (NARR), which is a high resolution climate data set (`http://www.emc.ncep.noaa.gov/mmb/rreanl/`) covering our time period (1993 - 2010) at 3-hour intervals and our region with 0.3° spatial resolution. We averaged the east-west wind over our domain (87°W to 94°W, 27°N to 31°N) and then filtered the data with a 40-hr low-pass filter to remove the diurnal sea breeze signal (*Zhang et al.*, 2009, 2010). The duration of wind (t_{Uwind}) was calculated by summing the number of days when the east to west wind velocity component was from the west during a 32-d period before the start of the annual shelf-wide survey (*Rabalais et al.*, 2001). The 32-d interval provided the best correlation between the area and t_{Uwind} when the window length was varied from 1 to 50-d (see Results).

The daily discharge of the Mississippi River was measured by the U.S. Army Corps of Engineers at Tarbert Landing, MS (`http://www.mvn.usace.army.mil/`); monthly nutrient loading was estimated by the U. S. Geological Survey at St. Francisville, LA (`http://nwis.waterdata.usgs.gov/`). All the data metrics (Table I) were normalized by the time-series standard deviation before the analyses.

Table I: Data for the regression analysis. [a] mt-N = metric ton nitrogen

Year	Cruise start date	Hypoxic area (km^2)	t_{Uwind} (days)	May-June NO_3 (mt-N[a]/day)	May NO_3 (mt-N/day)	$\bar{F}_{11}$ (m^3/s)
1993	July-24	17600	26	4279	4968	19304
1994	July-24	16600	26	2182	3032	20376
1995	July-21	18200	23	3705	3613	14497
1996	July-23	17920	18	3689	3548	13891
1997	July-23	15840	24	2859	3013	19762
1998	July-21	12480	24	3275	3968	15895
1999	July-23	20000	16	3902	4452	15755
2000	July-22	4400	27	1634	1461	8686
2001	July-20	20720	15	3557	3258	12910
2002	July-21	22000	12	3600	3935	16165
2004	July-21	15040	21	2746	2177	14500
2006	July-22	17280	12	2111	2755	8902
2007	July-21	20500	16	2879	3871	12984
2008	July-21	20720	18	4377	4774	17121
2009	July-18	8000	29	3459	3742	15771

The least square fit method was used to minimize the sum of the squares of the offsets of the points from the curve in single and multiple linear regressions. We used the t_{Uwind}, the 11-month averaged Mississippi River flow ($\bar{F}_{11}$) (*Wiseman et al.*, 1997), the May NO_3^- loading from the Mississippi River (*Turner et al.*, 2006) and the combined May-June NO_3^- loading from the Mississippi River as our predictors (*Donner and Scavia*, 2007).

We calculated the significance level (p) of each regression result as well as the coefficient of determination, r^2, assuming that the data were normally distributed. Because normality is difficult to prove using only fifteen measurements, we determined the robustness of the value of r using a bootstrap technique, randomly resampling the data with replacement, and repeatly estimating r^2 for each resampled series. The

median (r^2_{med}) and 95% confidence interval of r^2 for 10,000 resampled ensembles are used to characterize the results.

C. Results

When we varied the window length while calculating t_{Uwind}, the absolute value of r increased with longer window length (Figure 2). The best correlation is for a 32-d time window (r = -0.74). The negative correlation coefficient indicates that a long west wind duration results in a smaller hypoxic area.

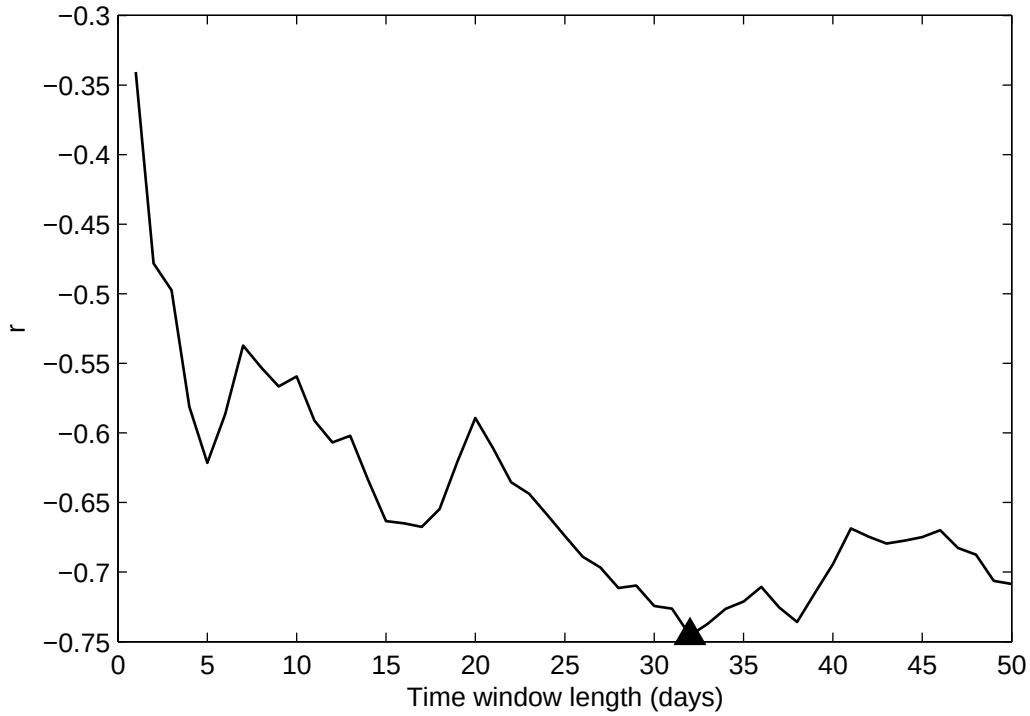

Fig. 2: The correlation coefficient (r) between the hypoxic area and the duration of west wind as a function of the window length in days before the cruise. The best correlation is for a 32-day window length (triangle).

The regression between hypoxic area and t_{Uwind} (r^2 = 0.55) has the strongest

correlation between hypoxic area and any single predictor (Table II). It is statistically significant ($p < 0.01$) and robust ($r^2_{mid} = 0.58$, 95% confidence interval [0.27 - 0.82], Figure 3d). There is also a significant correlation between hypoxic area and NO_3 loading. For May NO_3 loading, r^2 is 0.31 ($p = 0.03$, $r^2_{med} = 0.31$, [3×10^{-3} - 0.74], Figure 3c); for May-June, r^2 is 0.28 ($p = 0.04$, $r^2_{med} = 0.28$, [4×10^{-3} - 0.69], Figure 3b). There is no strong correlation between the area and flow, $\bar{F}_{11}$ (r^2= 0.07, $p = 0.3$, $r^2_{med} = 0.08$, [4×10^{-4} - 0.46], Figure 3a).

Despite the lack of a significant correlation between $\bar{F}_{11}$ and hypoxic area, a multi-linear regression analysis, which includes both t_{Uwind} and $\bar{F}_{11}$, has the strongest correlation of those considered ($r^2 = 0.86$, $p < 0.01$, $r^2_{med} = 0.86$, [0.5 - 0.97], Figure 3h). The improved correlation can be understood using a 3D plot (Figure 4). Although the hypoxic area and river discharge can not be fit to a line on the 2D plane, they fit well to a plane in the 3D space which includes t_{Uwind}. The multilinear regression with predictors t_{Uwind} and either May or May-June loading gives $r^2 = 0.74$ and 0.72, respectively. The regression with the May NO_3 load and Julian year as in *Turner et al.* (2006) has the smallest correlation ($r^2 = 0.31$, $p = 0.1$, $r^2_{med} = 0.39$, [0.04 - 0.78], Figure 3e).

Table II: Linear regression analysis result. All data are normalized by their standard deviations before calculation.

model: $Y = \beta_1 x + \beta_0$							
						Bootstrap	
x		r^2	β_1	β_0	p value	median	95% interval
$\bar{F}_{11}$		0.07	0.27	2.18	0.3	0.08	$4\times10^{-4} \sim 0.46$
May-June NO_3		0.28	0.53	1.25	0.04	0.28	$4\times10^{-3} \sim 0.69$
May NO_3		0.31	0.56	1.28	0.03	0.31	$3\times10^{-3} \sim 0.74$
t_{Uwind}		0.55	-0.74	6.06	<0.01	0.58	$0.27 \sim 0.82$
model: $Y = \beta_1 x_1 + \beta_2 x_2 + \beta_0$							
						Bootstrap	
x_1	x_2	r^2	β_1	β_2	β_0	p value	median	95% percentile
May NO_3	Julian year	0.31	0.55	-0.02	9.94	0.1	0.39	$0.04 \sim 0.78$
t_{Uwind}	May-June NO_3	0.72	-0.67	0.42	4.12	<0.01	0.75	$0.49 \sim 0.94$
t_{Uwind}	May NO_3	0.74	-0.66	0.45	4.11	<0.01	0.77	$0.48 \sim 0.92$
t_{Uwind}	$\bar{F}_{11}$	0.86	-0.94	0.60	4.20	< 0.01	0.86	$0.5 \sim 0.97$

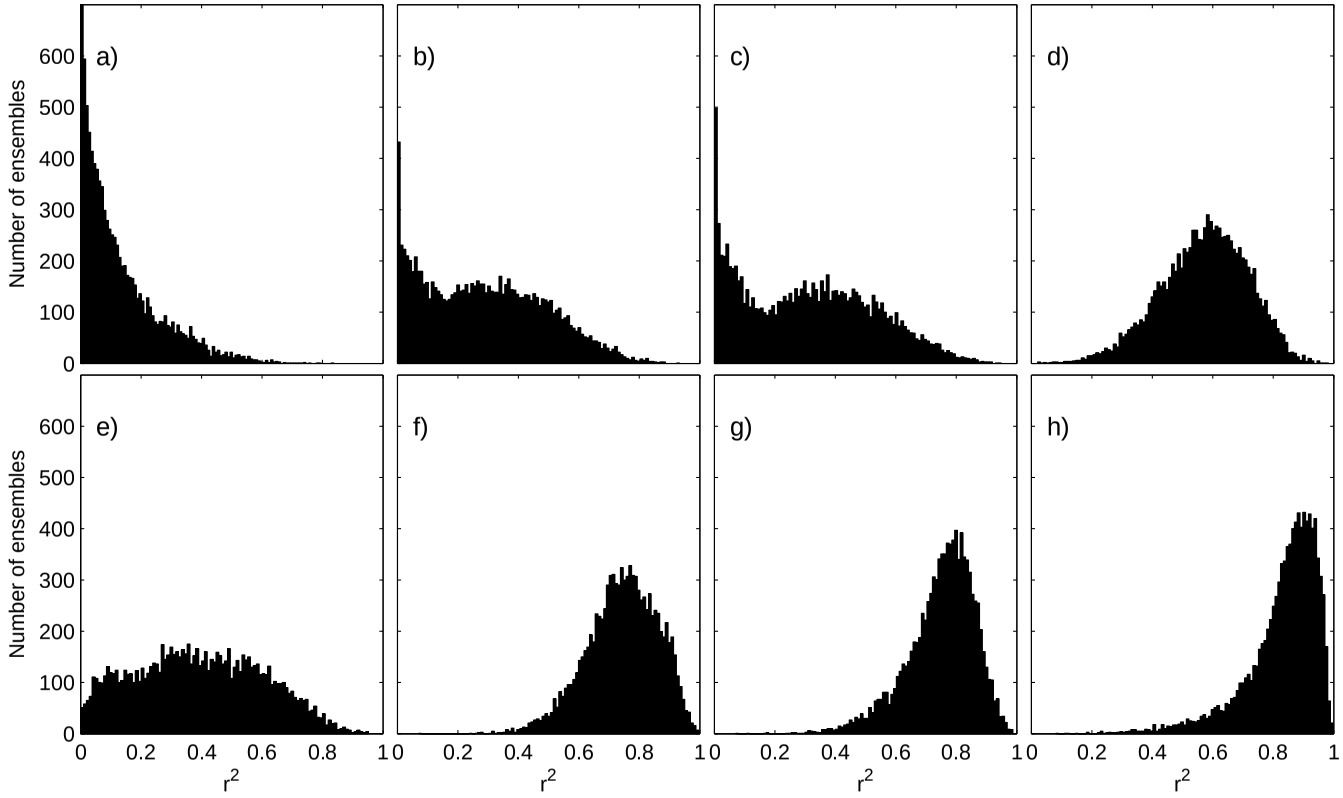

Fig. 3: Histograms of r^2 from bootstrap analyses of 10,000 ensembles. Regressed against the hypoxic area are (a) $\bar{F}_{11}$; (b) May NO_3 load from the Mississippi River; (c) May-June NO_3 load from the Mississippi River; (d) t_{Uwind}; (e) May NO_3 load from the Mississippi River and Julian year; (f) t_{Uwind} and May-June NO_3 load from the Mississippi River; (g) t_{Uwind} and May NO_3 load from the Mississippi River; (h) t_{Uwind} and $\bar{F}_{11}$.

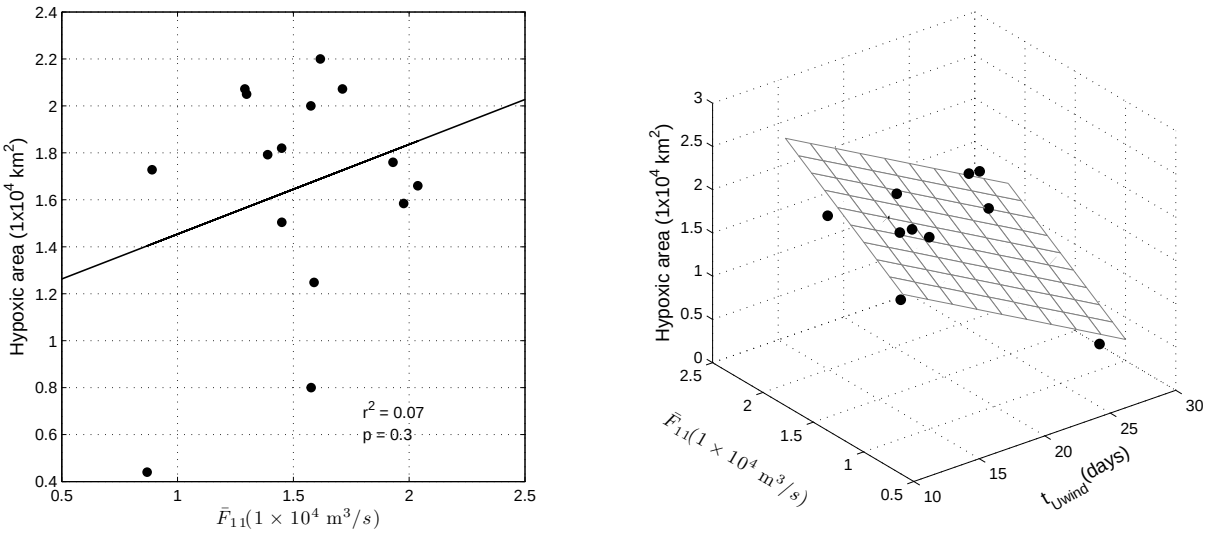

Fig. 4: The relationship between hypoxic area and $\bar{F}_{11}$ (a), and $\bar{F}_{11} + t_{Uwind}$ (b), two variable multiple linear regression fits a plane to the hypoxic area in 3D space.

D. Discussions

It is difficult to compare our statistical results with previous studies because the value of r^2 depends largely on the years being used in the regression and the specific dataset used for the calculations (*Wiseman et al.*, 1997; *Turner et al.*, 2006; *Donner and Scavia*, 2007; *Greene et al.*, 2009). Previous studies covered different periods and versions of USGS published data (Table III). In addition, the data from the Atchafalaya River were not always included in previous studies. Our r^2 values for regressions of nutrient loading and hypoxic area are smaller than those of *Turner et al.* (2006) (0.50) and Donner and *Scavia et al.* (2003) (0.61), although still significant at the 95% level, because we have used a newer version of the USGS water quality data. Our correlations between nutrient loading and hypoxic area are exactly the same as those of *Greene et al.* (2009), who used the same periods and dataset.

Table III: Comparing single linear regression results. [a]All r^2 values here are above the 95% significance level if data are assumed normally distributed. [b] A typo in the original paper, number is recalculated from Fig.10 of *Wiseman et al.* (1997) by *Hetland and DiMarco* (2008).[c] 1989 is 8574 km^2 as estimated from *Turner et al.* (2005); 2003 is excluded as a hurricane year. [d] A combined Mississippi-Atchafalaya River May NO_3 loading was used instead of only the Mississippi River in this calculation.

Variable	Reference	No. Records	Data Period	Previous r^2	[a]This Study r^2
$\bar{F}_{11}$	*Wiseman et al.* (1997)	N = 9	1985-1994(exclude 1989)	0.60[b]	0.65
May-June NO_3	*Donner and Scavia* (2007)	N = 19	1985-2004(exclude 1989)	0.61	0.45
May NO_3	*Turner et al.* (2006)	N=19	1985-2004(exclude 2003)[c]	0.5	0.44
	Greene et al. (2009)	N = 22	1985-2007(exclude 1989)	0.42[d]	0.42[d]

This study shows the importance of non-riverine physical driving, i.e., the duration of the west wind, as well as the riverine nutrient input in determining the area of hypoxia over the Louisiana shelf. *Wiseman et al.* (1997) found that a weak west wind during summer could drive the river plume eastward and offshore, creating a weak secondary pycnocline. This secondary pycnocline reduced the vertical mixing, further inhibiting ventilation of the subpycnocline, resulting in even lower near bottom oxygen concentrations. Although a west wind during summer facilitates hypoxia development by stratifying more of the continental shelf when the freshwater plume is moved further from the coast line, our regression results show that a persistent west wind actually reduces the areal extent because ultimately the plume moves south and east and leaves the continental shelf margin. Thus, a large region of the shelf becomes unstratified, promoting ventilation of near-bottom waters, and resulting in smaller hypoxic area.

The best correlation between the hypoxic area and t_{Uwind} is for a 32-d window length. Although there is no significant correlation between area and $\bar{F}_{11}$ for a single variable correlation, using $\bar{F}_{11}$ as a predictor in conjunction with the wind duration does yield an improved correlation. This unexpected high correlation for the multiple variable linear regression suggests that the influence of river discharge on hypoxia depends on how widely the water can be spread by the wind. The monthly-mean Mississippi River flow has a clear seasonality, typically high in spring and low in summer, however there is interannual variation in the average 11-month period that is considered in this study (*Dinnel and Wiseman*, 1986). The timing of the summer wind transitioning is different from year to year, and can range from early June (e.g. 2009) to mid July (e.g. 2002). An early wind transition thins the river plume and initially spreads it onto the broad Louisiana shelf by surface Ekman transport. However, as the west wind persists, the freshwater plume distribution to the east

gradually shrinks as the river flow onto the shelf from the eastern source at Southwest Pass moves south and offshore to the deep Gulf. The increased mixing resulting from lower density stratification on the west shelf reduces the hypoxic area. In contrast, a late wind transition completes the Ekman induced movement, but has insufficient time to move the river plume completely from the west shelf. The 32-d window length may reflect the response time for stratification on the west shelf to weaken from the low-energy wind. The variation of the river plume with wind during short time scales has been shown in a hydrological model (*Hetland and DiMarco*, 2008).

The regression models using the wind as a predictor can reproduce the hypoxic area for the non-hurricane years, especially for those years with extremely small (2000, 2009) and large area years (1999, 2001, 2002, Figure 5). The models generally over-predicted the observed hypoxic area for the hurricane and tropical storm years (2003, 2005 and 2010). We interpret this as indicating that the strong winds increase mixing and decrease hypoxic area relative to the prediction.

As we have shown, including the effect of the west wind greatly improves the skill of our prediction. When trying to forecast the hypoxic area, a regional climate model could be used to predict the wind field during the coming summer. Ultimately, we envision a coupled atmospheric - oceanic - biological modeling system as the best tool for the hypoxic area prediction. The effect of the wind complicates the management strategy for the hypoxic area. Unlike the riverine nutrient loading, which can be reduced by regulating the fertilizer use within the Mississippi river watershed, the variation of regional wind depends on the variation of the global climate system.

Precipitation over the central U.S. is expected to increase under global warming scenarios, resulting in an increase in Mississippi River flow (*Justic et al.*, 2003a,b; *Donner and Scavia*, 2007). The high flow brings both increased buoyancy and nutrients to the shelf, increasing the tendency for a large hypoxic area. Our study reminds

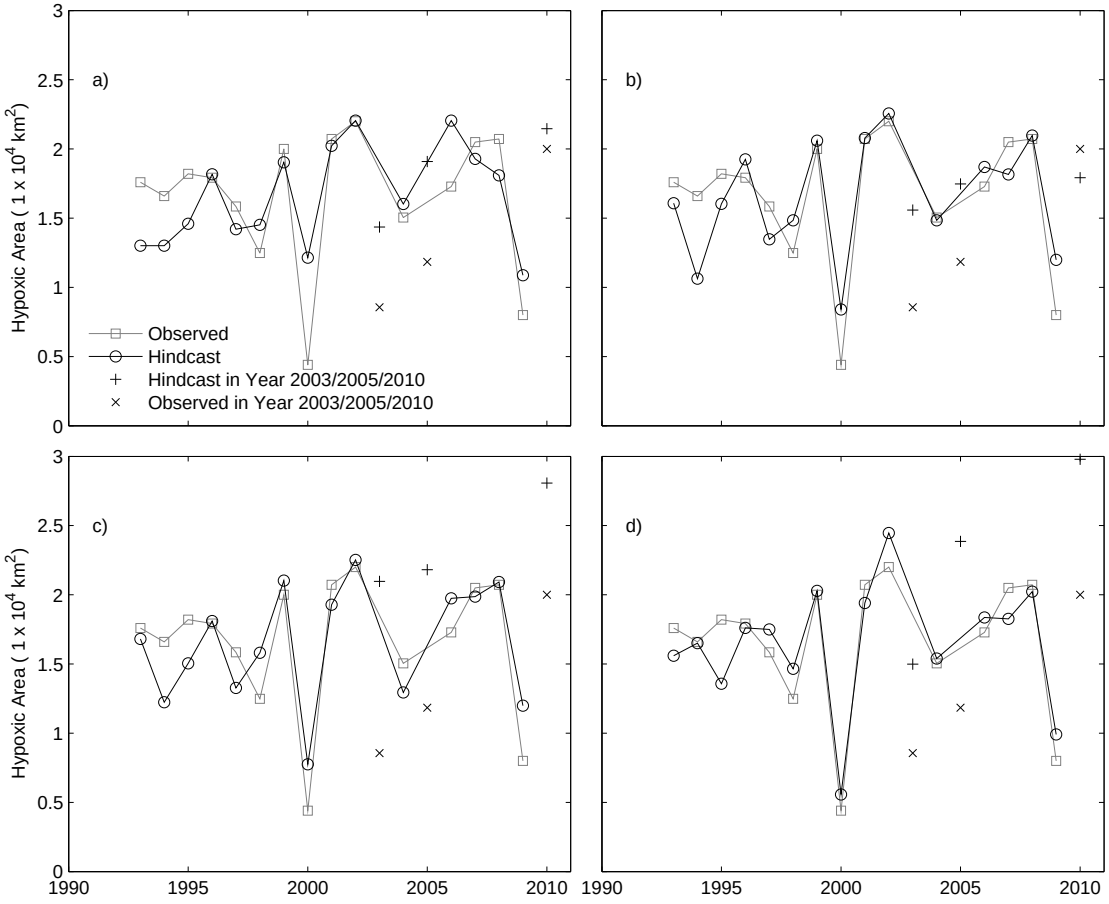

Fig. 5: The hypoxic area from the observation and the regression models. The regressed variables are (a) t_{Uwind} (b) t_{Uwind} and the May-June NO_3 load from the Mississippi River, (c)t_{Uwind} and the May NO_3 load from the Mississippi River, (d) t_{Uwind} and $\bar{F}_{11}$.

us that in addition to changing precipitation, global climate change can alter the extent of hypoxia by altering regional winds (*Scully*, 2010a). The shift of the transition time for the seasonal wind can influence the distribution of the river plume in mid summer, thereby influencing the hypoxic area. Details of how the transition time of the wind may change as a result of the evolving global system are not presently understood and are worth further investigation.

CHAPTER III

SIMULATING THE OXYGEN DYNAMICS OF THE NORTHERN GULF OF MEXICO USING A THREE-DIMENSIONAL, COUPLED PHYSICAL-BIOGEOCHEMICAL MODEL

A. Introduction

Oxygen depletion can cause detrimental ecological effects in coastal waters and therefore receives extensive scientific and management interest. In the Gulf of Mexico, water with oxygen concentration depleted to less than 2 mg/L (62 μM) is considered hypoxic. The region of hypoxia in the Gulf of Mexico is believed to have increased since the mid-20th century. Increases in the size and severity of the hypoxic zone have been driven by increased anthropogenic nutrient loading and the resulting coastal eutrophication (*Turner and Rabalais*, 1994; *Rabalais et al.*, 1996, 2002a,b). Nutrient management strategies have been suggested to improve the water quality in the northern Gulf of Mexico (*Mississippi River/Gulf of Mexico Watershed Nutrient Task Force*, 2001, 2008). The proposed measures include reducing the use of nitrogen-containing fertilizer, improving management of animal manure, reducing discharge from point sources, and restoring riparian wetlands (*Mitsch et al.*, 2001; *Dale et al.*, 2010).

Assessing the success of changed nutrient practices is made difficult by the complexity and variability of the physical processes in the coastal system. The density field that controls the strength of vertical mixing is itself controlled by multiple factors, including the amount of freshwater discharge, the wind strength and the wind direction. In addition, the currents that transport the oxygen-consuming materials produced by eutrophication are driven by the wind and by freshwater input. The

physical processes are tightly coupled to important biological processes and are not controlled by the proposed nutrient management policy. Understanding the role of physical processes is extremely challenging, but can improve nutrient management strategies.

Gulf hypoxia has been studied using numerical and statistical models for many years (*Justic et al.*, 2007). Past modeling work can be separated into two categories. The first category involves mechanistic or process studies. The model results cannot be used to predict the hypoxic area but help us better understand the relative importance of the various processes influencing hypoxia. Examples of this category include *Bierman et al.* (1994); *Chen et al.* (1997); *Justic et al.* (1996, 2002); *Rowe* (2001); *Breed et al.* (2004) and *Green et al.* (2006, 2008). The second category is used for management and either hindcasting or forcasting the observed hypoxic area. Examples of this category include *Scavia et al.* (2003), *Turner et al.* (2006), *Scavia and Donnelly* (2007) and *Greene et al.* (2009).

Bierman et al. (1994) divided the Louisiana shelf into regions and studied the changes in the dissolved oxygen (DO) concentration as a result of photosynthesis and respiration in each, as well as estimating oxygen exchange between regions. They concluded that photosynthesis and respiration could change the oxygen concentration more than physical exchange of oxygen through horizontal and vertical advection and mixing.

Chen et al. (1997) used a two dimensional, coupled biological and physical model through a cross-shelf section to study the algal growth in response to river discharge near Atchafalaya Bay. Their simulation predicted a well-defined density frontal zone and high nutrient concentrations near the bottom as a result of the coupling of physical and biological processes. However, their model lacked an alongshore component and did not consider oxygen dynamics. As a result, it could not be used to predict the

hypoxic area, but it was the first application of a coupled biological and hydrodynamic model to the Louisiana shelf.

Justic et al. (1996, 2002) focused on vertical processes using a two-box model to simulate the monthly oxygen concentration at a location with long-term observations. The model separated the water column into regions above and below the pycnocline. Above the pycnocline, the oxygen concentration was changed by exchange with the atmosphere and with the subpycnocline region, as well as by near-surface primary production. Below the pycnocline, oxygen was replenished by exchange with the overlying layer and consumed by respiration of settled organic matter in the water column and sediments. The model results indicated that the intensification of hypoxia since 1950 was caused by decadal changes of nitrogen loading from the Mississippi River.

Rowe (2001) used a simple model to compare different processes in the bottom water presumed to cause hypoxia. He concluded that benthic respiration, rather than water column respiration, was the greater consumer of oxygen.

Breed et al. (2004) used an inverse analysis of biological rate measurements to describe the carbon flow system in the Mississippi River plume. They showed a linkage between the primary production and sedimentation on the Louisiana shelf. *Green et al.* (2006) extended their work and investigated seasonal variability in organic carbon budgets at the Mississippi River plume. They found that the oxygen respiration in low salinity waters was much stronger than in intermediate to high salinity waters.

Green et al. (2008) used a more sophisticated ecosystem model for the Mississippi River plume to investigate the response of organic matter production and sedimentation to variable nitrate loading. Their model used a revised nitrogen-based *Fasham et al.* (1990) plankton model forced by simplified physical processes (plume residence time and light attenuation by non-algal material) varying along the river-ocean salin-

ity gradient. Their simulations found that a 30% decrease in NO_3 load would result in a 19% decrease in average plume primary production and 14% decrease in sedimentation. However, there was no oxygen component in the biological model, and the spatial variability was tied to the salinity gradient. As a result, the model could not provide information about the areal extent of hypoxia.

Scavia et al. (2003) made a coupled model that incorporated simple physical and biological processes to simulate the region below the pycnocline. Their model was driven by spring nitrogen loading (May-June) and considered oxygen exchange with the atmosphere and consumption in the bottom layer. Hydrodynamic processes were described as a constant alongshore velocity. Because the model was only one-dimensional along the shelf, it could not describe the cross shelf extent of the hypoxic zone. They used a linear regression between the observed hypoxic area and length to calculate the area of hypoxia.

Turner et al. (2006) described the change in hypoxic area using a multiple linear regression model, with May Mississippi River nitrogen loading and Julian year as predictors. The relationship to Julian year was later interpreted in a separated study as a proxy for carbon stored in the sediments. However, the performance of the model depends on years selected, and using Julian year as a predictor lacks a mechanistic basis.

Scavia and Donnelly (2007) investigated relationships among the hypoxic area, the nitrate input from the Mississippi River, and precipitation. From multi-linear regressions, they found that 70% of the May–June nitrate input could be explained by the November–December and March–May precipitation, and 37% of the hypoxic area could be explained by the May–August nitrate input in addition to the precipitation. Their results emphasized the importance of considering the climate variability in hypoxia management policy.

Greene et al. (2009) used multi-linear regression models to investigate the relationships between the hypoxic area and several individual nutrient inputs. The difference between their model and *Turner et al.* (2006)'s model was that they separated the total nutrient loading into two components: nutrient concentration and river discharge. They found that the hypoxic area had an abrupt increase in 1993, which meant that, with the same amount of discharge and nutrient concentration, the hypoxic area was 6,450 km^2 greater for the years post-1993 than before.

A consistent conclusion of above models is that the increase in anthropogenic riverine nutrient input has been responsible for the extent of bottom water hypoxia on the Louisiana shelf since 1975.

The model of *Hetland and DiMarco* (2008) was different from previous models by being three-dimensional, allowing the two-dimensional hypoxic region to be calculated directly. In addition, it emphasized physical rather than biological processes. Their model used the Regional Ocean Modeling System (ROMS) and a simple parameterization of oxygen dynamics to predict the hypoxic region. They concluded that the in-situ oxygen concentration was mainly changed by in-situ biological respiration and vertical mixing, instead of the advection of low-oxygen water from another region. Such a conclusion was similar to that of *Bierman et al.* (1994).

Although *Hetland and DiMarco* used a three-dimensional hydrodynamic physical model to simulate a complex physical environment, they noted that a more sophisticated description of the biological and chemical processes that alter oxygen concentrations was also needed for a better understanding of hypoxia. They suggested that a biological model incorporating a nitrogen budget be used in the future work.

The latest version of ROMS incorporates several elaborate biological modules, making it practical to relate nitrogen cycling to oxygen consumption. *Fennel et al.* (2006) used a revised version of the *Fasham et al.* (1990) plankton model embedded

in ROMS to quantify the nitrogen budget in the Middle Atlantic Bight (MAB). Their biological model has been expanded to include oxygen as an additional component and applied to understand hypoxia dynamics.

In this chapter, I use the *Fennel et al.* (2006, 2011) model with the expanded oxygen component to study hypoxia on the Louisiana shelf. First, I compare the simulated oxygen field with the available observations. Then, I examine the application of the model to hypoxic area estimation. Lastly, I use EOF analysis to identify typical spatial and temporal patterns of hypoxia. The standard survey of the hypoxic area occurs once per year. However, the DO concentrations change on much shorter time scales, varying over time scales ranging from minutes to decades. This modeling study allows us to expand our understanding of the hypoxic area variability on a variety of temporal and spatial scales.

The most commonly used units for dissolved oxygen are mg/L, ppm, ml/L, and μM. As mentioned above, hypoxia is defined as a dissolved oxygen concentration less than 2 mg/L, the equivalent of 2 ppm, 1.4 mg/L, or 62 μM. The observed data are commonly in units of mg/L, but the model outputs are in units of μM. Therefore, we use both mg/L and μM throughout this article, and provide conversions sometimes.

B. Methods

1. The Model

I used ROMS (version 3.0) (*Shchepetkin and McWilliams*, 2003, 2005; *Haidvogel et al.*, 2008) with one of its embedded biogeochemical modules (*Fennel et al.*, 2006, 2008, 2011) to describe the Louisiana shelf. The physical component was almost the same as *Hetland and DiMarco* (2008), with minor modifications. The biological part of the model was that of *Fennel et al.* (2011).

a. Physical Component

The model domain extended from 94.7 °W to 87.7 °W and from 27.4 °N to 30.4 °N, covering the shelf region where oxygen concentration has been surveyed during the past 25 years (Fig. 6). The model grid spacing changed with location. The horizontal resolution of the model was highest near the Mississippi River Delta (1 km) and lowest in the southwest corner of the domain (20 km), with an average grid spacing of 4 km. The offshore (southern) boundary was set along the 400–500 m depth contour to minimize the influence of the offshore boundary on the hypoxic region (typically at a bottom depth < 60 m). The model had 20 terrain-following vertical layers whose resolutions increased near the surface and bottom boundaries (Fig. 7).

The model was configured to use fourth-order horizontal advection of tracers, third-order upwind advection of momentum, and the *Mellor and Yamada* (1982) turbulence closure scheme for vertical mixing. The background diffusivities for momentum and tracers were set to 10^{-5} and 10^{-6} m^2/s, respectively.

The model was initialized with an average climatological profile of temperature and salinity. The temperature and salinity data were from World Ocean Atlas 2001 (`http://www.nodc.noaa.gov/`). The barotropic and baroclinic velocity fields and the free surface height were all set to zero. The model had three open boundaries, and boundary conditions included the gradient condition for the free surface, the radiation condition for the tracers and the baroclinic 3D velocities, and the *Flather* (1976) condition for the barotropic 2D velocities. The temperature, salinity, nitrate, ammonium and oxygen concentrations were nudged in and out to the external data with time scales of 1 d and 100 d, respectively (*Marchesiello et al.*, 2001).

The external data for nudging were from LATEX (*Nowlin et al.*, 1998) and NEGOM (*Jochens et al.*, 2002) observations. Both the seasonal and depth variations were considered. At the southern boundary, the model girds had uniform vertical resolution. I examined the data and found that there was not much variability along the southern boundary. Therefore, I ignored the spatial difference. All the data near the southern boundary were together, average by depth and season (spring Mar–May; summer Jun–Aug; fall Sep–Nov; and winter Dec–Feb), and linearly interpolated to the model grid. At the eastern and western boundaries, the model grids had a higher vertical resolution at the nearshore and lower resolution at the offshore. For the east boundary, I first found all the LATEX data close to the east boundary. Then, I separated the data into four seasons. For data in each season, I put them together and interpolated them to the model grid by the triangle-based linear interpolation in matlab. For the western boundary, I found all the NEGOM data close to the west boundary and processed them in the same way as the eastern boundary.

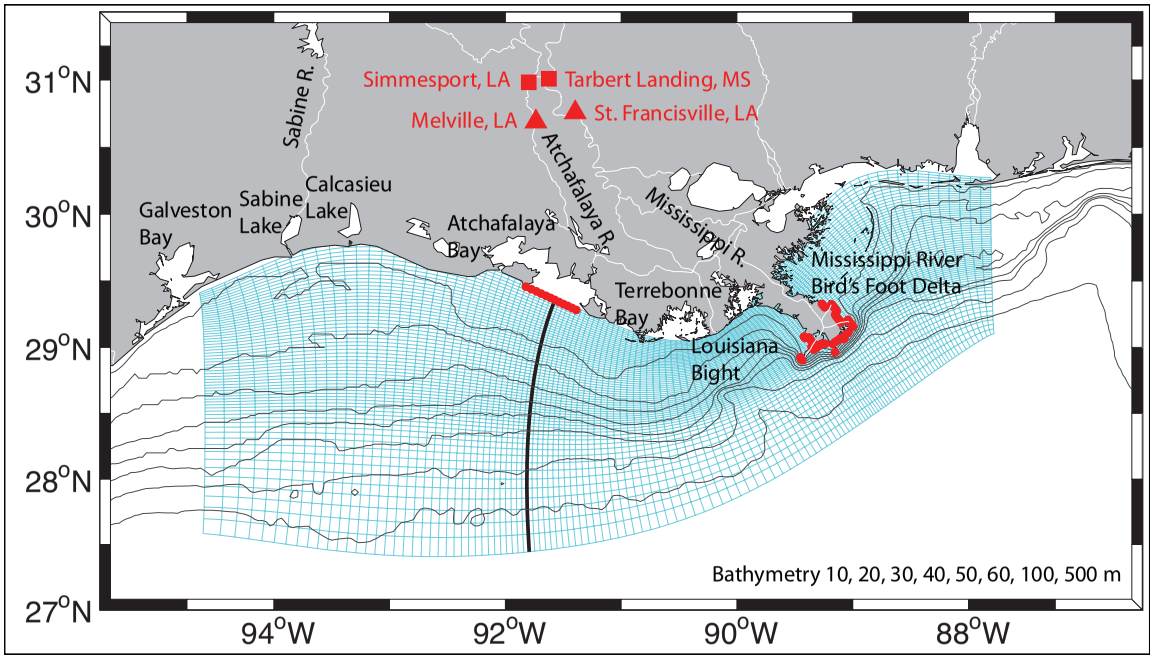

Fig. 6: The numerical model domain. The discharge and nutrient loading of Mississippi River use values measured at Simmesport, LA and Tarbert Landing, MS, respectively, but inputs to the model domain are at the computational grid. The discharge and nutrient loading of the Atchafalaya River are measured at St. Francisville, LA and Melville, LA, respectively, but input to the model domain is at the northern boundary of the model grid. The locations of Mississippi and Atchafalaya River inputs for the model (red dots) and observation (red triangle for USACE discharge; red square for USGS nutrient loading) are shown. The thick black line at 91.8°W shows the position of the vertical section (depicted in Fig. 7).

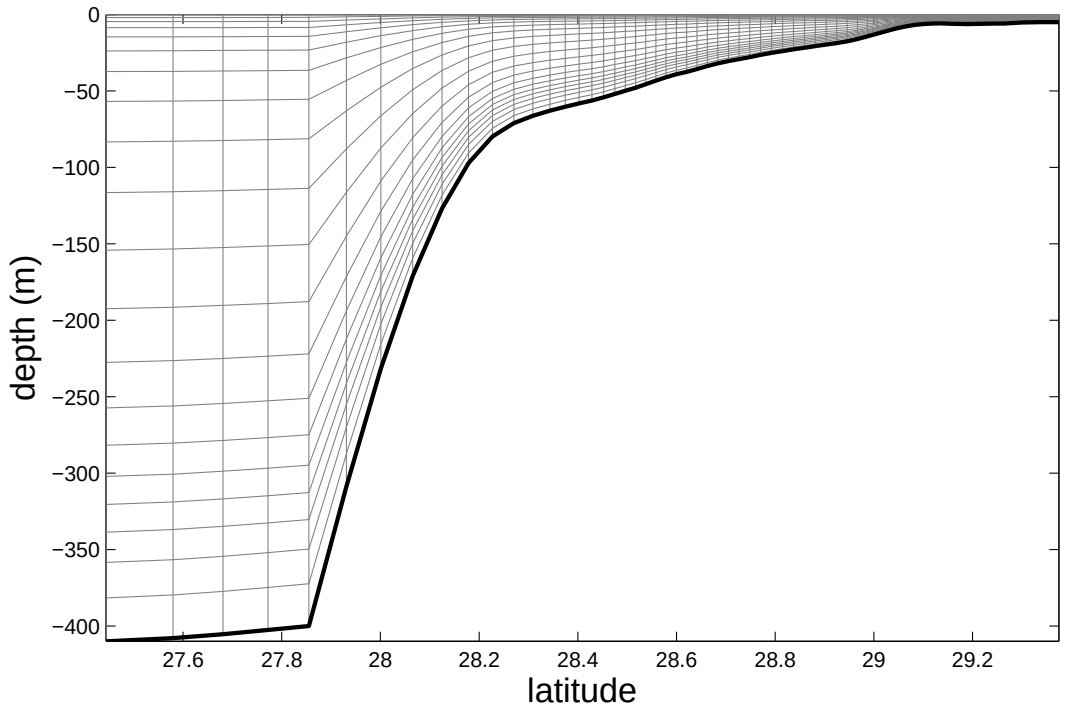

Fig. 7: A cross-shelf section. The map location of the section is shown in Fig. 6.

b. Biogeochemical Model Component

The Fennel module in ROMS was a modified version of the nitrogen-based *Fasham et al.* (1990) plankton model. The model components were modified to include two sizes of detritus, small and large, instead of a single detritus components. Small detritus could aggregate to form large detritus before sinking. The bacterial and labile dissolved organic matter components were not used in this study, and a chlorophyll component was added. As a result, the model included seven state variables: nitrate (N_{NO_3}), ammonium (N_{NH_4}), phytoplankton (P), zooplankton (Z), small and large particle detritus (D_S and D_L), and chlorophyll (C_{hl}). They could move physically as tracers. The biogeochemical equations describing them were (3.1) - (3.7). The model does not include any dissolved or particulate material from offshore or estuarine

sources other than the Mississippi and Atchafalaya Rivers.

The phytoplankton (P) component was:

$$\frac{\partial P}{\partial t} = \mu P - gZ - m_P P - \tau(D_S + P)P - w_P \frac{\partial P}{\partial z} \tag{3.1}$$

The specific growth rate of phytoplankton μ depended on the temperature T, the photosynthetically available radiation I, and the nutrient concentrations, N_{NO_3} and N_{NH_4}.

$$\mu = \mu_{max} \cdot f(I) \cdot (L_{NO_3} + L_{NH_4})$$

$$\mu_{max} = \mu_0 \cdot 1.066^T$$

$$L_{NO_3} = \frac{N_{NO_3}}{K_{NO_3} + N_{NO_3}} \cdot \frac{1}{1 + N_{NH_4}/K_{NH_4}}$$

$$L_{NH_4} = \frac{N_{NH_4}}{K_{NH_4} + N_{NH_4}}$$

$$f(I) = \frac{\alpha I}{\sqrt{\mu_{max}^2 + \alpha^2 I^2}}$$

$$I = I(z) = I_0 \cdot F_{rac} \cdot \exp\Big[- zK_w - K_{chl} \int_z^0 C_{hl}(\varsigma) d\varsigma \Big]$$

$$g = g_{max} \frac{P^2}{K_P + P^2}$$

The zooplankton (Z) component was:

$$\frac{\partial Z}{\partial t} = g\beta Z - l_{BM} Z - l_E \frac{P^2}{K_P + P^2} \beta Z - m_Z Z^2 \tag{3.2}$$

The small detritus (D_S) component was:

$$\frac{\partial D_S}{\partial t} = g(1 - \beta)Z + m_Z Z^2 + m_P P - \tau(D_S + P)D_S - r_{D_S} D_S - w_s \frac{\partial D_S}{\partial z} \tag{3.3}$$

The large detritus (D_L) component was:

$$\frac{\partial D_L}{\partial t} = \tau(D_S + P)^2 - r_{D_L} D_L - w_L \frac{\partial D_L}{\partial z} \tag{3.4}$$

The nitrate (N_{NO_3}) component was:

$$\frac{\partial N_{NO_3}}{\partial t} = -\mu_{max} f(I) L_{NO_3} P + n N_{NH_4} \tag{3.5}$$

The nitrification rate n was suppressed by light:

$$n = n_{max}\Big[1 - \max(0, \frac{I - I_0}{K_I + I - I_0})\Big]$$

The ammonium (N_{NH_4}) component was:

$$\frac{\partial N_{NH_4}}{\partial t} = -\mu_{max} f(I) L_{NH_4} P - n N_{NH_4} + l_{BM} Z + l_E \frac{P^2}{K_P + P^2} \beta Z + r_{D_S} D_S + r_{D_L} D_L \tag{3.6}$$

The chlorophyll (C_{hl}) component was:

$$\frac{\partial C_{hl}}{\partial t} = \rho_{chl} \mu C_{hl} - g Z \frac{C_{hl}}{P} - m_P C_{hl} - \tau(D_S + P) C_{hl} - w_P \frac{\partial C_{hl}}{\partial z} \tag{3.7}$$

$$\rho_{chl} = \frac{\theta_{max} \mu P}{\alpha I C_{hl}}$$

The *Fennel et al.* (2006) model had been extended by Katja Fennel (personal communication) to include DO as a state variable, and the descriptive equation was:

$$\begin{aligned} \frac{\partial O_2}{\partial t} &= \mu_{max} \cdot f(I) \cdot (L_{NO_3} \cdot r_{o_2:NO_3} + L_{NH_4} \cdot r_{o_2:NH_4}) P - 2 n N_{NH_4} \\ &\quad - (l_{BM} + l_E \frac{P}{P + K_P} \beta) r_{o_2:NH_4} \cdot Z - r_{D_S} \cdot r_{o_2:NH_4} \cdot D_S - r_{D_L} \cdot r_{D_L:NH_4} \cdot D_L \end{aligned} \tag{3.8}$$

In addition to the water column processes, gas-exchange across the air-sea interface changed the oxygen concentration in the top layer of the model:

$$\frac{\partial O_{2[top]}}{\partial t} = \frac{k_{o_2}}{\Delta z}(O_{2[sat]} - O_2) \tag{3.9}$$

where $\partial O_{2[top]}/\partial t$ (unit: μM-O_2/s) was the oxygen concentration change by exchange with the atmosphere. k_{o_2} was the gas exchange coefficient for oxygen (unit: m/s), $k_{o_2} = 0.31$ [unit: s/m] $\cdot u_{10}^2 \cdot \sqrt{660/Sc_{o_2}}$, Sc_{o_2} was the Schmidt number calculated using the relationship of *Wanninkhof* (1992), Δz was the thickness of the surface layer, and $O_{2[sat]}$ was the saturation concentration of oxygen, calculated as in *Garcia and Gordon* (1992). Parameters used in (3.1) - (3.8) were given in Table IV.

The initial values of N_{NO_3}, N_{NH_4}, P, Z, D_S, D_L and C_{hl} were uniform over the model domain (Table V). The oxygen concentrations were initialized with the saturation values calculated from the associated temperature and salinity profile. All other biological variables were set to small positive values (Table V).

The remineralization of deposited organic matter within the upper part of the sediment was formulated as a bottom boundary condition for the deepest water layer. *Fennel et al.* (2006) assumed that (1) the flux of sinking organic matter out of the bottom-most grid box resulted in a simultaneous influx of inorganic nutrients at the sediment/water interface; (2) the organic matter was remineralized through aerobic and anaerobic pathways at a fixed ratio.

Table IV: The parameters of the biogeochemical model.

Symbol	Parameter	Value	Unit
I_0	Threshold for light-inhibition of nitrification	0.0095	W m^{-2}
K_I	Light intensity at which the inhibition of nitrification is half-saturated	0.1	W m^{-2}
K_{NO_3}	Half-saturation concentration for uptake of NO_3	0.5	mmolN m^{-3}
K_{NH_4}	Half-saturation concentration for uptake of NH_4	0.5	mmolN m^{-3}
K_w	Light attenuation coefficient for water	0.04	m^{-1}
K_{chl}	Light attenuation coefficient for chlorophyll	0.02486	m^{-1}
K_P	Half-saturation concentration of phytoplankton ingestion	2	(mmolN m^{-3})^2
F_{rac}	The fraction of light that is available for photosynthesis	0.43	-
g_{max}	Maximum grazing rate	0.6	(mmolN m^{-3})$^{-1}d^{-1}$
l_{BM}	Excretion rate due to basal metabolism	0.1	d^{-1}
l_E	Maximum rate of assimilation related excretion	0.1	d^{-1}
m_P	Phytoplankton mortality	0.15	d^{-1}
m_Z	Zooplankton mortality	0.025	(mmolN m^{-3})$^{-1}d^{-1}$
n_{max}	Maximum nitrification rate	0.2	d^{-1}
r_{D_S}	Remineralization rate of suspended detritus	0.3	d^{-1}
r_{D_L}	Remineralization rate of large detritus	0.01	d^{-1}

Table IV: Continued

Symbol	Parameter	Value	Unit
$r_{o2:NO_3}$	Ratio of oxygen and nitrogen if taking nitrate for photosynthesis	8.625	-
$r_{o2:NH_4}$	Ratio of oxygen and nitrogen if taking ammonium for photosynthesis	6.625	-
w_P	Sinking velocity of phytoplankton	0.1	md^{-1}
w_{D_S}	Sinking velocity of suspended detritus	0.1	md^{-1}
w_{L_S}	Sinking velocity of large detritus	5	md^{-1}
Θ_{max}	Maximum chlorophyll to phytoplankton ratio	0.0535	mgChl mgC^{-1}
α	Initial slope of the P-I curve	0.025	molC $\mathrm{gChl}^{-1}(\mathrm{Wm}^{-2})^{-1}\mathrm{d}^{-1}$
β	Assimilation efficiency	0.75	-
μ_0	Phytoplankton growth rate at 0 °C	0.59	d^{-1}
τ	Aggregation parameter	0.02	$(\mathrm{mmolNm}^{-3})^{-1}\mathrm{d}^{-1}$

Table V: The initial values for biological variables.

Variable	Initial value	Unit
N_{NH_4}	0.1	μM
N_{NO_3}	3	μM
P	0.08	μM
Z	0.06	μM
D_L	0.02	μM
D_S	0.04	μM
C_{hl}	0.02	μg-ChlL^{-1}

The resulting chemical stoichiometry relationships were given by:

$C_{106}H_{263}O_{110}N_{16}P + 106O_2 \rightleftharpoons 91CO_2 + 15HCO_3^- + 16NH_4^+ + H_2PO_4^- + 91H_2O$

$NH_4^+ + 2O_2 \rightleftharpoons NO_3^- + 2H^+ + H_2O$

$C_{106}H_{263}O_{110}N_{16}P + 84.8HNO_3 \rightleftharpoons 106CO_2 + 42.4N_2 + 16NH_3 + H_3PO_4 + 148.4H_2O$

In the above relationships, if x is the fraction of organic matter remineralized by the anaerobic pathway, then oxygen is consumed at $106(1-x)+2\cdot 84.8\cdot x = 106+63.6x$ mol, since $84.8x$ mol NH_4^+ is oxidized to NO_3^-. *Fennel et al.* (2006) calculated that $x = 0.14$ using *Seitzinger and Giblin* (1996)'s assumption that the ratio of NH_4^+ oxidation to anaerobic respiration was 0.105.

The oxygen requirement was $106 + 63.6x \approx 115$ moles for oxidation of 1 mol of organic matter (expressed per mol N of organic matter it was 115/16). The NH_4^+ yield was $16(1 - x) + 16x - 84.8 \approx 4$ (expressed per mol of organic matter it was 4/16) during the remineralization of the organic matter.

The bottom boundary conditions for NH_4^+ and O_2 were:

$$\frac{\partial NH_4}{\partial t} = \frac{4}{16\Delta z}(w_P P|_{z=H} + w_{D_S} D_S|_{z=H} + w_{D_L} D_L|_{z=H}) \tag{3.10}$$

$$\frac{\partial O_2}{\partial t} = -\frac{115}{16\Delta z}(w_P P|_{z=H} + w_{D_S} D_S|_{z=H} + w_{D_L} D_L|_{z=H}) \tag{3.11}$$

c. Model Inputs

The model was forced by both physical and chemical inputs, including river flow, river-borne inorganic and organic nitrogen concentrations, wind velocity and direction, surface heat flux and surface freshwater flux (precipitation - evaporation). The river discharge values used were calculated from the daily reports of Mississippi and Atchafalaya River discharges made by the U.S. Army Corps of Engineers (USACE) at Tarbert Landing, MS, and Simmesport, LA, respectively (Fig. 6, `http://www.mvn.usace.army.mil/`).

River-borne nutrient concentrations are measured monthly and reported by the U.S. Geological Survey (USGS) for St. Francisville, LA, and Melville, LA (`http://toxics.usgs.gov/`). The monthly data were interpolated to provide daily values using a piecewise cubic hermite polynomial. The USGS measurements include the $NO_2^- + NO_3^-$, NH_4^+, and Total Kjeldahl Nitrogen (TKN). The organic nitrogen was calculated by subtracting NH_4^+ from TKN, and added to the model as small detritus (D_S) (*Fennel et al.*, 2011). The organic nitrogen included both the particulate and dissolved phases (PON + DON).

The Mississippi River and Atchafalaya River inputs to the model domain occurred at specific grid locations along the northern boundary (Fig. 6, red dots). Because the ocean was spatially separated from the river measurement sites, I used a 3-day offset between measured date and boundary forcing (*Corbett et al.*, 2004).

The model wind forcing was taken from the North American Regional Reanalysis

(NARR), which is a high resolution climate data set covering the shelf-wide survey period of hypoxia (1985–present) at 3-hour intervals. The temporal resolution can resolve vertical mixing related to the diurnal-inertial band weather activity (*Zhang et al.*, 2009, 2010). The spatial resolution of the dataset for the northern Gulf of Mexico region is 0.3°. Climate data were interpolated to the model grid by triangle based linear interpolation (*Watson and Philip*, 1984).

The surface heat and freshwater fluxes used the climatological fields of *da Silva et al.* (1994a,b). Tides were not included because they are small in this area (*DiMarco and Reid*, 1998).

2. Observations

Observed oxygen data were used to validate the simulated oxygen field and to develop a metric for applying the model to hypoxic area prediction. Three datasets were available at different temporal and spatial scales: a long-term time series from stationary moorings (stations C6A, C6B, C6C/CSI-6, CSI-9), a series of monthly to bimonthly cruises along two fixed cross-shore transects (C and F), and observations of chemical properties from annual shelf-wide surveys between 1985–2008. All observations were part of an ongoing program at the Louisiana Universities Marine Consortium (LUMCON). The data were retrieved from National Oceanographic Data Center (NODC, `http://www.nodc.noaa.gov/`). Note that not all measurements made during the 25-year program were publicly available (Table VI, Fig. 8).

Measurements from moorings documented the vertical structure and monthly DO concentrations at fixed sites near the Mississippi River mouth. Several moorings have been deployed in about 20 m water depth south of Terrebonne Bay since 1989. The temporal coverage from these moorings varied from year to year. Because most stations (C6A, C6B, C6C/CSI-6) were too close to each other to be resolved by

the numerical model, I considered them as one station (C6X) for model/observation comparisons (Table VI).

Two cross-shore transects have been sampled monthly or bimonthly for oxygen distributions near the discharges from the Mississippi (C) and the Atchafalaya Rivers (F). The C transect has been conducted monthly since 1990. The F transect has been conducted bimonthly since 2000. The observations were separated into summer (June, July and August) and non-summer months (the rest).

There has been an annual shelf-wide cruise to measure the extent of hypoxia during the summer, when hypoxic area is usually greatest. The measurements have been made annually in mid-July to late-July since 1985, except for 1988 and 1989. In 1988, the cruise was in mid-August (08/12-08/16). In 1989, there was no cruise. This dissertation only considered LUMCON data collected between 1985 and 2008.

Table VI: The available LUMCON data from NODC.

Year	Moorings	Transecs	Shelf-wide
1985	N/A	C Jun - Dec F Jul	Jul 15 - Jul 20 Sep 10 - Sep 12
1986	N/A	C Jan, Mar - Nov; F Jul	Jul 07 - Jul 17
1987	N/A	C/F Jul	Jul 01 - Jul 05
1990	C6 Apr - Jun, Aug - Nov C6A Mar - Jun, Aug - Nov	C Apr - Nov F Jul	Jul 23 - Jul 26
1991	C6 Feb - Jun, Aug - Oct, Dec C6A Feb - Jun C6B Feb - Dec	C Feb - Dec F Jul	Jul 16 - Jul 20
1992	C6 Mar - Jun, Aug, Sep C6B Mar - Oct	C Mar - Oct F Jul	Jul 24 - Jul 29
1993	N/A	C/F Jul	Jul 24 - Jul 30
1998	C6B Jan - Sep, Nov - Dec	C/F Jul	Jul 21 - Jul 25
1999	C6B Jan, Mar - Dec	C Jul, Aug; F Jul	Jul 23 - Jul 28
2000	N/A	C/F Jul	Jul 22 - Jul 26
2001	C6 Jan, Mar, Apr, Oct C6B Jan, Mar, Apr, Jul, Oct - Dec	C Jan, Mar, Apr, Jul, Oct - Dec F Jan, Mar, Jul, Nov, Dec	Jul 20 - Jul 25
2002	C6 Jan, Feb, May, Jun, Aug - Oct C6B Jan - Oct	C Jan - Oct F Feb, Apr, Jun - Aug, Oct	Jul 21 - Jul 26
2003	C6 Apr, Jun, Sep - Dec C6B Jan, Feb, Apr, Jun, Jul, Sep - Dec	C Jan, Feb, Apr, Jun, July, Sep - Dec F Jan, Feb, Apr, Jun, Jul, Sep - Dec	Jul 23 - Jul 28
2004	C6 Jan - Jun, Aug, Oct, Nov C6B Jan C6C Feb - Aug, Oct, Nov	C Jan - Aug, Oct, Nov F Feb, Apr, Jun, Jul, Nov	Jul 24 - Jul 25
2005	C6 Jan, Feb, Jul, Nov, Dec C6C Jan, Feb, Jul, Nov, Dec	C Jan - Dec F Feb, Jun - Aug, Oct	Jul 25 - Jul 29
2006	C6 Jan - Aug, Nov C6B Mar, Jun - Aug, Nov C6C Jan - Aug, Nov	C Jan - Aug, Nov F Feb, Apr, Jun - Aug	Jul 22 - Jul 26
2007	C6 Jan, Feb C6B Jan, Mar, May - Aug, Oct, Nov C6C Jan - Mar, May - Dec	C Jan - Mar, May - Dec F Jan, Mar, May, Jul	Jul 22 - Jul 28
2008	C6B Apr - Aug C6C Jan - Aug, Oct, Nov	C Jan - Aug, Oct, Nov F Feb, Apr, Jun, Jul, Nov	Jul 22 - Jul 27

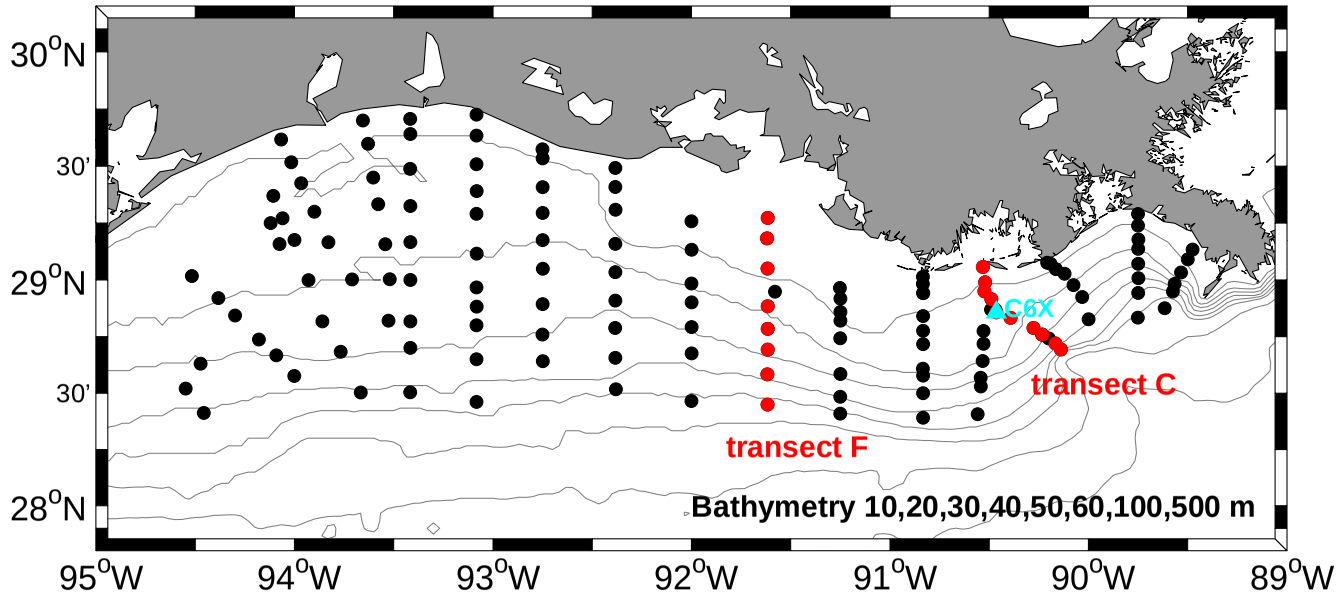

Fig. 8: The sites for sampling programs (listed in Table VI). Actual locations may vary from year to year. The fixed moorings are close to each other and shown as C6X (Blue triangle). Two transects (C and F) are shown. The stations on transect C from nearshore to offshore are C1, C3, C5, C6, C7, C8, C9, C10 and C11. The stations on transect F from nearshore to offshore are F0, F1, F2, F3, F4, F5, F6 and F7.

3. Assessing Model Skill Metrics

I used four metrics to compare model results with observations, including:

(1) the correlation coefficient (r)

$$r = \frac{\sum_{i=1}^{n}(O_i - \bar{O})(P_i - \bar{P})}{\sqrt{\sum_{i=1}^{n}(O_i - \bar{O})^2 \sum_{i=1}^{n}(P_i - \bar{P})^2}}$$

(2) the root mean square difference (RMS)

$$RMS = \sqrt{\frac{\sum_{i=1}^{n}(P_i - O_i)^2}{n}}$$

(3) the bias

$$Bias = \frac{\sum_{i=1}^{n}(P_i - O_i)}{n} = \bar{P} - \bar{O}$$

(4) the model efficiency (MEF)

$$MEF = 1 - \frac{\sum_{i=1}^{n}(P_i - O_i)^2}{\sum_{i=1}^{n}(O_i - \bar{O})^2}$$

where O_i was the observation at time t_i, P_i was the model result at t_i, $\bar{O}$ was the mean observation, and $\bar{P}$ was the mean prediction.

These metrics capture different aspects of model performance. r measures the tendency of the predicted and observed values to covary. Bias and RMS measure the sizes of the discrepancies between model result and observation. MEF measures how well a model predicts relative to the variance of the observations. A value of r near one indicates a close match between model results and observations, a value

of zero indicates that the model predicts individual observations no better than the observation average, and a value less than zero indicated that the observation average was a better predictor than the model (*Stow et al.*, 2009). These four metrics are often used together for a comprehensive skill assessment. Values of 0 for Bias and RMS and values of 1 for r and MEF indicate a perfect fit to the observations.

The model skill metrics were calculated for three different data sets for three different purposes: (1) to assess the model's ability to capture the monthly variation of DO concentration at different depths of the water column at station C6X; (2) to determine the model's ability to describe the cross-shore variability of DO concentration for transects C and F; and (3) to estimate the model's performance in reproducing the areal extent of hypoxia using the mid-summer hypoxic areas from 1985–2009.

The model outputs were processed in different ways. To compare the output with the data from the time series station C6X, the model results at the location (latitude: 28.87 °N; longitude: 90.46 °W; bottom depth: 18.23 m) closest to C6X on observation days were used. Because the topography was smoothed, the bottom depth of the model was shallower than the actual depths at C6X by 2–4 m.

For transect C and transect F, the model outputs at each observation station were processed in the same way as for the station C6X, but the data were separated into summer (collected in Jun–Aug) and non-summer (the rest) months.

For the annual shelf-wide survey, the model skills between the observed hypoxic area and the "low oxygen" areas in the model were calculated. The sampling cruises required several days to collect the oxygen measurements, but the model produced the oxygen distributions simultaneously at every time step. As a result, there was a substantial mismatch in time scales between the model and the observations. I calculated the total low oxygen area for the model results and compared the results with the observations. The calculation procedure was: (1) determine the number

of days that the oxygen concentration was less than the given level (1–5 mg/L) on each model grid point from the beginning to the end of the cruise (e.g. 16–20 July, 1991); (2) calculate the area of model regions with one or more days below a given DO concentration.

4. EOF Analysis on the 25-year Model Run

EOF analysis provides a means to identify and quantify recurring spatial patterns. I performed the EOF analysis for the 25-year simulated (1985–2009) oxygen field to study typical spatial and temporal patterns of hypoxia. Because of the rapid changes in hypoxic area, a simple analysis of area was not very useful. The frequency of hypoxia in the region with DO < 3 mg/L, designated as hypoxia* in the results at monthly time intervals provided a more statistically robust pattern than the simple DO concentration.

Before the EOF calculation, the monthly frequency had been averaged over all months (25 years $\times$ 12 month/year $= 300$ months) for that grid point and substracted, therefore, the hypoxia* frequency has a mean of 0. The frequency is a measure of the severity of the hypoxia* events. The locations where the frequency of hypoxia* was 0 had no hypoxia* during a month, locations with frequencies near 1 had persistent hypoxia*.

To explain the relationships between the EOF modes, I performed cross-correlations between the PC time series of different modes. The lags between the cross-correlations were limited to 6 months to avoid strong annual cycles of the PC time series.

To understand the mechanisms that control different EOF modes, cross-correlations was calculated between PC time series and physical and biogeochemical variables, including: (1) the combined Mississippi-Atchafalaya River flow; (2) the dissolved inorganic nitrogen (DIN $= NO_2^- + NO_3^- + NH_4^+$); (3) the DIN concentration of the

Atchafalaya River; (4) the PON + DON concentration of the Mississippi River; (5) the PON + DON concentration of the Atchafalaya River; (6) the wind strength; (7) the wind duration time at soutwest (SW) direction; (8) the wind duration time at southeast (SE) direction. The wind strength was calculated as the wind power density (G_w) (*Jamil et al.*, 1995):

$$G_w = \frac{1}{2} \times \rho \times V^3 \tag{3.12}$$

where $V = \sqrt{(u^2 + v^2)}$ is the wind speed, and ρ is the air-density. The duration of wind was calculated as the number of days that the wind came from a given direction in one month. All other variables were averaged by month.

C. Results

1. Comparisons with Long Term Observations at C6X

The model captured the vertical structure and the seasonal variation of the observed DO concentration for the time series station C6X (Fig. 9). In the observation, the surface DO concentration was high. It ranged from 162–383 μM (5.2–12.4 mg/L), and averaged 243 μM (7.8 mg/L) in the top 1 m. From 1–5 m, the surface DO concentration decreased. It ranged from 90–375 μM (2.9–12.1 mg/L), and averaged 233 μM (7.5 mg/L). The surface DO concentration had a strong seasonality. In the layer above 5 m, the average DO concentration was 263.5 $\pm$ 37.2 μM (8.5 $\pm$ 1.2 mg/L) before June, 207.7 $\pm$ 24.8 μM (6.7 $\pm$ 0.8 mg/L) from June to August, and 213.9 $\pm$ 27.9 μM (6.9 $\pm$ 0.9 mg/L) after August. As a contrast to the surface measurements, the bottom DO concentrations were low. Below the 15 m depth, the DO concentration ranged from 0.16–275 μM (0.01–8.9 mg/L), and averaged 123 μM

(3.97 mg/L). The DO concentration was further reduced near the bottom. Below 18 m, the DO concentration ranged from 0.24–261 μM (0–8.4 mg/L), and averaged 106 μM (3.4 mg/L). Consistent with the surface, the bottom DO concentration also had a strong seasonal cycle. Near the bottom (below 18 m), the average DO concentration was 141.4 $\pm$ 61.3 μM (4.56 $\pm$ 1.98 mg/L) before June, 24.7 $\pm$ 33.9 μM (0.8 $\pm$ 1.09 mg/L) from June to August, and 134 $\pm$ 66 μM (4.33 $\pm$ 2.13 mg/L) after August.

The model was consistent with the observation in that the surface DO concentration was high and bottom DO concentration was low. However, at the surface, the simulated DO concentration was lower and the seasonal cycle was weaker than in the observations. In the top 5 m, the simulated average DO concentration was 238.1 $\pm$ 9.5 μM (7.7 $\pm$ 0.3 mg/L) before June, 231.8 $\pm$ 28.7 μM (7.5 $\pm$ 0.93 mg/L) from June to August, and 214.4 $\pm$ 8.3 μM (6.9 $\pm$ 0.3 mg/L) after August. Contrary to the surface, the simulated DO concentration at the bottom was higher than the observations, but the seasonal cycle was as strong as the observations. Below 18 m depth (the last model grid), the simulated average DO concentration was 197.3 $\pm$ 31.1 μM (6.4 $\pm$ 1.0 mg/L) before June, 85.4 $\pm$ 60.8 μM (2.8 $\pm$ 1.9 mg/L) from June to August, and 186.7 $\pm$ 37.2 μM (6.0 $\pm$ 1.2 mg/L).

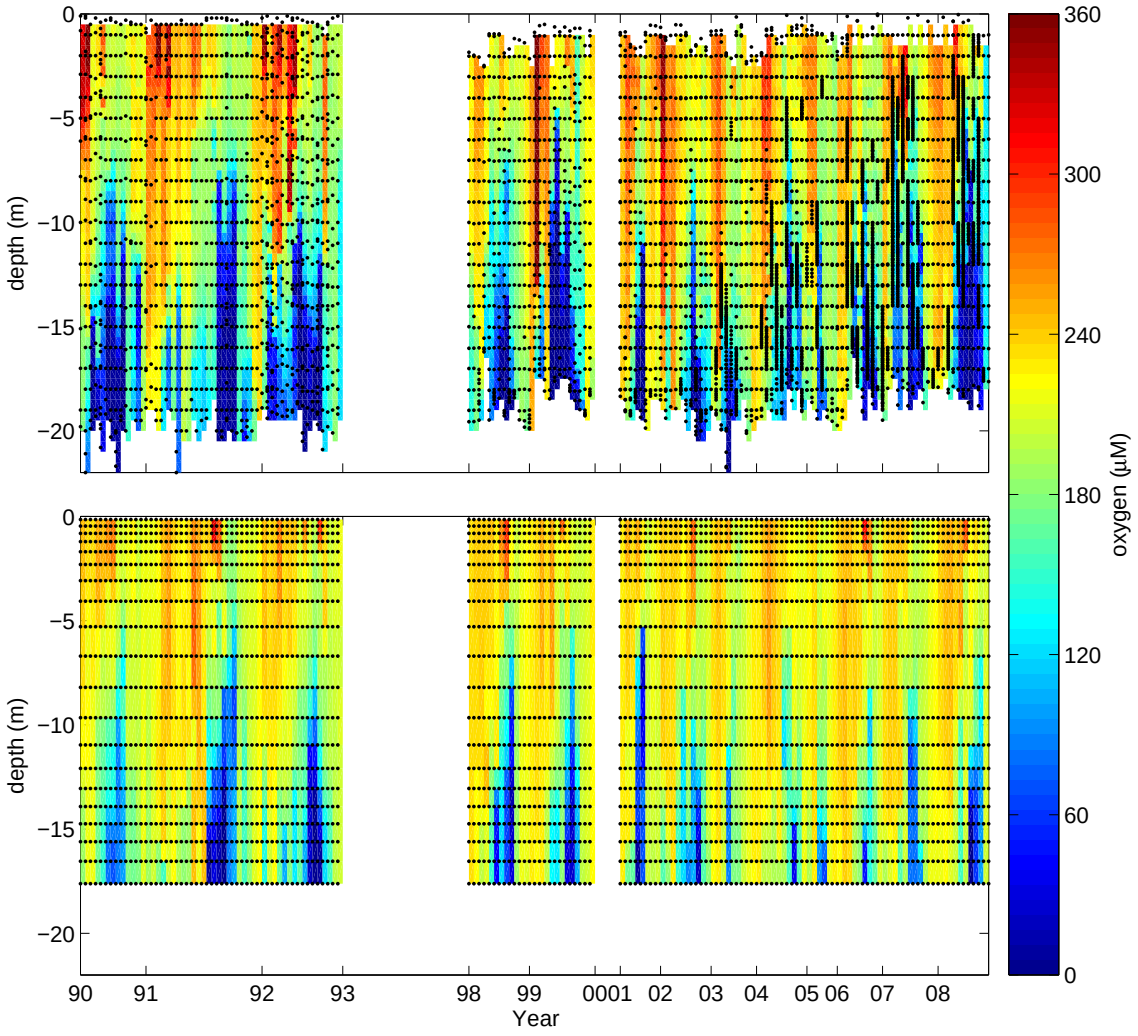

Fig. 9: The observed (above) and simulated (below) oxygen concentrations at the stationary mooring C6X. Black dots denote the sample (above) and model grid locations (below). The observational data for C6X were interpolated to depth interval of 0.5 m to make the contour diagram.

The observations were interpolated to the depths of the model grid to calculate the different skill indices (Fig. 10). Because few observations were available shallower than 0.5 m, the analysis started at around 0.8 m depth. The MEF was positive for the whole water column. It increased from 0.8 m (0.009) to 3 m (0.21), and was

approximate to 0.2 from 3 m to the bottom of the model grid. The correlation coefficient r was lowest near the surface (0.3), gradually increased to 4 m (0.56), decreased to 6.7 m (0.43) and increased again to the bottom of the model grid (0.68). The bias increased from 0.8 m to the bottom. It was negative from surface to 4 m, positive from 4 m to the bottom. The RMS decreased from 0.8 (48 μM) to 4 m (32 μM), and increased from 4 m to bottom (71 μM).

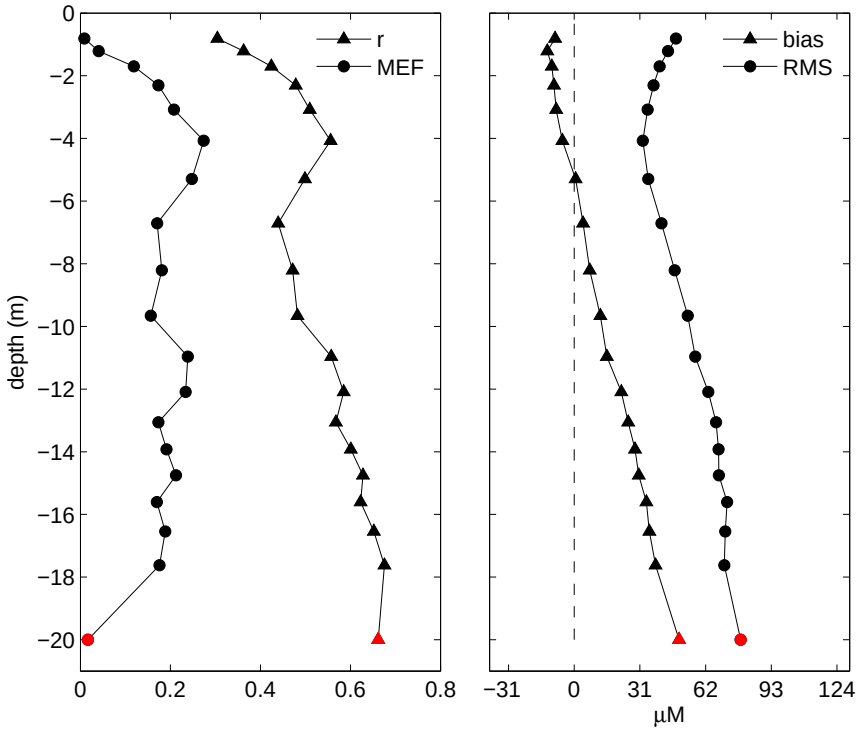

Fig. 10: The model skill metrics. Left: MEF and r; Right: bias and RMS. The model and observed DO values are compared at the same depth by interpolating observational data to model vertical grids. The red dots and triangles show the results from comparing the deepest model grids to the observations nearest the bottom.

The simulated DO concentration had its highest correlation with the observed DO ($r = 0.68$) at the bottom grid point at 18.23m. The bias (38 μM) and RMS (71

μM) were larger at the surface. The MEF was relatively small (0.18).

The deepest simulation results (18.23 m) compared with the deepest observations (20–22 m) yielded a greater bias (49 μM) and RMS (78 μM); the MEF decreased to 0.02. However, the correlation between the two remained high (r = 0.66). All the reported r values were significant at the 95% level (Red values in Fig. 10).

A point to point comparison showed where the model systematically deviated from the observations (Fig. 11). At the surface (> 5m), the observations were larger than model results before summer (January–May), smaller than the observations for summer (June–August), and fit the model results for the fall and winter (September–December). Near the bottom depth (> 15m), the observed concentrations were lower for most months. The differences were greatest during May–July.

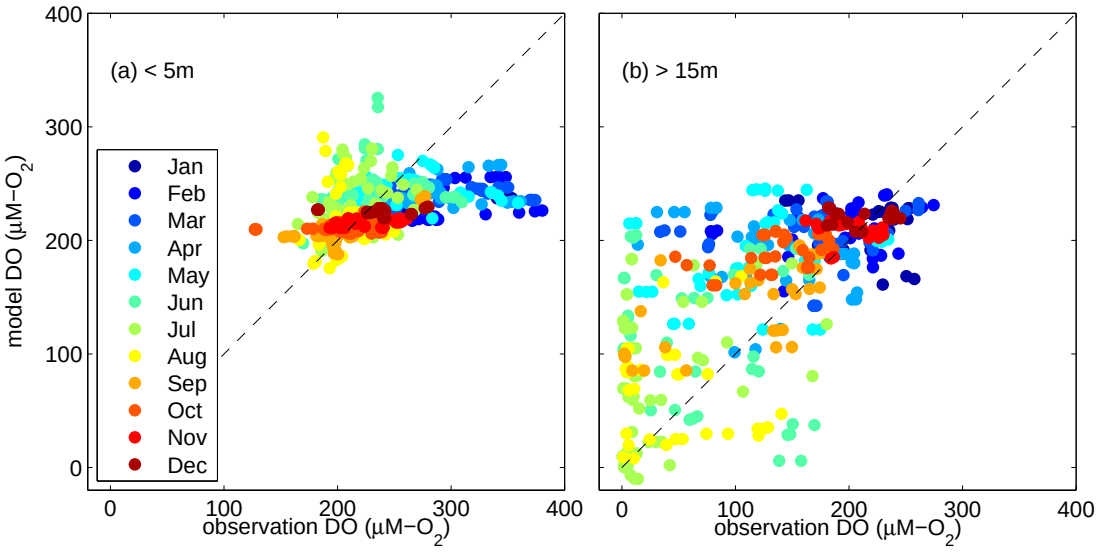

Fig. 11: Point-to-point model and observation comparisons at C6X station for surface (> 5 m, a) and bottom (< 15 m, b). The points are color coded to indicate the time of year. The dashed line indicated the 1:1 reference.

In summary, at the time series station C6X, our model reproduced the seasonal patterns of the observed DO concentration, especially at the bottom where the hypoxia was observed ($r = 0.68$). The simulated bottom DO concentration had a systematic offset with the observation (bias = 38 μM).

2. Model/Observation Comparisons for C and F Transects

In both transects C and F (Fig. 12 and Fig. 13), there were strong vertical differences in average oxygen concentrations for all stations across the shelf. The model reproduces the seasonality of those differences but has a positive bias compared with the observations.

In the observations along transect C, the oxygen concentration was high at the surface, especially during non-summer months. In the top 5 m, the averaged oxygen concentration was 240.87 $\pm$ 25.42 μM (7.77 $\pm$ 0.82 mg/L) during non-summer months, and 203.36 $\pm$ 28.21 μM (6.56 $\pm$ 0.91 mg/L) during summer months. The oxygen concentration decreased at the bottom. It was extremely low during summer months. In the bottom 5 m, the averaged oxygen concentration was 148.80 $\pm$ 60.14 μM (4.80 $\pm$ 1.94 mg/L) during non-summer months, and 82.77 $\pm$ 48.36 μM (2.67 $\pm$ 1.56 mg/L) during summer months. The oxygen concentration had a cross-shore variation during summer. It was lower in the middle of the transects (C4–C8, 20–30 m depth, average 56.42 $\pm$ 42.47 μM (1.82 $\pm$ 1.37 mg/L)), and higher for the nearshore and offshore stations (C1, C3 <15 mand C9–C11 > 30 m, average 105.09 $\pm$ 41.54 μM (3.39 $\pm$ 1.34 mg/L)).

The simulated oxygen concentration was consistent with the observation that the surface oxygen concentration was high. However, contrary to the observations, the seasonal variation of the simulated oxygen concentration was small at the surface. Above 5 m, the average oxygen concentration was 228.28 $\pm$ 2.16 μM (7.36 $\pm$ 0.07

mg/L) during non-summer months, 217.2 ± 18.85 μM (7.01 ± 0.61 mg/L) during summer months. Consistent with the observations, the simulated oxygen concentration also decreased at the bottom, and the seasonal variation became stronger. In the bottom 5 m, the average oxygen concentration was 207.23 ± 14.46 μM (6.68 ± 0.47 mg/L) during non-summer months, 127.10 ± 34.77 (4.1 ± 1.12 mg/L) during summer months. The simulated oxygen concentration also had a cross-shore variation during summer. The averaged bottom oxygen concentration was 108.2 ± 23.18 μM (mg/L) (3.49 ± 0.75 mg/L) in the mid stations of the transects (C4–C8), 143.86 ± 34.73 μM (4.64 ± 1.12 mg/L) for the nearshore and offshore stations.

The spatial and temporal variation of DO on transect F was similar to transect C. In the observations, the average DO concentration was 240 ± 23.64 μM (7.74 ± 0.76 mg/L) in the top 5 m, and 209.60 ± 28.08 μM (6.76 ± 0.91 mg/L) within the bottom 5 m during non-summer months. This contrasts with 196.02 ± 35.55 μM (6.32 ± 1.15 mg/L) in the top 5 m, and 123.82 ± 44.94 μM (3.99 ± 1.45 mg/L) within the bottom 5 m during summer months. As a comparison, in the model, the average DO concentration was 228.64 ± 7.70 μM (7.37 ± 0.25 mg/L) in the top 5 m, 225.73 ± 7.79 μM (7.28 ± 0.25 mg/L) within the bottom 5 m during non-summer months, and 198.04 ± 26.72 μM (6.39 ± 0.86 mg/L) in the top 5 m, and 181.64 ± 32.10 (5.86 ± 1.04 mg/L) within the bottom 5 m during summer months. There were a cross-shore variations in the observation during summer, but this was not seen in the model. In the observations, the average DO concentration in the bottom 5 m of F2–F3 was 93.81 ± 44 μM (3.03 ± 1.42 mg/L); of the other stations (F0, F1, and F4–F7) it was 133.82 ± 40.58 μM (4.32 ± 1.31 mg/L). In the model, the averaged DO concentration in the bottom 5 m of F2–F3 was 182.08 ± 36.63 μM (5.87 ± 1.18 mg/L); at the other stations (F0, F1, F4–F7) it was 181.50 ± 30.45 μM (5.85 ± 0.98 mg/L).

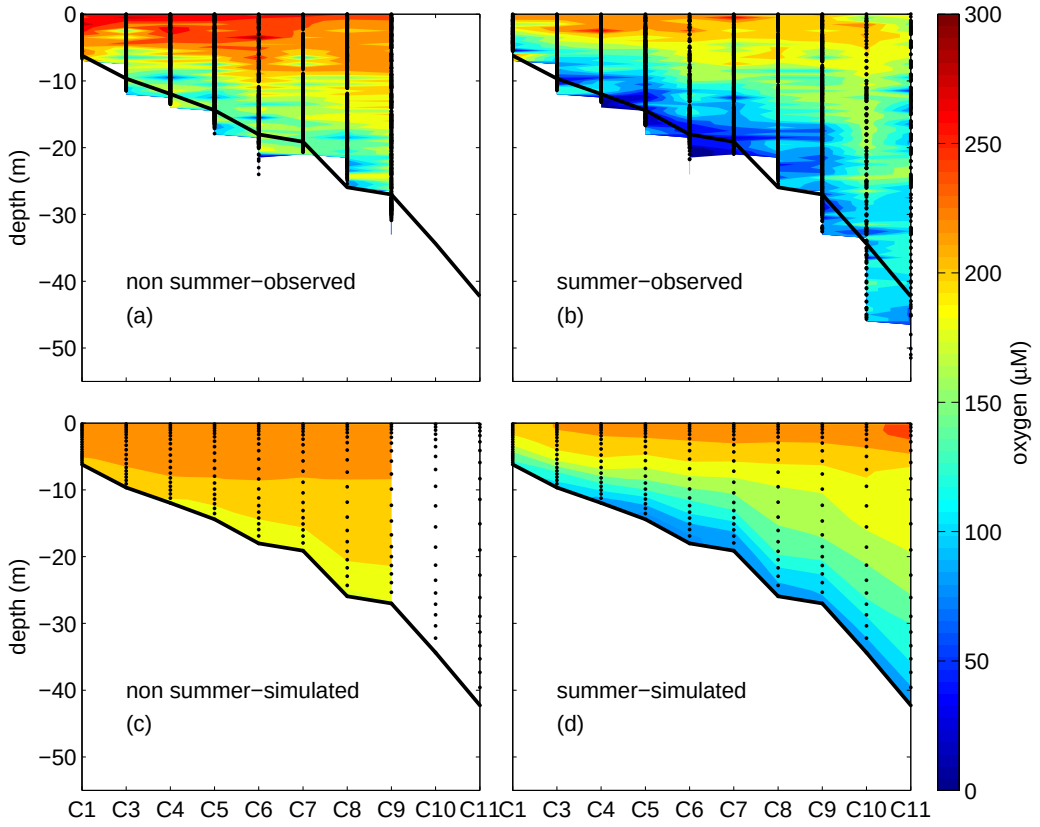

Fig. 12: The observed (a & b) and simulated (c & d) seasonal average oxygen concentrations along the C transect. The observational (above, a & b) and model depths (c & d) are indicated with black dots. The bottom topography of the model is indicated by the black line at the base of the graphs.

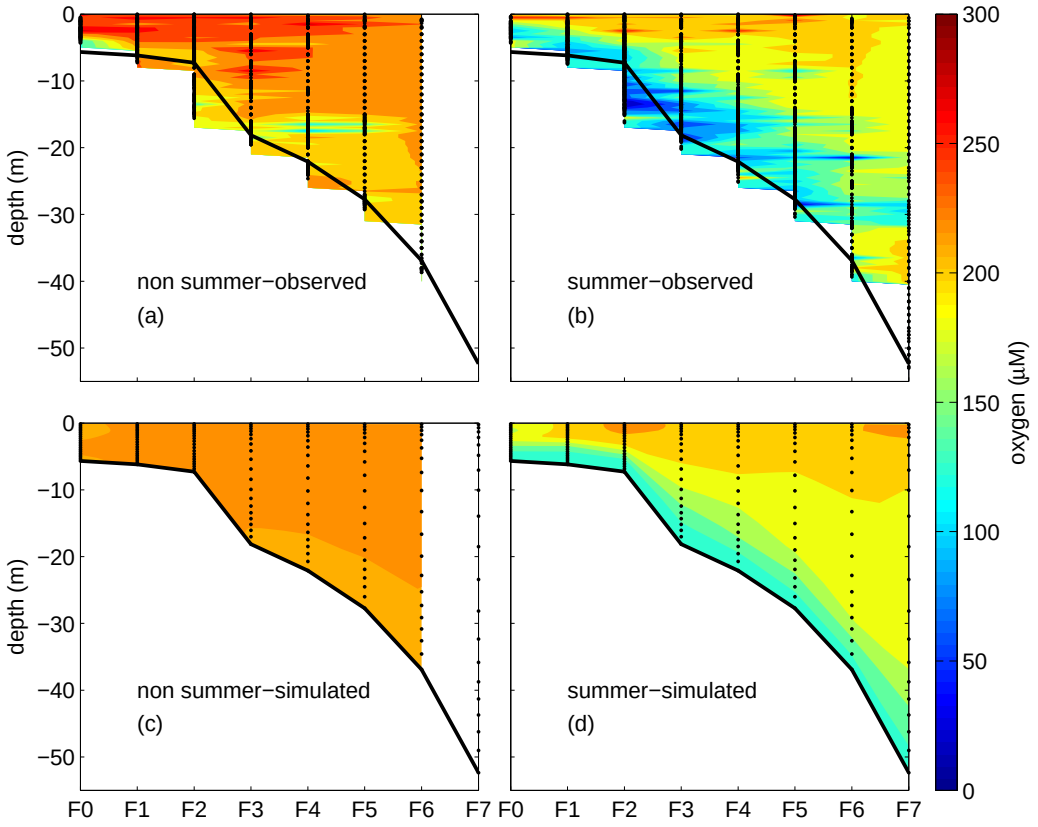

Fig. 13: The observed (a & b) and simulated (c & d) seasonal average oxygen concentrations along the F transect. The observational depths (a & b) and model grid points (c & d) are shown as black dots. The bottom topography of the model is indicated by the black line at the base of the graphs.

The model skill varied from nearshore to offshore in transect C (Fig. 14). The simulated and observed data were correlated throughout most of the water depth of C1–C5 with r between 0.3 and 0.6. The values of r increased as the depth increased. At the bottom of the water column, r was greater than 0.6 at C1–C5, and averaged at 0.68.

The model systematically deviated from the observations. At C1–C4, the model underestimated DO concentrations for the upper water column (bias = -4 μM), but overestimated DO concentrations for the lower water column (bias = 15 μM). At C5–C9, the model overestimated the DO concentrations for most of the water column (bias = 20.5 μM) except at the surface (bias = -8.9 μM). Stations C10 and C11 were different from the other stations with DO concentrations being underestimated for the bottom (bias = -9.8 μM) and overestimated for the surface (bias = 26.5 μM). The bias at those stations was small compared to the hypoxia definition that DO concentration less than 62 μM. As the bias varied greatly with depth, the RMS ranged from 28 to 89 μM, with most of the values from 60 to 80 μM.

The model efficiency was positive for most of the water column at C1–C5 (mean MEF = 0.13). It was negative for most depths at C6 (mean MEF = -0.06), and changed from positive to negative for C8 and C9, and had a larger negative value at most depths of C10–C11 (mean MEF = -4.4).

At the bottom of C1–C9, the average r was 0.64, bias was 30.7 μM, RMS was 73 μM, and MEF was 0.11. In contrast, at the bottom of C10 and C11, the model and observations were not significantly correlated, the bias was -16 μM, RMS was 55 μM, and MEF was -8.4.

The model showed a greater skill on transect F than C (Fig. 15). The averaged r and MEF were 0.43 and -0.1 at transect F, but were 0.28 and -0.8 at transect C. The averaged bias and RMS was 10 and 64 μM at transect F, but was 13 and 66 μM

at transect C. The best model skill was in the lower water column at F2–F4, where r was about 0.6–0.9; MEF was about 0.4–0.8; Bias was 15–30 μM; RMS was 40–70 μM. At the bottom depth from F1–F6, the averaged r was 0.68, bias was 18 μM, RMS was 59 μM, and MEF was 0.35.

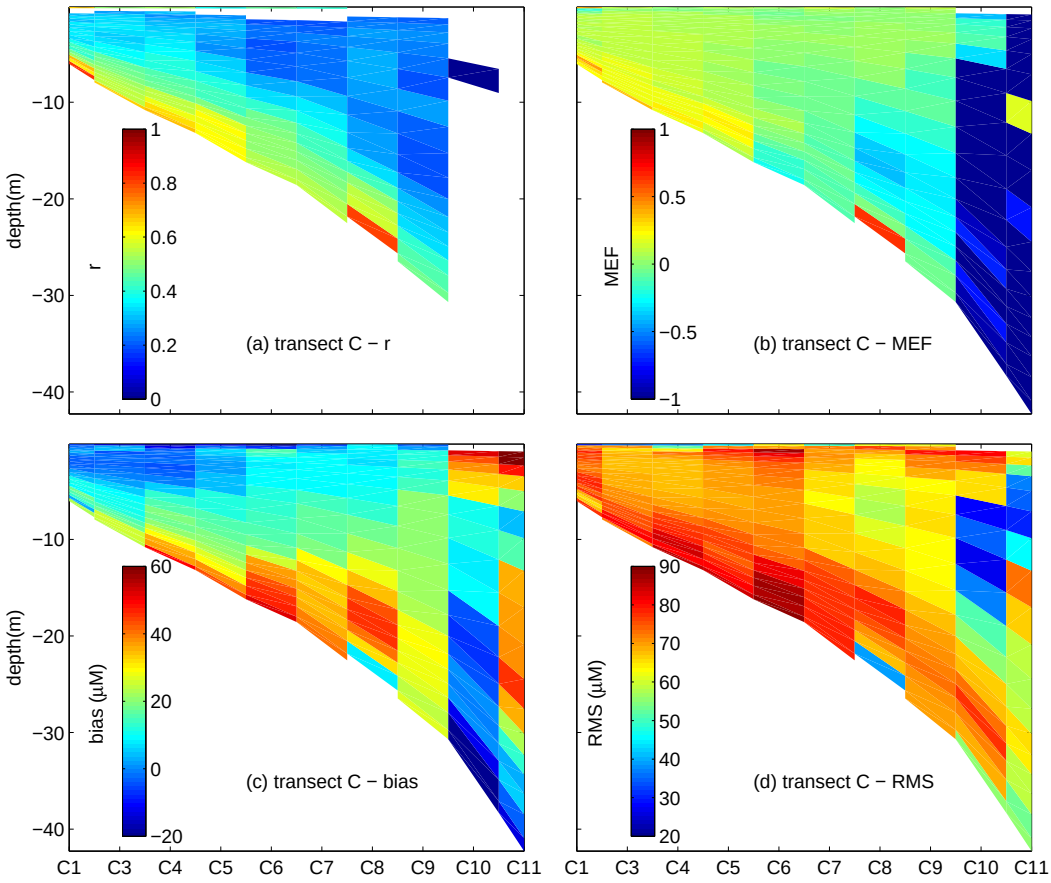

Fig. 14: The model skill metrics for transect C. Values r (a), the MEF(b), the bias (d) and the RMS(d) are shown. Only values of r statistically significant at the 95% level are shown. Non-significant values are depicted with white background.

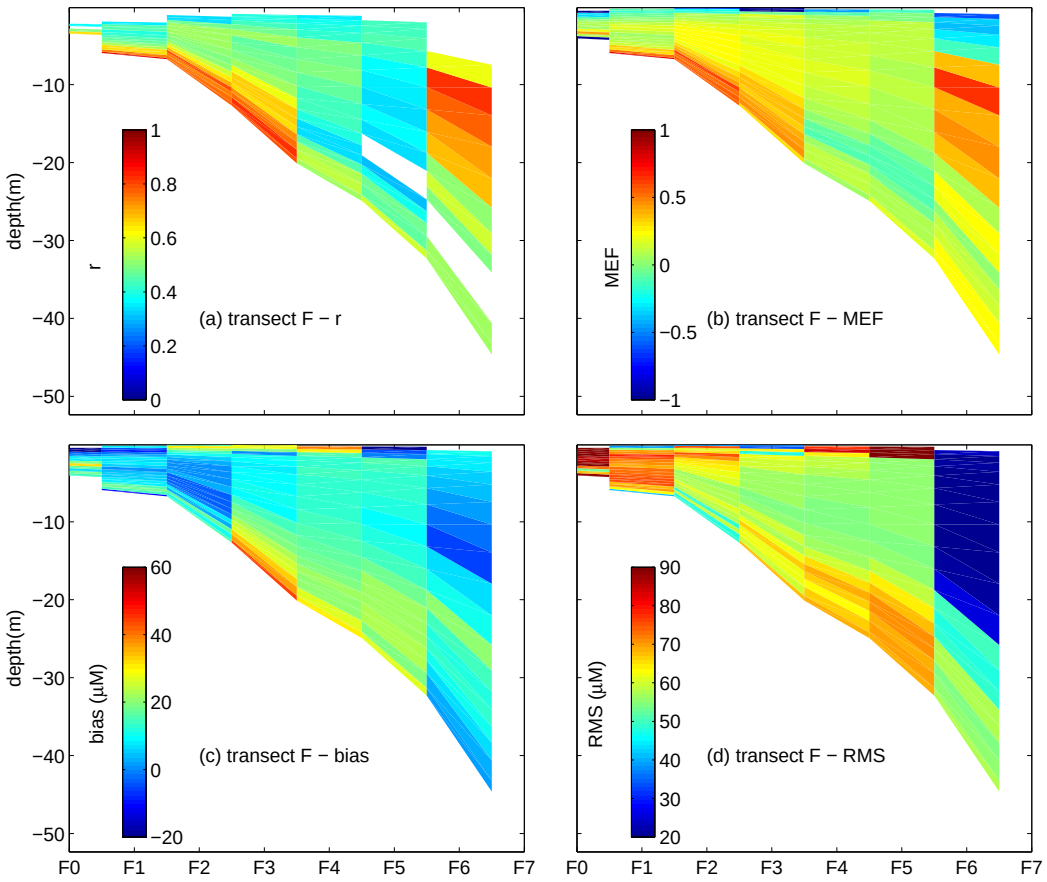

Fig. 15: The model skill metrics for transect F. Panel descriptions are the same as in Fig. 14.

3. Spatial Pattern Near the Bottom

Both the observed and simulated DO concentrations near the bottom were low on the Louisiana shelf (Fig. 16). The low oxygen zone started at the Mississippi River Bird's Foot Delta and extended westward to 93°W. The observed oxygen concentrations were again lower than those of the simulation, except in the Louisiana Bight, where the average observed DO concentration was 23 μM greater than simulated values. The low oxygen zone had a small break between the Mississippi and Atchafalaya River discharge. In the observations, the break was at 91.5°W, in 10–30 m, while in the

model, the break was at 90.8°W, 0–20 m. West of 93°W, there was a relatively low oxygen zone in 20–40 m depth and relatively high oxygen zone at shallower depth.

The model and observations had many similarities, however, important differences remain. The mean observed oxygen concentration was high south of Atchafalaya Bay in water shallower than 10 m, but model values were extremely low there. The low oxygen zone extended further west in the observations than in the model. Because the oxygen concentration has a positive bias at the bottom of C6X (38 μM), transect C (31 μM) and transect F (18 μM), I took DO concentration less than 93 μM as the low oxygen zone in the observation, less than 124 μM as the low oxygen zone in the model. The low oxygen regions extended to the Sabine Lake in the observations, but were limited to the region east of Calcasieu Lake (93°W) in the model. In the cross-shelf direction, the observed low oxygen zone was limited to the near bottom regions deeper than 30 m in the observations, but was over 60 m in the model.

I calculated the areas covered by regions less than a certain DO concentration for a range of concentrations using the model results for 1991. The area studied was limited to locations with bottom depths between 7–100 m and west of the Mississippi River Bird's-Foot Delta. The LUMCON shelf-wide survey region was within these bounds. The total areas showed strong seasonal variations for all concentrations (Fig. 17). The change in total area could be quite dramatic, particularly in summer. All low oxygen areas were small during spring and winter (Jan 01–Apr 01; Oct 01–Dec 31), large during summer and fall (Apr 01–Oct 01); and even larger during late summer (Jul 15–Aug 15). There were two abrupt decreases during spring and summer of 1991. One was just before June 15, the other was just before July 15. These decreases were associated with intense storm activity. The LUMCON cruise was July 16–July 20 (dashlines), immediately after the second storm. The simulations indicated that the hypoxic area extended further west at the end of the cruise (Fig. 18). Although the

Table VII: The integrated low oxygen areas during the 1991 cruise time (July 16 - July 20). The oxygen level increases from 1 to 5 mg/L by every 1 mg/L to calculate the area.

Oxygen level	1 mg/L	2 mg/L	3 mg/L	4 mg/L	5 mg/L
Area	3,600 km^2	6,900 km^2	11,800 km^2	24,400 km^2	44,400 km^2

low oxygen areas increased in these five days, the areal extent on July 20 was still less than on July 16. The total areas containing DO at concentrations less than 1, 2, 3, 4 and 5 mg/l are shown in Table VII. The observed low oxygen area (11,920 km^2) was close to the total low oxygen area using 3 mg/L as the DO upper level in the model (11,800 km^2). The addition of 1 mg/L (= 31 μM) to the standard hypoxia definition (DO $<$ 2 mg/L (62 μM)) was consistent with the fact that the simulated bottom oxygen concentration was higher than the observation by 20 – 40 μM.

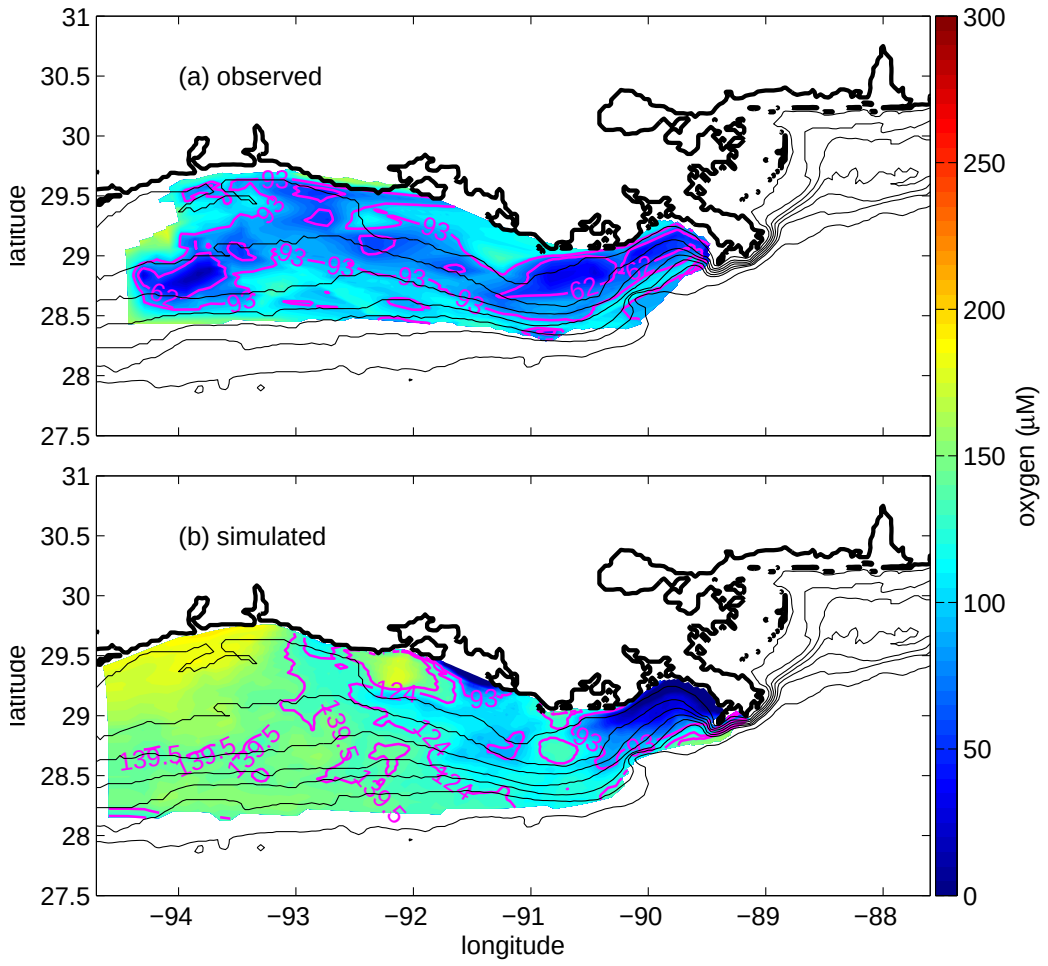

Fig. 16: The average DO concentration near the bottom for observations (a) and model (b). For the model data, we averaged the bottom DO concentration during the shelf-wide survey time in each year, and then averaged all the 25 years (1985 - 2009). For the observations, we interpolated the observational data in each year to the model grid, and then averaged all the 25 years (Table VI, Fig. 8). The contours are 10, 20, 30, 40, 50, 60 and 100 m isobaths.

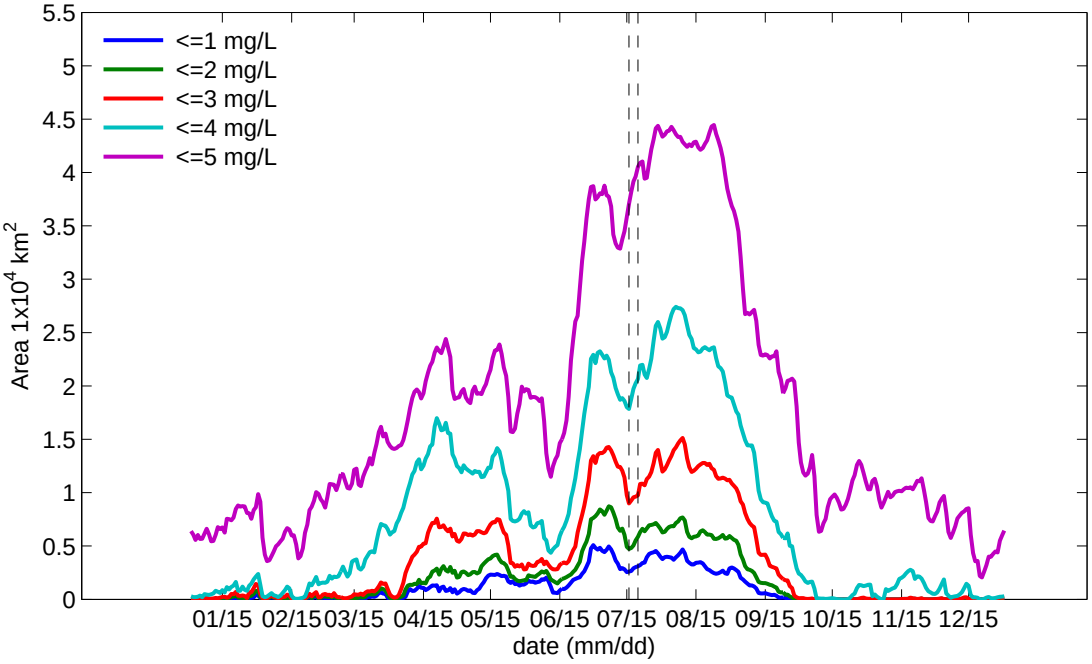

Fig. 17: The model simulated low oxygen areas in 1991. The model output has a result every 1 day. The upper limit of the oxygen concentration increases from 1 mg/L (31 μM) to 5 mg/L (155 μM). Dashed lines show the observation time for this year (July 16 - July 20).

A similar calculation using the 25-year time series (1985–2009) showed large interannual variations (Fig. 19). The hypoxic area calculated from observations for DO less than 2 mg/L was within the range of values for the simulation, and similar to that for 3 mg/L in all simulations apart from 2005. The similarity in the two calculations can be understood in the context of the model bias for bottom DO concentrations of about 30 μM, about 1 mg/L.

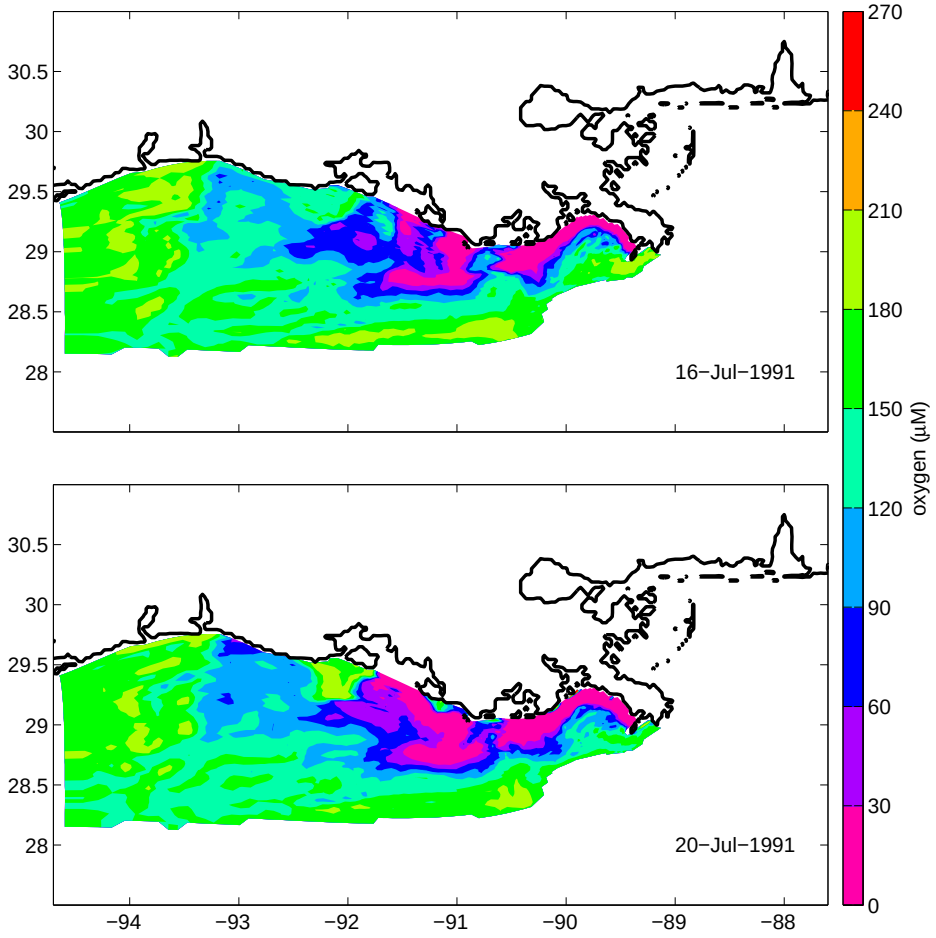

Fig. 18: The simulated bottom oxygen concentration at the beginning (July 16) and end of the cruise (July 20) in 1991. The region for which the DO concentration is less than 3 mg/L (93 μM) on July 20 is not as large as that of July 16.

I defined the condition that DO concentrations were less than 3 mg/L as hypoxia* to distinguish from the traditional definition (< 2 mg/L). Using 3 mg/L as the DO upper level to calculate the simulated hypoxic area and compare with the observed hypoxic area was consistent with that used in simulations in *Scavia et al.* (2003).

The model skill metrics between the observed hypoxic region and simulated low oxygen areas showed that all the r values were significant at the 95% level (Table VIII). The maximum r was between observed hypoxic area and the calculated hypoxic* area ($r = 0.71$). The only positive model efficiency was for hypoxia* (0.31), because bias and RMS were relatively small.

It was noteworthy that the match between the simulated and observed hypoxic areas had a "jump" (Fig. 19). Before 1991, the observations were close to using 2 mg/L as the upper level of DO concentration for area calculation. After that, they were close to hypoxia*. If we consider this "jump" in skill assessment by using 2 mg/L as upper level before 1991, and hypoxia* from 1991, the model skill metrics improve considerably ($r = 0.87$; MEF = 0.72; Bias = -207km^2; RMS = 3,010 km^2; Table VIII).

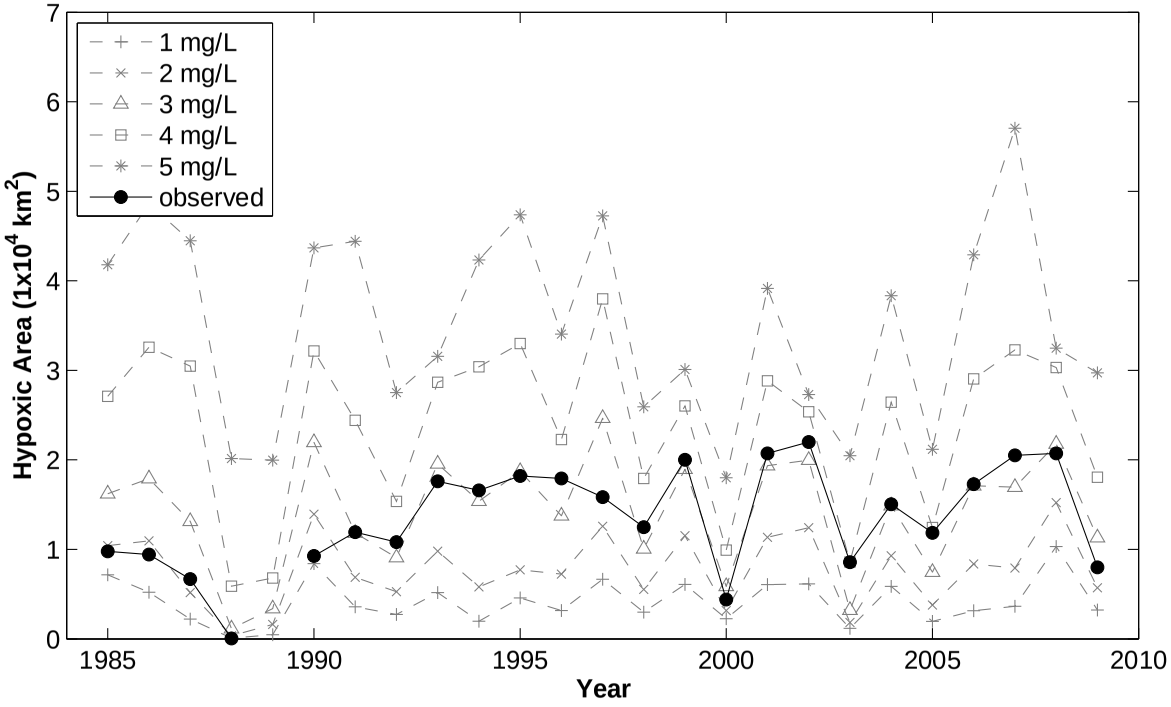

Fig. 19: The observed hypoxic area and simulated total low oxygen areas from 1985 - 2009. The low oxygen areas were calculated using different DO concentration as the upper limit. The total low oxygen areas are the integrated areas during the cruise time. The observed area was calculated for the region with DO less than 2 mg/L.

Table VIII: The model skill metrics between the observed hypoxic area and model simulated low oxygen areas for years 1985–2009. The oxygen upper level increases from 1 mg/L to 5 mg/L to calculate the low oxygen areas. "jump" means using 2 mg/L as the upper level for calculation before 1991; 3 mg/L as the upper level from 1991.

	1 mg/L	2 mg/L	3 mg/L	4 mg/L	5 mg/L	"jump"
r	0.50	0.63	0.71	0.59	0.35	0.87
MEF	-2.36	-0.55	0.35	-4.03	-16.9	0.72
RMS (km^2)	10,500	7,110	4,600	12,800	24,200	3,010
Bias (km^2)	-9,240	-5,560	1,020	10,800	22,100	-207

The overall low oxygen areas in the model captured most of the hypoxia spots in the observation (Fig. 20). For the model results, I used 2 mg/L as the upper level of DO for the area calculation in the model before the year 1991, and hypoxia* from the year 1991. For those years that the hypoxic area was distributed discontinuously on Louisiana shelf (including the year 1985, 1986, 1987, 1990, 1992, 2003 and 2005), the simulated low oxygen area did not overlap the observed hypoxia. The simulation and the observations both show patchiness and small spatial variability. In contrast, for those years that the hypoxic area was distributed continuously on the east and west shelves (including the year 1991, 1993, 1999, 2001, 2002, 2004, 2006, 2007 and 2008), the model-simulated low oxygen areas was also mostly continuous.

4. EOF Analysis for the 25-year Model Simulations

The averaged annual monthly hypoxia* frequency showed that hypoxia* occurred in the areas < 100 m deep east of the Sabine Lake with a monthly frequency $\geq 1\%$ (Fig. 21). Hypoxia* was more frequent ($\geq 10\%$) for bottom depths between 10–60 m east of Atchafalaya Bay. In the Louisiana Bight, the hypoxia* frequency was greater

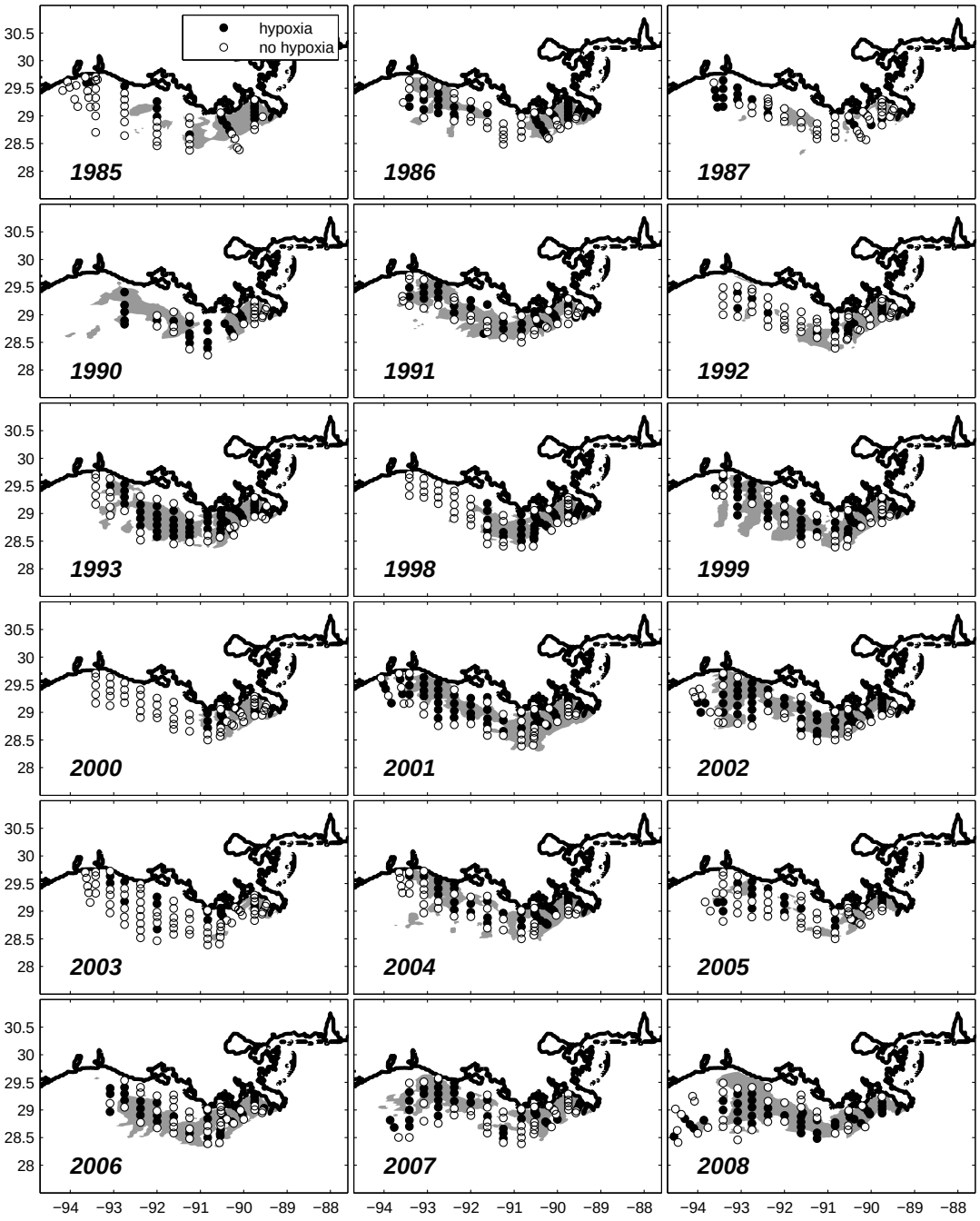

Fig. 20: The simulated low oxygen area (gray, shadow) and the observational stations. Black dots for hypoxic locations; white dots for non-hypoxic locations. For the simulations, a value of 2 mg/L was used for calculating low oxygen area from 1985–1990, and 3 mg/L was used from 1991–2008.

than 20%. It was highest ($\geq$ 50%) near the mouth of the Mississippi and Atchafalaya Rivers.

An EOF analysis of hypoxia* frequency after removal of the mean on a monthly time interval over the 25-year simulation period highlighted the spatial and temporal natural variability of hypoxia (Fig. 21, Fig. 22 and Fig. 23). The first three modes explained 62%, 8.1%, and 4.9% of the spatial variance (Fig. 22). A spectral analysis of the PC time series associated with the EOFs (not shown) indicated that the first three modes had strong seasonal cycles. The seasonality is shown in the monthly averages of the PC values (Fig. 24).

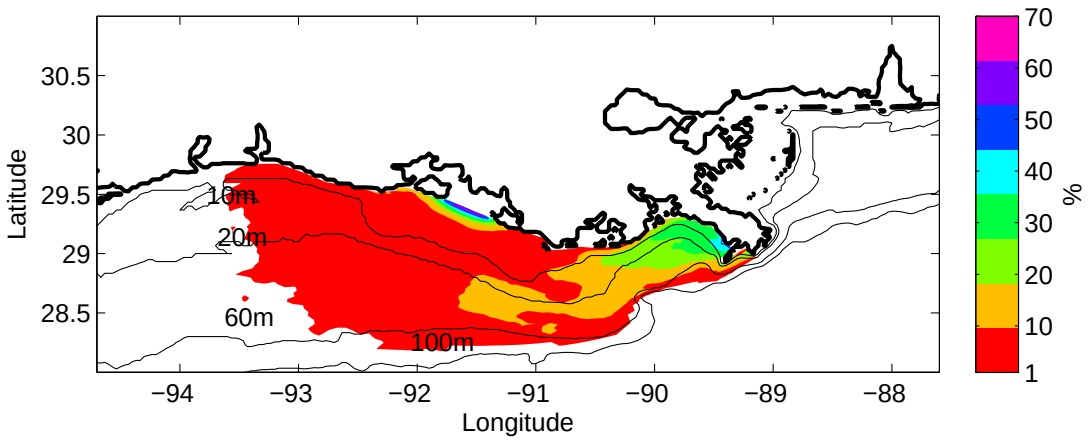

Fig. 21: The mean of the monthly hypoxia* frequency. The monthly frequency of hypoxia* was calculated at each model grid by counting the number of days that the DO concentration was less than 3 mg/L. The model simulation was for 300 months 1985–2009.

The spatial pattern of the first EOF mode describes east-west variation (Fig. 22). West of Calcasieu Lake (about 93°W), the hypoxia* signal vanished. It increased gradually eastward to the Mississippi River Bird's-Foot Delta. The annual cycle

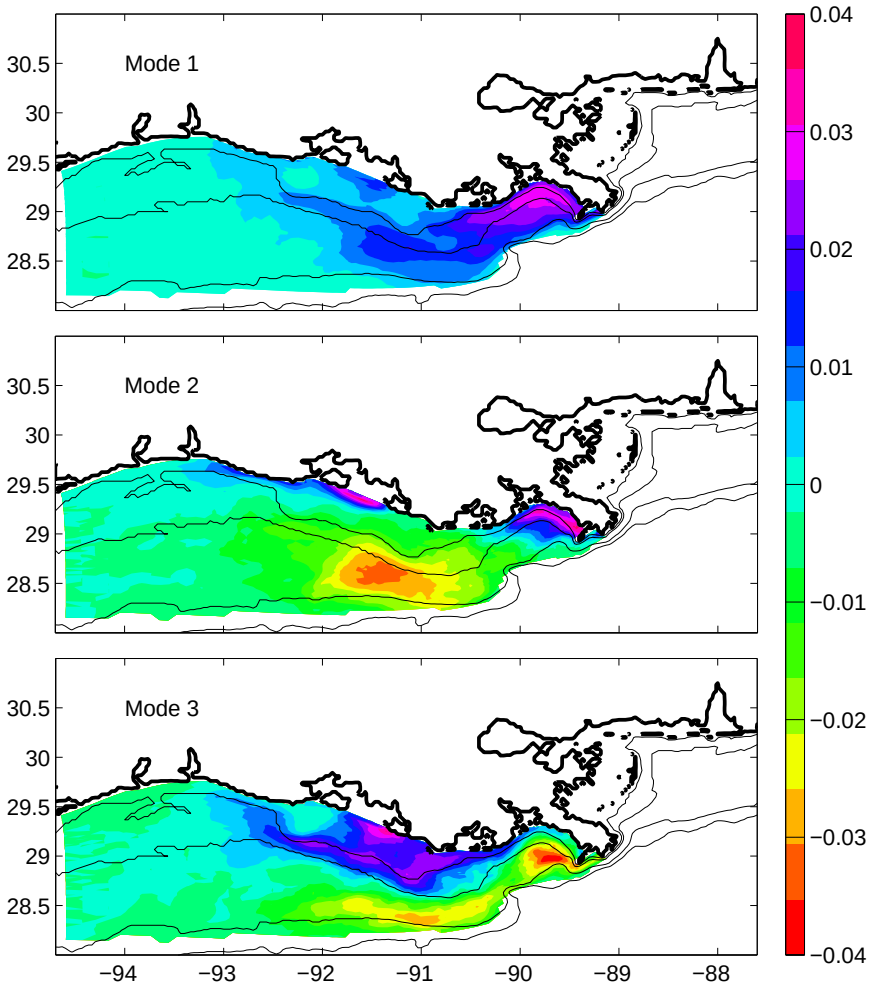

Fig. 22: The spatial pattens of the first-three EOF modes. The first-three modes explain 62%, 8.1%, and 4.9% of the variance. Contours are 10, 20, 60, 100m isobath.

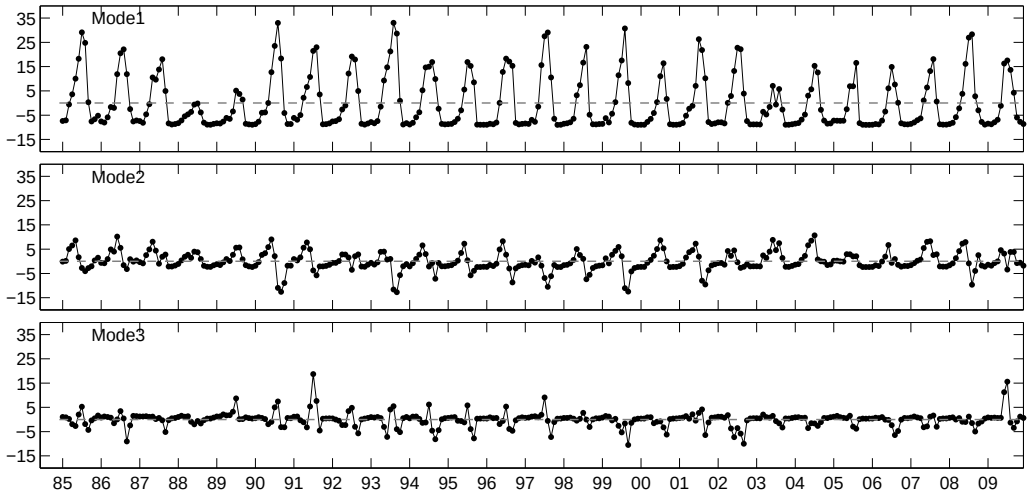

Fig. 23: PC time series of the first three EOF modes.

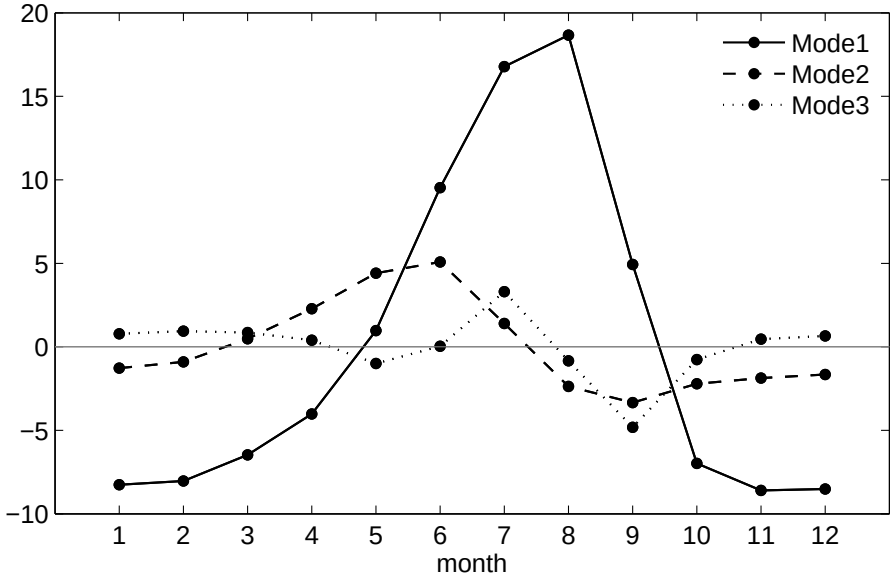

Fig. 24: The annual cycle of the PC time series for the first three EOF modes. Each data set was calculated by averaging the 25-year data in Fig. 23.

shows that its contribution was positive from late spring to early fall (May–Sep, Fig. 24), and peaked in mid-summer (July–August). Thus, hypoxia* intensified during May–September, and is largest in July–August.

The spatial structure of the second and third EOF modes had strong onshore-crossshore pattern. The pattern reversed signs near the 20 m isobath. For the second EOF mode, the strong hypoxia* regions were the Mississippi and Atchafalaya River plumes which were separated from each other. The PC time series of the two most impacted regions had a strong hypoxia* signal from March–July. August through November this mode increases oxygen values offshore.

5. The Cross-correlation Between EOF Modes and Physical and Biogeochemical Variables

Most of the significant correlation coefficients were between Mode 1 and Mode 2 (Fig. 25). The correlation coefficient r was as high as -0.73 and -0.59 when the PC time series of Mode 1 was lagged with the wind power density (G_w) by 0 and 1 months. The r value was as high as 0.62 when Mode 1 and the duration of southwest (SW) wind compared at 0 lag. Mode 1 was also highly correlated with the combined Mississippi–Atchafalaya River flow at a lag of 2 for Mode 1 ($r = 0.52$), 3 ($r = 0.66$), and 4 ($r = 0.62$) months. Mode 1 was also correlated with the Mississippi River DIN concentration when lagged by 1 ($r = 0.54$), 2 ($r = 0.66$) and 3 ($r = 0.58$) months, and with the Atchafalaya River DIN at lags of 0 (r= 0.50), 1 (r= 0.65), and 2 (r= 0.56) months.

The correlation of Mode 2 with environmental measures was not as strong as for Mode 1. Mode 2 was statistical significantly correlated with the duration of southeast (SE) wind at lags of 0 ($r = 0.28$) and 1 ($r = 0.41$) months, the combined Mississippi–Atchafalaya River flow at lags of 0 ($r = 0.42$), 1 ($r = 0.39$) and 2 ($r = 0.26$) months,

the Mississippi River DIN concentration at lags of 0 ($r = 0.37$) and 1 ($r = 0.28$) months, and the Atchafalaya River DIN concentration for no lag ($r = 0.25$).

D. Discussion

1. Mechanisms Controlling Hypoxia

The EOF analysis demonstrated a region with persistent hypoxia* conditions in the Louisiana Bight. This persistence could be caused by the recirculation structure associated with the Mississippi River plume (*Ichiye*, 1960). Most transport of the Mississippi River water is to the west on the Louisiana shelf and is driven by the easterly wind and by the Coriolis force after the water exits the river mouth. However, a small amount returns to the Mississippi River Bird's Foot delta, forming an eddy in the Louisiana Bight, which retains nutrients and organic matter in the region, and supports high primary production and subsequent organic matter sinking there. The organic matter consumes a large amount of oxygen and increases the intensity of hypoxia.

Observations have shown that the duration of hypoxia in the Gulf of Mexico can be nearly continuous from mid-May to mid-September, with maximum spatial extent in late July (*Rabalais et al.*, 2001). The model results presented here are consistent with these observations. The PC time series of Mode 1 increased from May to September, and peaked in July and August. The seasonality of hypoxia is related to the seasonal variation of the wind strength. The wind is weak during summer (May–September, minimum in July and August), and strong during the other seasons (Oct–Apr). The strong wind causes strong vertical mixing and ventilates bottom waters. As a result, there is little hypoxia in non-summer months. As summer starts and wind decreases, vertical mixing decreases, which slows reoxygenation of low-oxygen bottom

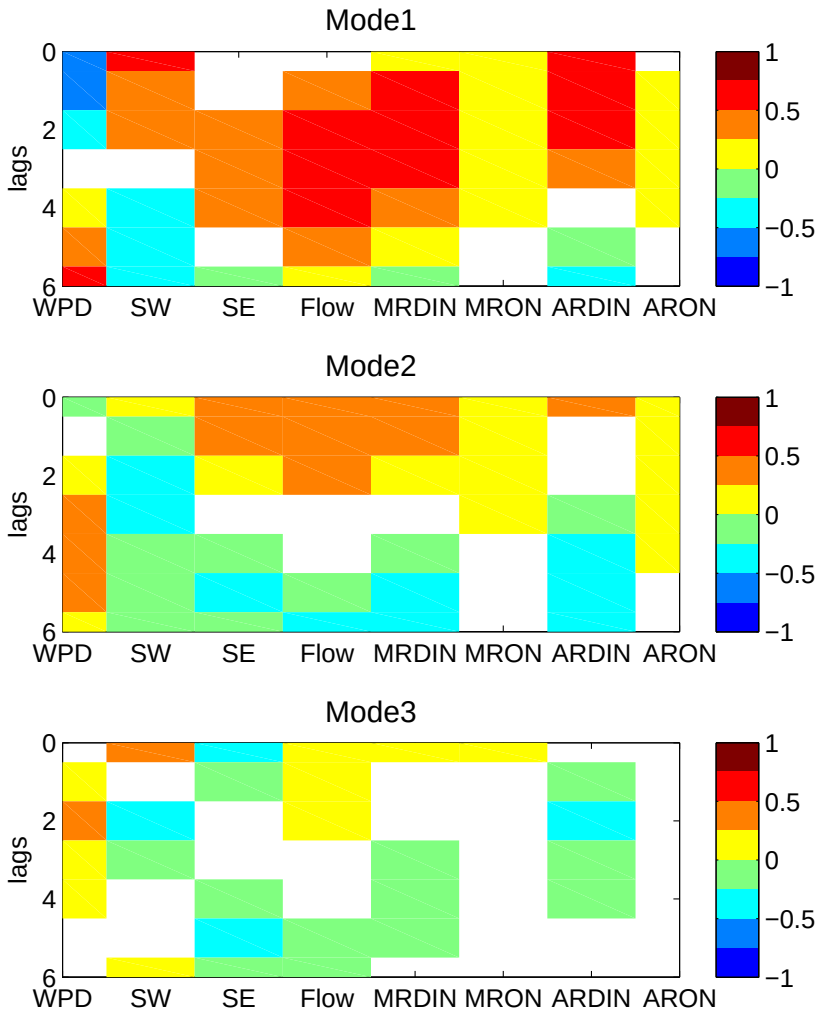

Fig. 25: The cross-correlation between PC time series of modes and eight physical and biogeochemical variables. Included are: (1) the combined Mississippi-Atchafalaya River flow (Flow) (2) the DIN concentration of the Mississippi River (MRDIN) (3) the DIN concentration of the Atchafalaya River (ARDIN) (4) the PON+DON concentration of the Mississippi River (MRON) (5) the PON+DON concentration of the Atchafalaya River (ARON) (6) the wind power density (G_w) (7) the southwest wind duration time (SW) (8) the wind southeast duration time (SE). Negative lags are removed from the results because they have no physical meaning. All the r values here are statistically significant ($p < 0.05$).

water. As a result, the wind regime facilitates the development of the hypoxic area. The relationship between the wind strength and hypoxia intensity is documented by the cross-correlation between the PC time series of Mode 1 and wind power density. The high correlation (r = -0.73) at 0 lag indicates the instant response of the oxygen concentration to the wind-induced high mixing. Negative r is consistent with the fact that the strong wind increases the oxygen concentration and reduces the hypoxia intensity.

The cross-correlations between the PC time series document the development of hypoxia in space and time. In late spring to early summer (May–June), hypoxia is predominantly confined to the nearshore region (< 10 m). There are two distinct regions beneath the Mississippi and Atchafalya River plumes. By mid to late summer (July–August), the two hypoxic regions move offshore and merge into one large region, located on the mid–east Louisiana shelf in water shallower than 60 m depth.

The spatial variation of hypoxia is caused by the movement of the river plume steered by the wind. In the northern Gulf of Mexico, the wind direction has a seasonal component. It is upwelling favorable (from the west) during summer months, downwelling favorable (from the east) during the rest of the year (*Cochrane and Kelly*, 1986; *Cho et al.*, 1998; *Nowlin et al.*, 2005). The switch in predominant wind direction usually occurs in early to mid July.

With the upwelling-favorable summer wind, hypoxia develops more easily on the mid–east Louisiana shelf because two conditions are met at the same time. First, nutrients and freshwater are transported offshore, supporting high primary production and resulting in the accumulation of a large amount of oxygen-consuming material on the mid–east Louisiana shelf. Second, the freshwater moves offshore at the surface and seawater moves on-shore near the bottom, intensifying density stratification and preventing high-oxygen surface water mixing with the lower-oxygen bottom water in

the region. In contrast, downwelling favorable winds (May and June) trap freshwater in a nearshore band and drive relatively high vertical mixing. As a result, downwelling favorable winds inhibit the development of hypoxia.

In the model, organic matter is deposited rapidly nearshore in water shallower than 10 m and consumes all the oxygen, forming a low oxygen band next to shore. In reality, the decomposition of the organic matter takes time (see next section). The influence of the wind direction is shown by the correlation between the PC time series and the duration of wind. The PC time series of Mode 1 (high hypoxia* frequency on mid-east Louisiana shelf above 60 m) was correlated with the duration of SW wind (upwelling favorable). The PC time series of Mode 2 (high hypoxia* frequency nearshore) was correlated with the duration of SE wind (downwelling favorable).

Previous studies found a strong relationship between the hypoxic area and the nitrogen loading of the Mississippi–Atchafalaya River. *Justic et al.* (2002)'s model simulated the dissolved oxygen concentration at station C6X using the nitrate loading of the Mississippi River during the current and previous months. *Scavia et al.* (2003)'s simple biophysical model calculated the hypoxic area using May–June Mississippi–Atchafalaya River nutrient loading as the model forcing. *Turner et al.* (2006)'s regression model forecast the mid-July hypoxic area using the May Mississippi River nitrate loading as the predictor. *Greene et al.* (2009)'s multi-linear regression model used nitrogen and phosphate concentration and river discharge as their predictors of hypoxia. The discharge in May, nitrate concentration in May, and the phosphate concentration in February explained the greatest percentage ($\geq 60\%$) of the area variability. All of these studies indicated that the river discharge, nitrate concentration, or their combined effect (nitrate loading, which equals to the discharge times the concentration) is best correlated with the July hypoxic area at 0 to 2-month lag. In this study, the PC time series of Mode 1 was highly correlated with the combined

Mississippi-Atchafalaya River flow at 2-month lag ($r = 0.52$), with the Mississippi River DIN concentration at 1- ($r = 0.54$) or 2-month ($r = 0.66$) lag, and with the Atchafalaya River DIN concentration at 1- ($r = 0.65$) or 2-month ($r = 0.56$) lag, which were consistent with the previous model results. The 0–2 month lag between the nitrogen flux and hypoxia events is caused by the time needed for nutrient transport, nutrient conversion to organic matter, and the sinking and benthic remineralization of the organic matter.

It was noteworthy that the correlation between the PC time series of Mode 1 and inorganic nutrient concentration (DIN of Mississippi and Atchafalaya River) was stronger than the correlation with organic nutrient (DON + PON of Mississippi and Atchafalaya River). The greater importance of DIN implies that the intensity of hypoxia at the mid-east Louisiana shelf is mainly determined by the inorganic type of nutrients. It is primary production that stimulated the inorganic nutrient and the resulting in organic matter sinking that provides the oxygen-consuming material on the mid-east Louisiana shelf. The organic type of nutrients from the river is deposited rapidly near the river-mouth, and consumes the bottom oxygen inshore.

2. Model Assessment

a. Assessing the Model's Ability to Predict DO Concentrations

Four skill metrics have been used to measure the model's ability to reproduce the observed dissolved oxygen field. The model captures the vertical structure and seasonal variations of DO concentrations. Generally speaking, the model is better for transect F than transect C, for nearshore stations than offshore ones, and perform better in deeper water than in shallower (i. e., nearer the bottom). Although the model captures the variability of DO concentrations, the bottom DO concentration

overestimates the observation by 38 μM at station C6X, 31 μM along transect C, 18 μM along transect F, and 23 μM for the shelf-wide survey. In contrast, the DO concentration at the surface is underestimated by the model in pre-summer months (Jan–May).

The internal settings of the model have an impact on model performance. The importance of these settings can be summarized into four factors: (1) conversion of organic matter to oxygen consumption; (2) organic matter transport; (3) strength of the pycnocline; (4) model grid limitations. I next discuss each of these individually.

First, the model assumes that the organic matter is consumed immediately upon reaching the bottom. Measurements have shown that the organic matter consumption can take up to four-months (*McKee et al.*, 2004; *Dagg et al.*, 2004). In reality, a large amount of organic matter reaching the bottom during the spring is not fully decomposed until summer. The instantaneous-consumption assumption has two effects on the model results: (1) bottom DO is consumed during spring. Because of rapid vertical mixing at this time, the low bottom DO concentration can not be maintained but exchanges with the surface. As a result, the surface DO concentration in the model is reduced in the spring. (2) Because the organic matter was consumed in spring, less was left to be consumed during the summer. As a result, oxygen consumption near the bottom was too low and DO concentrations too high in the model.

Second, the model describes the fate of organic matter from the river too simply. About 36% of nitrogen entering the model domain is organic nitrogen. Most of it deposits near the river mouths, resulting in a high frequency of hypoxia* (70%) there. However, in the real world, after the organic matter deposits, it is transported as fluid mud and undergoes numerous cycles of resuspension-deposition (*McKee et al.*, 2004; *Dagg et al.*, 2004; *Geyer et al.*, 2004; *Bianchi et al.*, 2010). The near-bottom movement of organic matter supplies additional oxygen-consuming material that adds

to that from primary production. Not including this movement in the model results in insufficient DO consumption in the offshore region.

Third, the strength of density stratification during summer is underestimated by the model. The observed bottom temperature during July is about 4°C less than at the surface (Fig. 26e). However, the simulated temperature is almost uniform vertically. Although the strength of the pycnocline on the shelf is mainly determined by the vertical salinity gradient on the Louisiana shelf, the vertical temperature gradient also plays an important role (*Belabbassi*, 2006). Underestimating the strength of the thermocline reduces the intensity of the stratification and causes the bottom DO concentration to increase. In addition, the high temperature in the model may also influence the oxygen solubility, which decreases the oxygen concentration at the bottom.

Wiseman et al. (1997) suggested that a stronger pycnocline and associated reduced mixing was an important factor for reducing the near-bottom DO concentration. A weak secondary pycnocline can be distinct or merge with the primary pycnocline in June. *Wiseman et al.* suggested that the secondary pycnocline might result from interactions between the strength and phasing of mixing, summer heating, and the return flow of low salinity waters from the Texas shelf. Such double-pycnocline structure (or the one-merged strong pycnocline) is not well captured by the model.

Fourth, the model grid setting affects the bottom oxygen concentration. Two reasons are (1) the topography of the model has been smoothed, making the water depth in the model shallower than the actual depth by about 1–4 m and increasing the mixing of surface oxygen downward. (2) the thickness of the bottom-most model grid element is greater than the distance above bottom for the deepest measurements by as much as 0.5–3 m for offshore stations. The finite difference approximation to the vertical gradient could then be smaller than that close to the bottom.

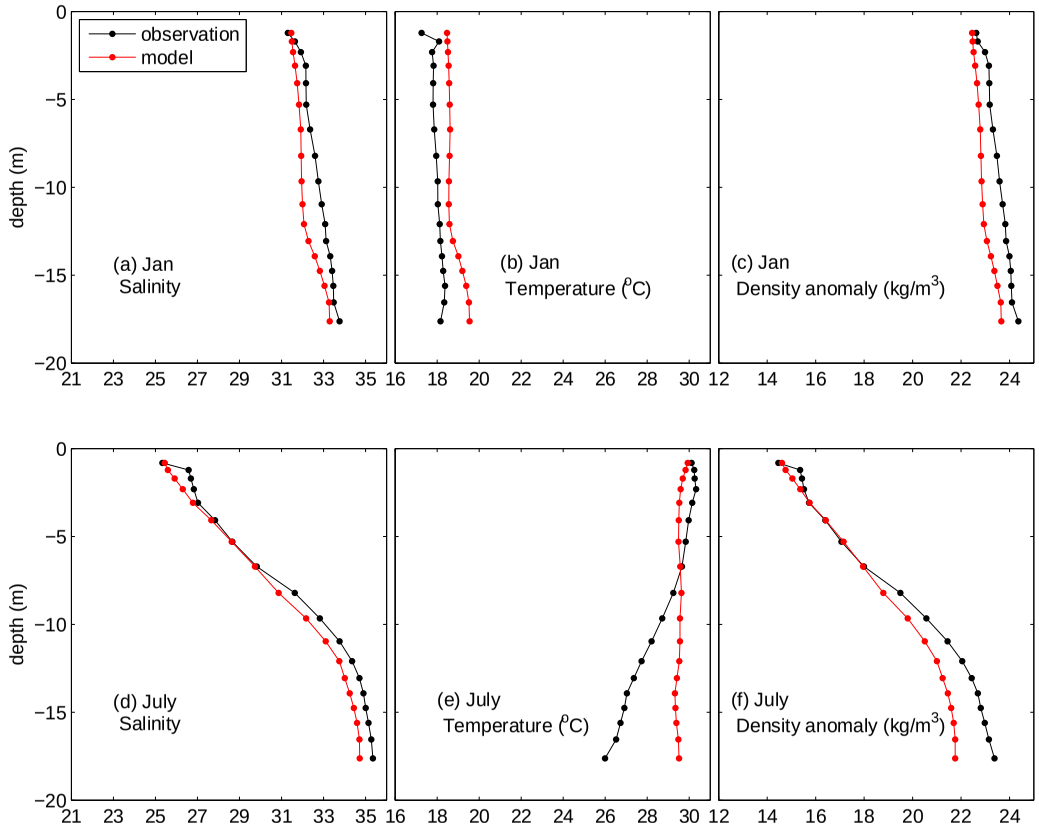

Fig. 26: The multiple year averaged temperature, salinity and density profile in Jan and July at C6X station. The data used for calculation is in Table VI. (a) salinity in January; (b) temperature in January; (c) density anomaly in January; (d) salinity in July; (e) temperature in July; (f) density anomaly in July.

b. Hindcasting the Observed Hypoxic Area from the Coupled Model

Although the model over-estimated the bottom DO concentrations, it captured the seasonal and annual variability of the bottom DO. As a result, the model can be used for hypoxic area hindcasting by adjusting the upper level of DO concentration as has been done with hypoxia*. The bias between model and observation is 20–30 μM for three different types of data, or about 1 mg/L (31 μM). Adding this 1 mg/L offset to the commonly used 2 mg/L as the bound for hypoxia allows the calculation of a simulated hypoxic area that is close to the observation. *Scavia et al.* (2003) also used 3 mg/L as the DO upper level to calculate the hypoxic area in the model. They explained that this was because they simulated the mean subpycnocline oxygen concentration instead of that at the bottom.

After 1991, the observed hypoxic area fits the model hypoxia*. However, before 1991, the observed area fits the model results for standard hypoxia value of 2 mg/L. The switch between values of DO that allow the model to fit the observation is consistent with the existence of a hypoxic area "shift", postulated by *Turner et al.* (2008). They found that the same May nitrogen loading in 1999–2004 interval calculated using a regression analysis yielded a hypoxic zone about twice as large than that calculated for in 1981–1988 interval. *Greene et al.* (2009) made an extensive regression analysis of the data and proposed that the hypoxic area increased abruptly by about 6,500 km^2 in the early 1990s. This area "shift" has been included in the improved version of the *Scavia et al.* (2003)'s model (*Liu et al.*, 2010). The mechanism proposed by *Turner et al.* (2008) for the area "shift" was that the "left-over" organic material from the previous years increased the oxygen demand. As a result, the hypoxic area was large even with a small amount of nitrogen loading. However, the method used for estimating the hypoxic area may create artifacts and be responsible for the

"shift" (DiMarco's personal communication). The improvement and application of our current model to the hypoxic area problem require a better understanding of the existence and cause of the "area shift". If the shift is real, one way to improve the model is to include an organic matter storage term (see section 3). Otherwise, the hypoxia* definition should be used for these simulations.

3. Conclusions

The ROMS model has previously been shown to be good at reproducing the seasonal variation of physical properties, such as the temperature, salinity, and current velocity (*Hetland and DiMarco et al.* 2011). It can also reproduce changes in biological properties, such as surface NO_3 concentration, chlorophyll, phytoplankton and zooplankton, primary production, phytoplankton growth rate, and zooplankton grazing rate (*Fennel et al.*, 2011). This study here is the first comparison of the oxygen field from the enhanced model with the observations.

By using four skill metrics, the model captured the vertical structure and seasonal variation of the observed DO concentration. At station C6X, the simulated DO concentration was correlated with the observations at $r = 0.68$, but overestimated the DO concentration by 38 μM. Along transect C and transect F, the model had a better skill for stations nearshore than offshore, and for deeper water depths. On the bottom of transect C, the average r was 0.64, and the bias was 31 μM. On the bottom of transect F, the average r was 0.68, and the bias was 18 μM. For the annual shelf-wide survey, the bias of the bottom DO concentration was 23 μM.

I defined hypoxia* in the model as a DO concentration less than 3 mg/L. On an annual basis, the model simulated hypoxic* area was close to the observed hypoxic area, with $r = 0.71$, RMS = 4,600 km^2, bias = 1,020 km^2 and MEF = 0.35. The simulated hypoxic area had a "jump": the observed hypoxic area was close that

calculated using 2 mg/L as the upper level of DO before 1991, but 3 mg/L after 1991. If the "jump" was considered in the comparison, the model skills improved ($r = 0.87$, MEF = 0.72, RMS = 3,010 km^2, bias = -207 km^2). The existence of the "jump" in the observed hypoxic area may result from the storage of carbon from the previous years, or from human errors in interpolation or measurements.

The EOF analysis of the model simulated hypoxia* frequency on a monthly time interval from 1985–2009 explained 62%, 8.1% and 4.9% of the spatial variability in the first three modes. The PC time series had strong seasonal cycles. The PC time series of Mode 1 showed two high-frequency hypoxia* regions nearshore related to the Mississippi and the Atchafalaya Rivers in May–June. Mode 1 was highly correlated with the duration of southwest wind, the combine Mississippi-Atchafalya River flow, the Mississippi River DIN concentration and the Atchafalaya River DIN concentration. The PC time series of Mode 1 showed one highly-frequent hypoxia* region stretching from the Mississippi River Bird's-Foot Delta to Calcasieu Lake in July–August. It was highly correlated with the wind power density, the duration of southwest wind, the combined Mississippi-Atchafalaya River flow, the Mississippi River DIN concentration, and the Atchafalaya River DIN concentration.

The coupled model that was used in this study is better than the other hypoxia models as it includes a full hydrological model, giving it a unique advantage for investigating the role of physical processes on hypoxia area variability. The coupled model describes the water column processes well. However, hypoxia is also affected by many processes that occur in the benthic boundary layer (*Rowe*, 2001; *McKee et al.*, 2004; *Dagg and Breed*, 2003). The model could be improved further by coupling it to a sediment model describing the organic matter transport as well as a diagenetic model describing the complex biogeochemical processes in the benthic boundary layer. However, such a big model requires more computer time to run and it is hard to

test the sensitivities. In addition, model tuning is a time-consuming work and the uncertainty of the model is very difficult to quantify. Such a big model may be less applicable than the simple ROMS model for the purpose of predicting hypoxic area and studying hypoxia mechanisms. It is worth mentioning that constraining the surface boundary condition of dissolved oxygen to saturation in this model has important implications and ramifications for the total oxygen and carbon budget. In nature, high primary production rates may lead to supersaturation of oxygen in the surface layers, a situation not allowable in the present model. Future versions of this model must consider relaxing or modifying the surface boundary condition for oxygen concentration.

CHAPTER IV

SCENARIO STUDY OF THE RELATIVE ROLE OF WIND AND RIVER DISCHARGE ON HYPOXIC AREA USING A COUPLED PHYSICAL-BIOGEOCHEMICAL MODEL

A. Introduction

Hypoxia is the term used to describe oxygen concentrations in aquatic environments low enough to have deleterious effects on aquatic environments. Hypoxic conditions can cause suffocation and aberrant behavior of benthic fauna, as well as reduce the fishery production. As a result, hypoxia has received extensive scientific study and management interest (*Caddy*, 1993; *Diaz and Rosenberg*, 1995; *Diaz*, 2001; *Diaz and Rosenberg*, 2008; *Bianchi et al.*, 2010). The interest is especially great for the Gulf of Mexico, where the Mississippi River delivers a large amount of freshwater and nutrients to the Louisiana shelf. The freshwater it introduces caps Gulf of Mexico seawater, causing increased density stratification and inhibiting oxygen exchange between the near bottom water and the atmosphere. The nutrients it provides stimulate phytoplankton growth, producing more carbon which is decomposed by bacteria consuming oxygen at the bottom. These two effects cause a large and sustained hypoxic area every summer. The hypoxic area averaged over 16,000 km^2 from 1993 – 2009. The hypoxic region is the largest in North America and the second largest in the world (the first largest is the Black Sea, about 70,000 km^2) (*Goolsby et al.*, 2001; *Rabalais et al.*, 1999, 2001, 2002b; *Stow et al.*, 2005; *Dale et al.*, 2010).

There has been a great interest in studying the relative roles of anthropogenic activity and natural climate variability on controlling hypoxia in the Gulf of Mexico. Analysis of benthic foraminifera and of biologically-bound silica in diatom remains

from sediment cores have shown that the intensification of seasonal hypoxia on the Louisiana shelf since the 1950s is associated principally with the wide-spread use of nitrogen-contained fertilizer. However, high freshwater discharge related to natural climate variability also caused sporadic low oxygen conditions before 1910 (*Nelsen et al.*, 1994; *Turner and Rabalais*, 1994; *SenGupta et al.*, 1996; *Osterman*, 2003; *Osterman et al.*, 2005, 2009).

Understanding the influence of natural factors on the extent of hypoxic area is of great management interest (*U.S. Enviromental Protection Agency*, 1998, 2004, 2007; *Mississippi River/Gulf of Mexico Watershed Nutrient Task Force*, 2001, 2008). While anthropogenic nitrogen inputs to the river can be controlled by changing agricultural practices, natural factors, including the variability of river discharge and the wind field are greatly affected by climate changes.

Previous models have explored how the hypoxic area is influenced by the variability of river discharge associated with climate change (*Justic et al.*, 2003a,b, 2005; *Greene et al.*, 2009; *Donner and Scavia*, 2007). These models separated the total nutrient loading (concentration multiplied by river discharge) into a nutrient component (mainly $NO_2^- + NO_3^-$, but also phosphate) and a river discharge component, studying how their variability affects the sensitivity of the resulting dissolved oxygen concentrations or hypoxic area to changes in them. However, separating the roles of river discharge and nutrient concentration is extremely difficult. The river discharge, which determines the intensity of stratification, also affects the strength of the geostrophic currents and, thus, the transport of the nutrients and dissolved oxygen. Such changes in currents are not predicted by these models. Thus, their predictions are incomplete.

Regional wind variability is another natural factor that can strongly affect the hypoxic area. The wind field in the Gulf of Mexico varies seasonally. Winds are weak and upwelling-favorable during summer, strong and downwelling-favorable dur-

ing other seasons. Alternation of wind direction changes the circulation pattern and strength of stratification of the Louisiana shelf (*Cochrane and Kelly*, 1986; *Cho et al.*, 1998; *Nowlin et al.*, 2005). *Wiseman et al.* (1997) suggested it could be an important influence on hypoxic area. The influence of wind direction on hypoxia has been studied in other regions (*Wilson et al.*, 2008; *Scully*, 2010b), but no such study has been done in the Gulf of Mexico previously.

The Mississippi–Atchafalaya drainage system has changed over the centuries. By the 1950s, the Atchafalaya River carried about 30% of the Mississippi River flow as a result of managed diversions (*Fisk*, 1952). *Krug* (2007) argued that the increase of the shelf hypoxic area was a consequence of wetland loss during the river-switching, but he did not consider changes in nutrient and freshwater movement on the Louisiana shelf as a result of the flow diversion changes. Changes resulting from the river diversion not only change the amount of organic matter delivered to the shelf, but also change where hypoxia occurs on the shelf. If the river flow to the Atchafalaya River were increased, would the hypoxic region move to the west of the Louisiana shelf as a result of more freshwater there? How far offshore and along the west Louisiana shelf would the hypoxic region extend in this case? Such changes can be predicted by a three-dimensional model. *Hetland and DiMarco* (2008) showed the relative influence of the Mississippi and Atchafalaya River plumes in controlling the hypoxia, but made no projections about effects if the relative flow through the Atchafalaya River were to be reduced or increased.

Besides an interest in the variability of coastal circulation structure induced by climate change, there is also great interest in understanding the role of other sources of nitrogen on hypoxia, especially the transport of organic material to the shelf by fluid and mobile muds (*Aller*, 1998; *Bianchi and Allison*, 2009; *Bianchi et al.*, 2009). Inorganic nutrients and organic materials go through different biogeochemical processes.

Distinguishing the role of the organic matter from that of the inorganic nutrients is important for better understanding the mechanisms that control the hypoxia. Incorporating organic matter as well as the inorganic nutrient in numerical models can improve their predictions.

The *Mississippi River/Gulf of Mexico Watershed Nutrient Task Force* (2001) established the goal of reducing the size of the hypoxic area to a five-year running mean of 5000 km^2 by 2015. It proposed voluntary actions to reduce nitrogen loads to the Gulf of Mexico by 30%. However, simple numerical models suggested that the role of physical processes needed to be considered as well, and that doing so resulted in a need for an additional 10%–40% nitrogen reduction to meet the goal (*Scavia et al.*, 2003; *Scavia and Donnelly*, 2007; *Donner and Scavia*, 2007; *Liu et al.*, 2010). Although simple models have served as useful tools to adjust the amount of nitrogen reduction required to meet the action plan, hypoxia is such a complex issue that more sophisticated models, with the ability to separate different forcing of the system, including wind, freshwater flow, and nutrients loading are needed for an accurate estimation of the amount of nitrogen reduction needed to meet the 5000 km^2 goal. Such models would provide a better understanding of the mechanisms that control the hypoxia.

The purpose of this study is to use a sophisticated coupled numerical model to study the sensitivity of the hypoxic area to physical and biological forcing. The model is the three-dimensional, coupled physical-biogeochemical model introduced in the previous chapter. Here, I explore seven scenarios, six with the same total nitrogen loading to the Louisiana shelf but with different river input conditions or wind forcing. The altered factors include wind patterns, total freshwater discharge, nitrogen components, and changes in the division of flow between Mississippi and Atchafalaya Rivers. In addition, I tested a seventh scenario with the same freshwater

discharge but half of the total nitrogen loading used previously to investigate the response of the hypoxic area to nitrogen concentration reduction.

B. Methods

The seven scenarios are labeled A through G (Table IX). The first scenario is the base case (A). All the other cases were compared to it to study the impact of upwelling favorable (i.e., west) wind duration (B), river discharge (C), reduced nitrogen concentration (D), river diversions (E, F), and components of nitrogen input (G). All simulations were forced by otherwise unaltered observed wind and river data. All seven experiments had the same initial distributions of biomass, oxygen and physical conditions. The initial conditions were set using the physical and biological fields on 25 May 2009 from the continuous 25-year (1985–2009) simulations. Each case ran for a 100 d period (25 May–01 Sep) that was chosen to include a typical summer season (June, July, August). The model, the wind and river forcing data, and the 25-year model results were all introduced in the previous chapter.

The seven scenarios are separated into four groups for discussion. The first group (A and B) was designed to test the effect of upwelling favorable wind duration. I used the 2002 and 2009 wind fields as the model forcings for several reasons. First, the wind fields during the summer of 2002 (2 m/s, -34° to the north) and 2009 (2.3 m/s, 22° to the north) were comparable in magnitude, but differed in mean direction by about 90° (Fig. 27). The wind direction in 2009 provided longer duration of upwelling favorable winds (03 June–06 August) than in 2002 (12 July–02 August, Fig. 28). Second, the observed hypoxic areas during 2002 (22,000 km^2) and 2009 (8,000 km^2) were considerably different. Lastly, the May–June river discharges and total nitrogen loadings in both 2002 (162 km^3, 3.8×10^5 metric ton) and 2009 (207 km^3, 3.5×10^5

metric ton) were high (Fig. 29). Their similarity implies that it was not the changes in nutrient inputs, but the duration of upwelling favorable wind, that was responsible for any differences in hypoxic area. Since the sensitivity of the hypoxic area to the duration of upwelling favorable wind was the experiment at focus, the same 2009 river discharge was used for both of scenario A and scenario B.

The second group of scenarios (A, C and D) was designed to test the sensitivity of the hypoxic area to total nitrogen loading, freshwater discharge and nitrogen concentration. Scenario C had the same amount of total nitrogen loading as scenario A, but with the river discharge increased by 50% and the DIN and PON concentrations decreased to 2/3 of the base case. Scenario D had the same amount of river discharge as scenario A. However, the total nitrogen loading was reduced to one half of the original by reducing the DIN and PON concentration to one half of the original.

The third group of scenarios (A, E and F) was designed to study the influence of a hypothetical diversion of freshwater on the hypoxic area. The three cases had the same amount of freshwater discharge and total nitrogen loading, but the Mississippi River had different fractions of the total river flow. In scenario E, the Mississippi River had all the river flow. In scenario A, the Mississippi River had 67% of the river flow and the Atchafalaya River had 33%. In scenario F, the Mississippi River had 33% of the river flow and the Atchafalaya River had 67%. The concentrations remained the same.

The fourth group of scenarios (A and G) was designed to study how nitrogen components influence the hypoxic area. Here, all of the nitrogen was added as DIN in scenario G, rather than 65% in DIN and 35% in PON in scenario A.

In the following analysis, I compared the time series of hypoxic* areas and hypoxia* frequency for the seven scenarios. I have mentioned in the previous chapter that the results from the numerical model used to calculate hypoxic* area were defined

as dissolved oxygen less than or equal to 3 mg/L. The hypoxic* area was calculated for the region with bottom depth 7 – 60 m, west of the Mississippi River Bird's Foot Delta. The hypoxia* frequency was calculated for two periods: (a) the early summer period, 01 June – 30 June, (b) the late summer period, 14 July – 12 August. The two periods I selected encompassed the development to decay cycle of hypoxia* for different scenarios. The days from 01 July to 13 July were not considered because the hypoxic* area varied little in all scenarios. To assess the impact of upwelling favorable wind duration (A and B), hypoxia* frequency was calculated for both the early and late summer periods. To assess the impact of changes in river discharge, nutrient concentration, river diversion and nitrogen components (A, C, D, E, F and G), hypoxia* frequency was calculated for late summer period, during which hypoxic* area showed dramatic changes for the different scenarios.

I also compared the averaged salinity and chlorophyll concentration fields for the two selected periods, which I used to show differences in physical and biological fields. I was interested in the region west of the Mississippi River Bird's Foot Delta (Fig. 30), because it is the region where hypoxia has been observed frequently. To describe the spatial variability, I separated the region into east and west components. The boundary between the two was near 90.8°W.

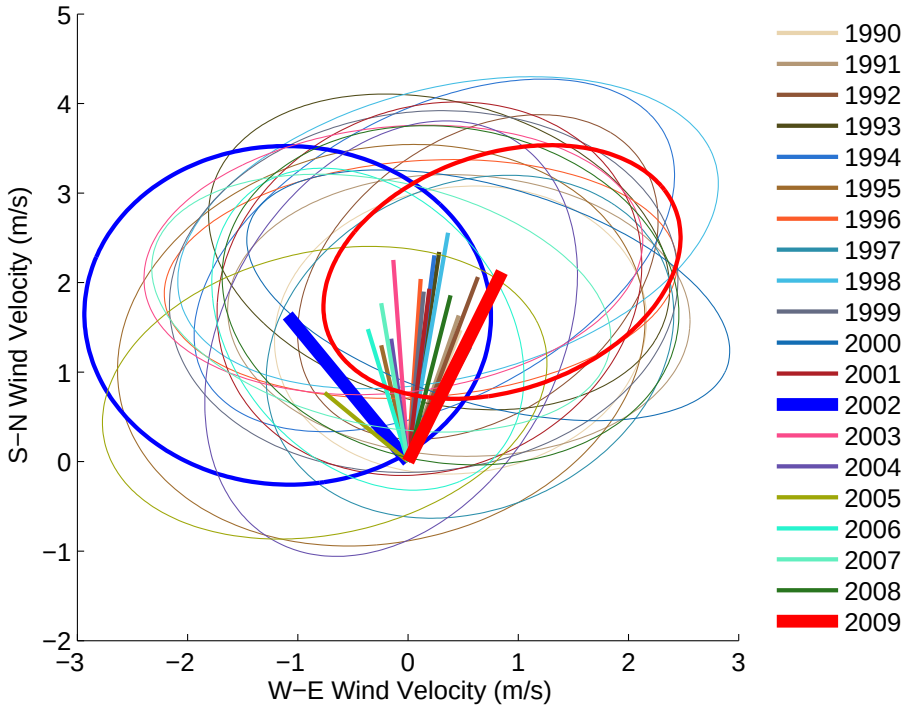

Fig. 27: The observed wind variance ellipses for summer (25 May - 01 Sep) from 1990 to 2009. The mean 2002 and 2009 winds are noted by thick blue and red lines, respectively. The sticks are the time-averaged wind magnitude for each year. The ellipses show the wind variance along the two principal axes. The wind time series is taken from spatially averaged NARR wind data and filtered using a 40-hr low-pass filter. Positive W-E winds are from west to east (upwelling favorable).

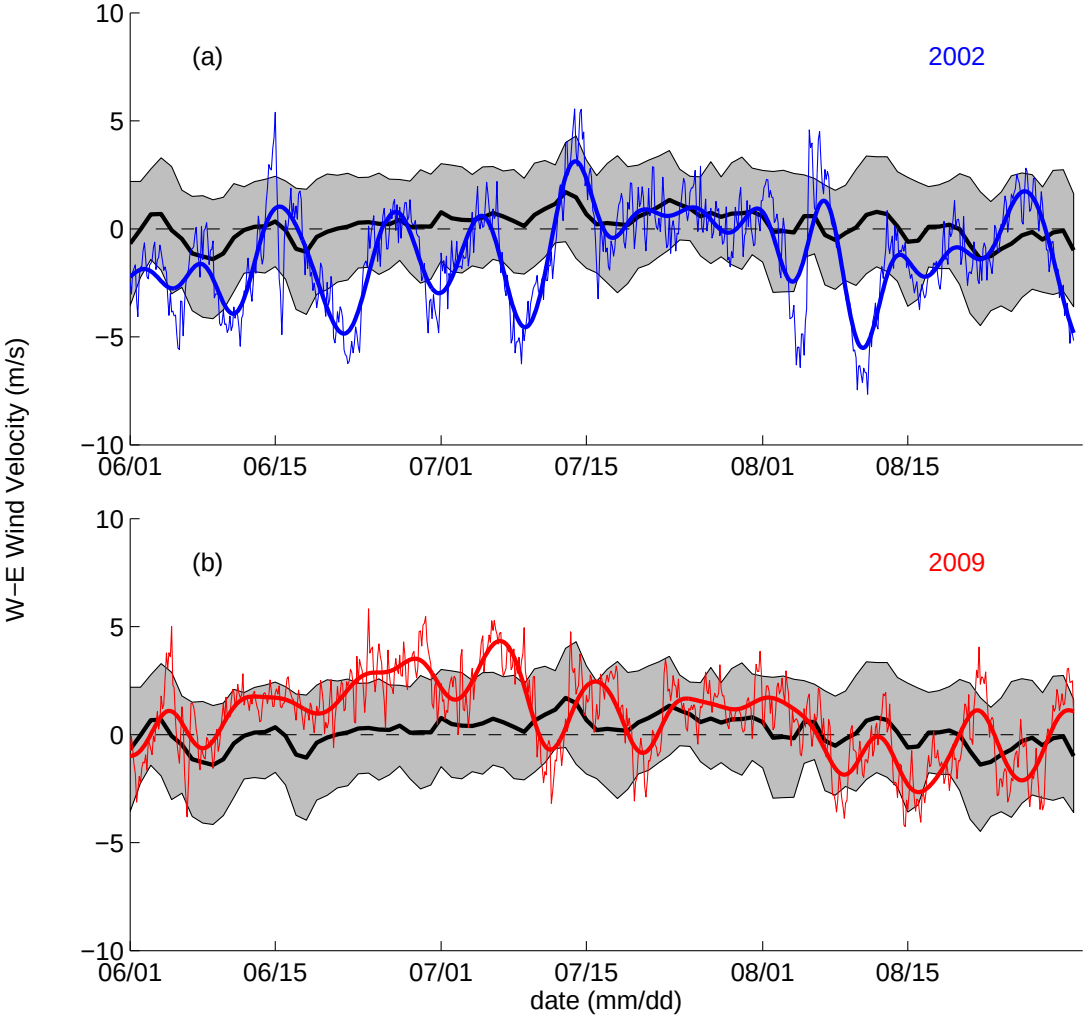

Fig. 28: Spatially averaged W-E winds of summer 2002 (a) and 2009 (b). Positive values indicate wind from west to east (upwelling favorable). The original time series was measured at 3-hr time intervals; it was filtered with a 40-hr low-pass filter for usage here. Black line is average wind velocity component based on climatology. Shaded area is mean velocity plus and minus one standard deviation.

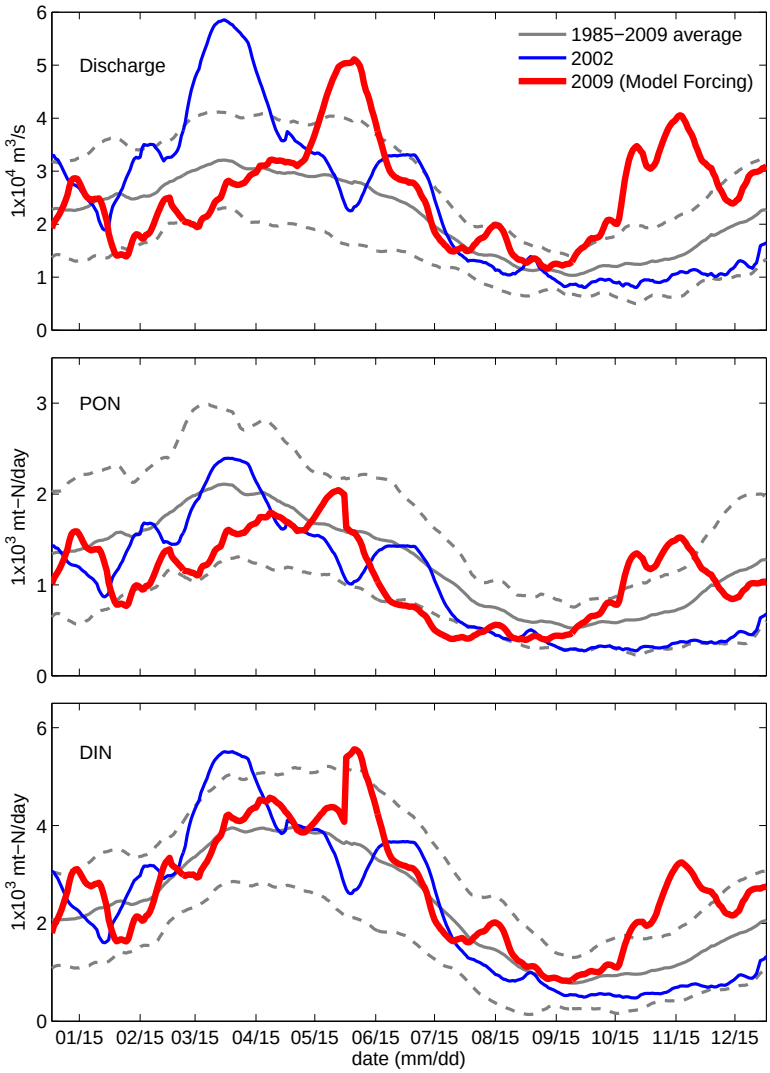

Fig. 29: The measured river discharges (top), riverine PON loadings (middle), and DIN loadings (bottom). Blue lines are for 2002, red lines are for 2009. The grey lines are the 25-year (1985–2009) averaged daily value (solid line) with ± 1 standard deviation (dash lines). The total nitrogen loading includes both PON loading + DIN loading, where nitrogen loading = nitrogen concentration × river discharge. The river discharge data were from the U.S. Army Corps of Engineers (USACE); the nutrient concentration data were from the U.S. Geological Survey (see Chapter III).

Table IX: Description of seven scenarios and their forcings. MR is the Mississippi River. AR is the Atchafalaya River.

Scenario ID	Scenario Name	Model forcings
A	base	2002 Wind (short west wind) 2009 River Discharge (1/3 from AR + 2/3 from MR) 2009 Nitrogen Concentration (DIN + PON)
B	long upwelling wind	2009 Wind (long west wind) 2009 River Discharge (1/3 from AR + 2/3 from MR) 2009 Nitrogen Concentration (DIN + PON)
C	high discharge	2002 Wind 3/2 × [2009 River Discharge (1/3 from AR + 2/3 from MR)] 2/3 × [2009 Nitrogen Concentration (DIN + PON)]
D	low concentration	2002 Wind 2009 River Discharge (1/3 from AR + 2/3 from MR) Half of 2009 Nitrogen Concentration (DIN + PON)
E	all MR	2002 Wind 2009 River Discharge (All from MR) 2009 Nitrogen Concentration (DIN + PON)
F	1/3 MR	2002 Wind 2009 River Discharge (2/3 from AR + 1/3 from MR) 2009 Nitrogen Concentration (DIN + PON)
G	all DIN	2002 Wind 2009 River Discharge (1/3 from AR + 2/3 from MR) 2009 Nitrogen Concentration (All in DIN form)

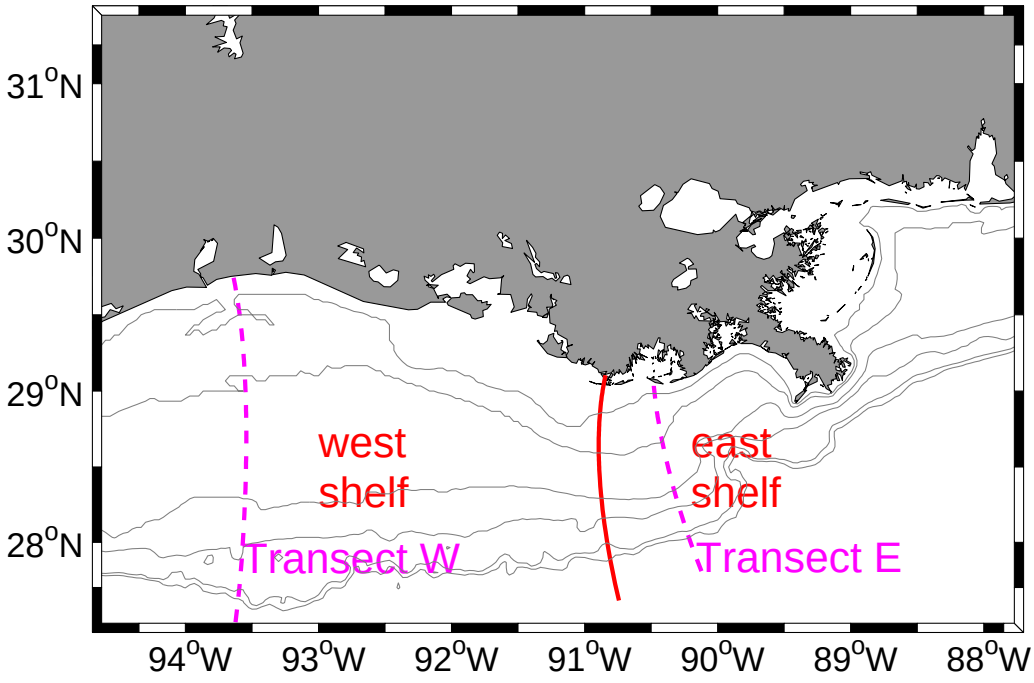

Fig. 30: The east and west Louisiana shelf regions selected for analysis (Table IX). Dashed lines indicate the position of the vertical section in the west and the east (Fig. 34 and Fig. 35). The depth contours shown are at 10, 20, 60, 100, 300, and 400 m. The solid red line is the boundary between the two regions.

C. Results

1. The Effect of West Wind Duration

a. Hypoxic* Area

The time series of hypoxic* area for the long upwelling wind (scenario B) and base (short upwelling wind, scenario A) cases differed substantially (Fig. 31). Although the maximum hypoxic* areas were comparable (16,200 km^2 vs 16,500 km^2), the dates of maximum area were different. For the long upwelling wind case, the maximum hypoxic* area occurred in the mid-June (June 15th). For the base case, the maximum

hypoxic* area occurred in the late July (July 27th). The long upwelling wind case was forced by 2009 winds and river flow. The averaged hypoxic* area during the cruise time (July 18th - July 23rd) of the upwelling case was 9,860 km^2, about 23% larger than the 2009 observational hypoxic area (8,000 km^2).

The hypoxia* had different spatial patterns for the base and long upwelling wind cases during the two summer periods (Fig. 32). During the early summer of the long upwelling wind case, the hypoxic* region extended westward past the Sabine River mouth and southward over the 20 m isobath. Most of the region was hypoxic* for more than 2 weeks ($> 50\%$). In contrast, during the early summer of the base case, the hypoxic* region was limited to the east Louisiana shelf having bottom depth 10 – 20 m. The duration of hypoxia* was less than two weeks ($< 50\%$). During the late summer of the long upwelling wind case, the hypoxic* region was limited to the east Louisiana shelf and shoreward of the 40 m isobath. The duration of hypoxia* was more than three weeks ($> 75\%$). In contrast, during the later summer of the base case, hypoxic* area extended to the west, covering much of the Louisiana shelf. The duration of hypoxia* was over two weeks ($> 50\%$).

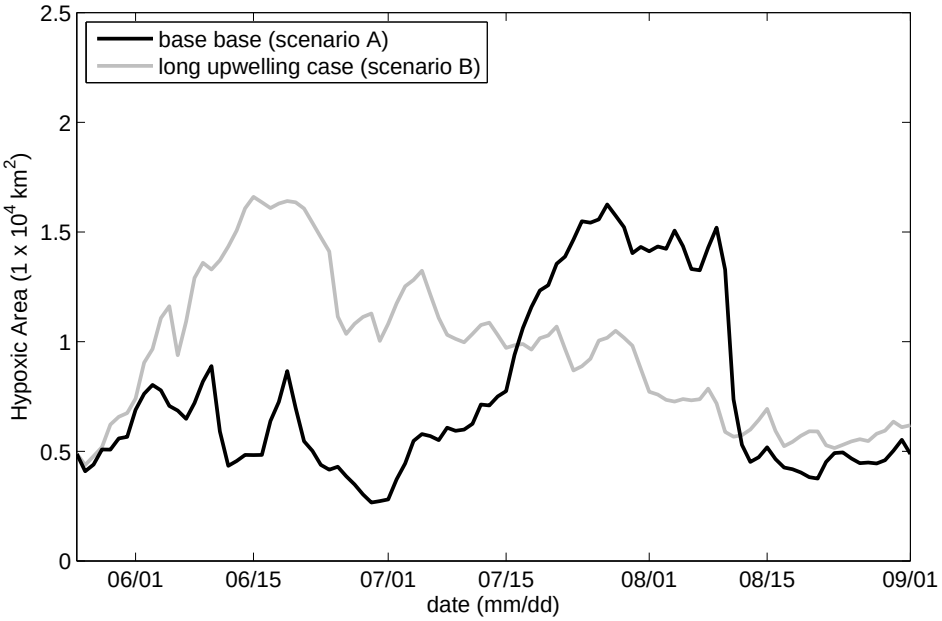

Fig. 31: The hypoxic* areas for the long upwelling wind (scenario B, gray) and base (scenario A, black) cases during summer (Table IX).

b. Salinity and Chlorophyll Distributions

The salinity patterns were different for the two cases. During the early summer of the base case, low-salinity surface water was confined to a narrow nearshore band where bottom depth was less than 20 m on the Louisiana shelf (Fig. 33). During the early summer of the long upwelling wind case and during the late summer of the base case, the low-salinity surface water extended further offshore on the Louisiana shelf. This extension is clearly visible in the two vertical sections on the east and west shelf (Fig. 30, Fig. 34 and Fig. 35). The isohalines during the early summer of the upwelling wind case and late summer of the base case were aligned more horizontally than for the early summer of the base case, suggesting stronger stratification extending further offshore waters. The surface salinity increased greatly in the late summer of the long

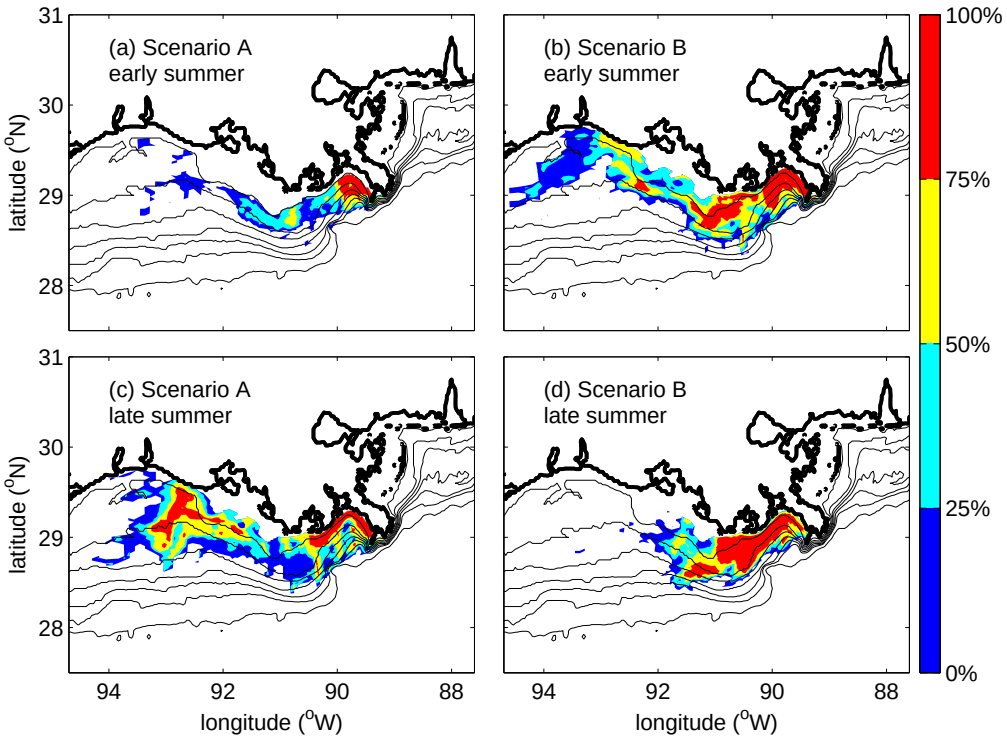

Fig. 32: The frequency of hypoxia* during the early (June 1st – June 30th) and late (July 14th – August 12th) summer periods of scenario A (base case) and B (long upwelling wind case). (a) The early summer period scenario A, (b) the early summer period of scenario B, (c) the late summer period of scenario A, (d) the late summer period of scenario B. The depth contours are 10, 20, 30, 40, 50, 60, and 100 m isobaths.

upwelling wind case, particularly on the west shelf (Fig. 33).

The surface chlorophyll concentration was usually low where the salinity was high (Fig. 36). The chlorophyll concentrations decreased more for the long upwelling wind case than for the base case between the early to late summer periods. In the base case, the mean west shelf chlorophyll concentration decreased by about 34% during the summer (7.38 to 4.88 mg-Chl/m^3). On the east shelf, it decreased by about 21% (14.32 to 11.32 mg-Chl/m^3). In the long upwelling wind case, the west shelf chlorophyll concentration decreased by about 77% (7.24 to 1.70 mg-Chl/m^3). On the east shelf, it decreased by about 54% (17.83 to 8.17 mg-Chl/m^3). Although the low salinity surface water was confined to the nearshore during the early summer period of base case, the mean surface chlorophyll concentration on the west shelf was relatively high (7.38 mg-Chl/m^3).

The chlorophyll and salinity fields covaried on the two vertical transects (Fig. 34 and Fig. 35). The highest chlorophyll concentration was consistently at the surface within the river plume. The chlorophyll concentration decreased rapidly with increasing depth. Both salinity and chlorophyll concentration contours were more parallel to the surface on the east transect than the west transect. The chlorophyll concentrations extended further offshore in the late summer period of both cases, as well as during the early summer of the upwelling wind case than the early summer of the base case.

2. The Relative Importance of River Discharge and Nitrogen Concentration

a. Hypoxic* Area

The high discharge case (C) was forced with the 2002 wind field, high freshwater discharge and low nitrogen concentration. It had the same total N loading as the

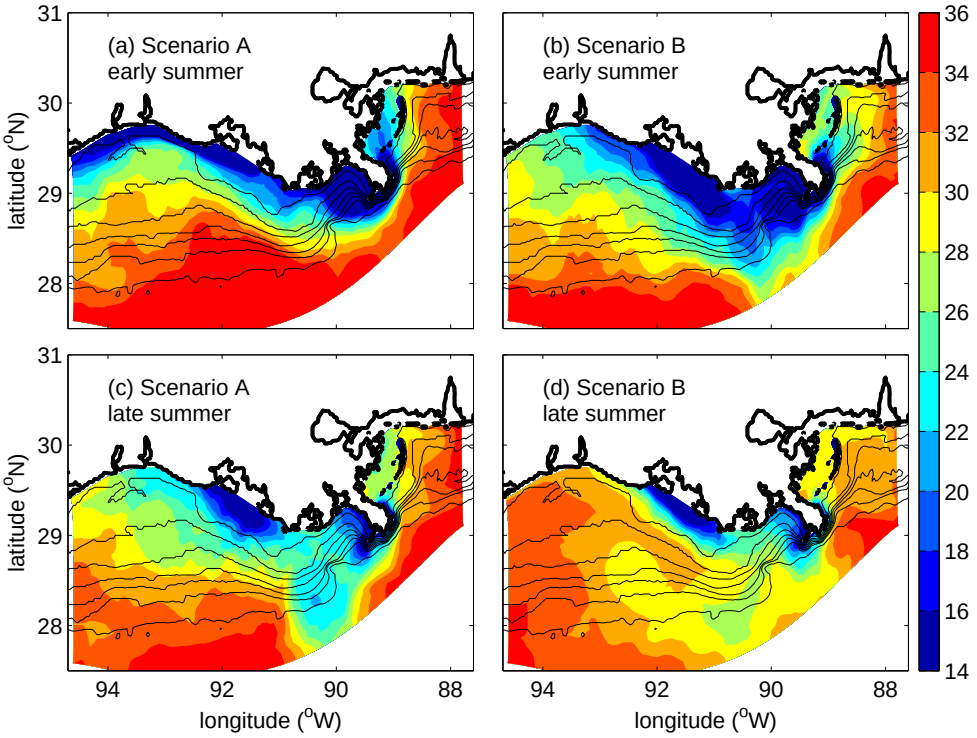

Fig. 33: The average sea surface salinity at the early (June 1st - June 30th) and late (July 14th - August 12th) summer periods of scenario A (the base case) and B (the long upwelling wind case). (a) The early summer period scenario A, (b) the early summer period of scenario B, (c) the late summer period of scenario A, (d) the late summer period of scenario B. The depth contours are 10, 20, 30, 40, 50, 60, and 100 m isobaths.

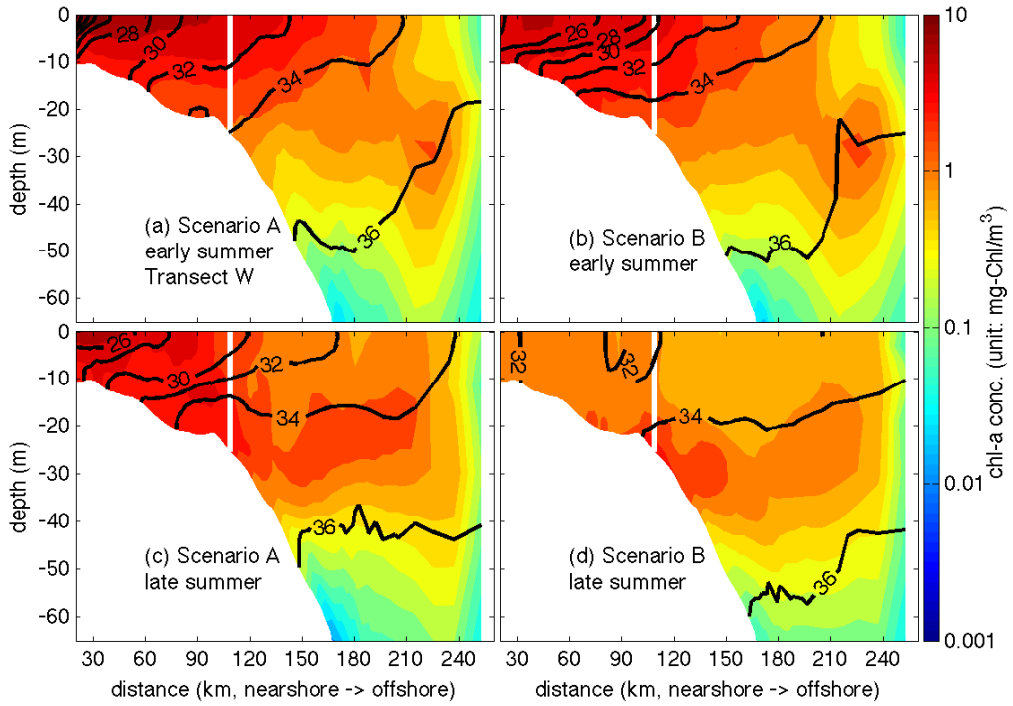

Fig. 34: West vertical sections distribution of the average salinity (contours) and chlorophyll concentration (color, mg-Chl/m^3) at the early (June 1st - June 30th) and late (July 14th - August 12th) summer of scenario A (the base case) and B (the long upwelling wind case). (a) The early summer scenario A, (b) the early summer of scenario B, (c) the late summer of scenario A, (d) the late summer of scenario B. The distance is from nearshore to offshore. The salinity contour interval is 2. The position of the west transect is in Fig. 30

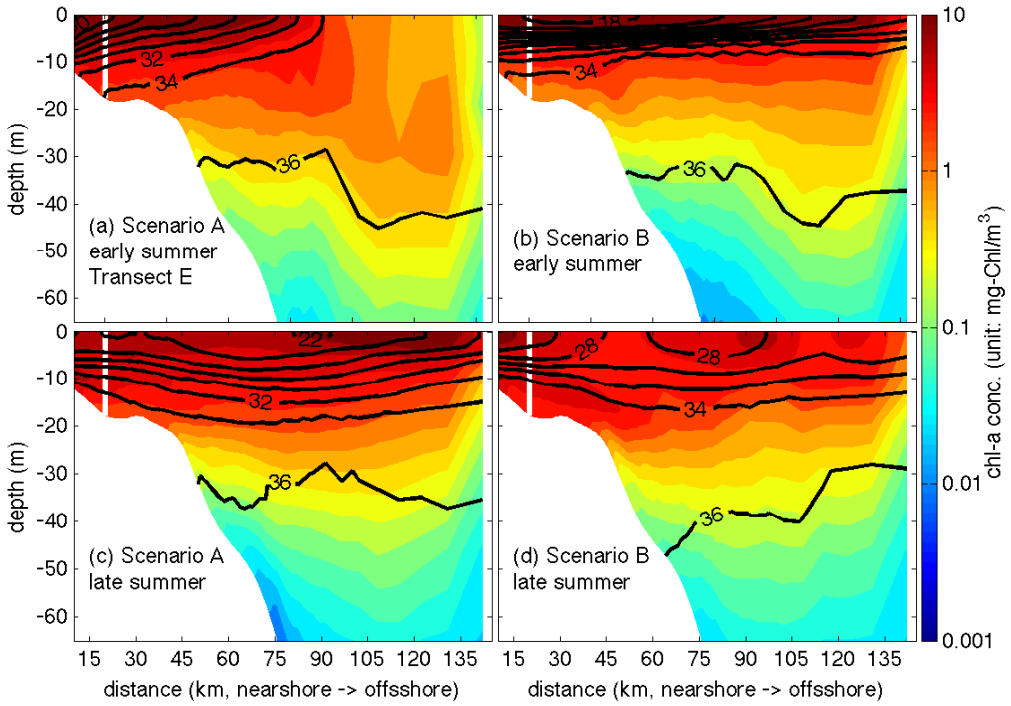

Fig. 35: East vertical sections distribution of the average salinity (contours) and chlorophyll concentration (color, mg-Chl/m^3) at the early (June 1st - June 30th) and late (July 14th - August 12th) summer of scenario A (the base case) and B (the long upwelling wind case). (a) The early summer scenario A, (b) the early summer of scenario B, (c) the late summer of scenario A, (d) the late summer of scenario B. The distance is from nearshore to offshore. The salinity contour interval is 2. The position of the east transect is in Fig. 30

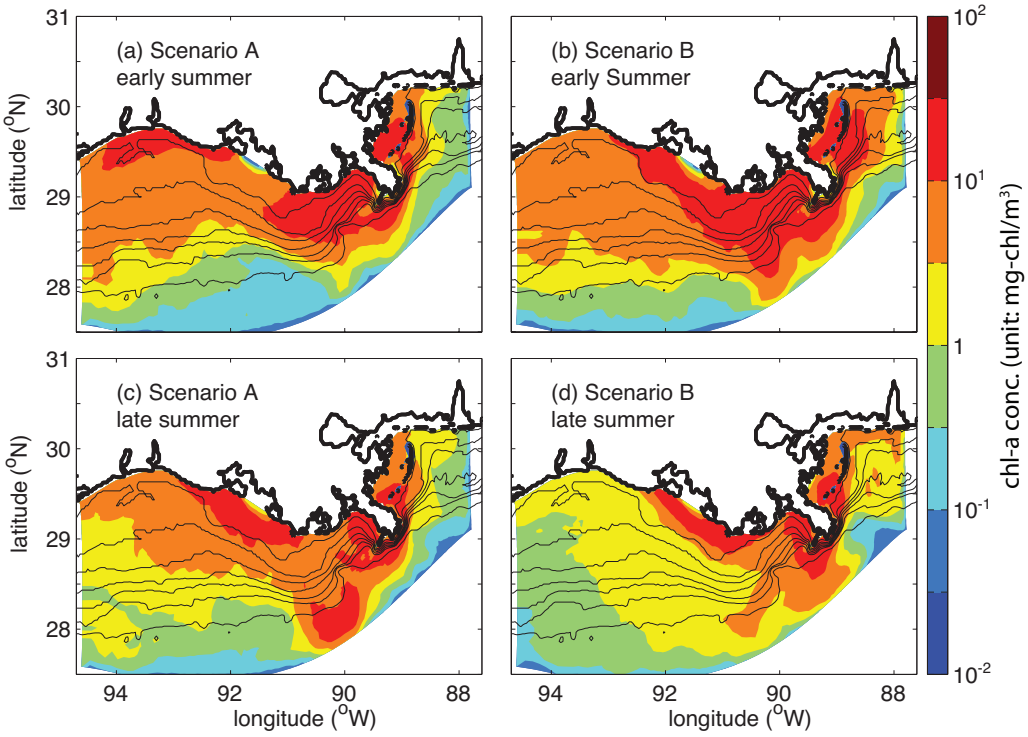

Fig. 36: The average surface chlorophyll concentration (mg-chl/m^3) at the early (June 1st - June 30th) and late (July 14th - August 12th) summer of scenario A (the base case) and B (the long upwelling wind case). (a) The early summer of scenario A, (b) the early summer of scenario B, (c) the late summer of scenario A, (d) the late summer of scenario B. The contours show 10, 20, 30, 40, 50, 60, and 100 m isobaths.

base case (Table IX). The resulting hypoxic* area was maximum during the late summer period and larger than that of the base case (Fig. 37, average 18,500 km^2 versus 13,000 km^2). During this time, the hypoxic* region extended further west and south than the base case (Fig. 38). The hypoxic* region for the base case extended west to about 93.3 °W and south to the 20 m isobath. As a comparison, the hypoxic* region for the high discharge case extended west to about 93.7°W and south to the 30 m isobaths.

The low nitrogen concentration case (D) has the same river discharge as the base case but the nitrogen concentration was reduced to one half that of the base case (Table IX). The resulting hypoxic area was small during the whole summer period, and limited to east of the Terrebonne Bay (Fig: 37 and Fig. 38). The average hypoxic area during the late summer period was 3300 km^2, about 75% less than the base case.

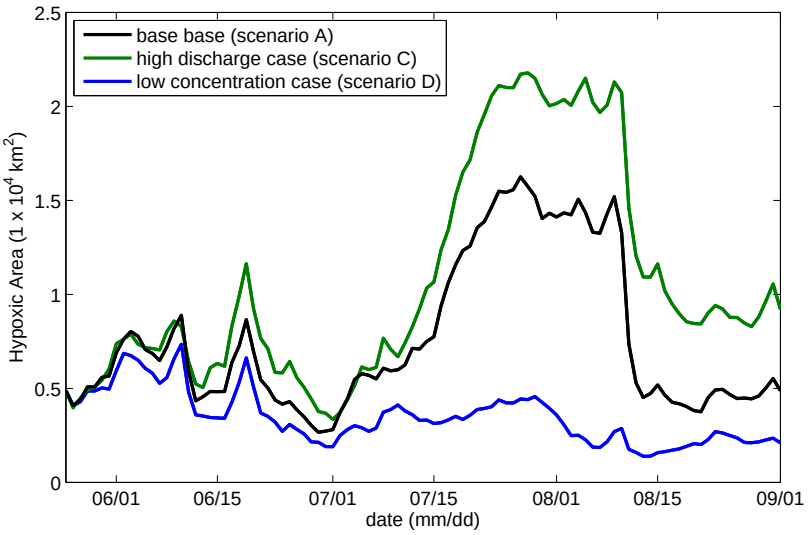

Fig. 37: The hypoxic* areas for the base (scenario A, black), high discharge (scenario C, green) and low concentration (scenario D, blue) cases through the season (Table IX).

b. Salinity and Chlorophyll Distribution

The surface low salinity (Fig. 39) and high chlorophyll concentration (Fig. 40) extended further south and west for the high discharge case. The main change in physical and biological properties occurred on the west shelf, where the average surface salinity was 24 in the high discharge case, 4 lower than the base case. The chlorophyll concentration was 5.8 mg-Chl/m^3, 20% larger than the base case. As a comparison on the east shelf, the average surface salinity was 20 in the high discharge case, 2 lower than the base case. The chlorophyll concentration was 11.58 mg-Chl/m^3, 2% larger than the base case.

Because of the same physical forcings (wind and freshwater discharge), the surface salinity distribution in the low concentration case is the same as that of the base case. However, the reduced nitrogen concentration caused the chlorophyll decrease. On the west shelf, the average chlorophyll concentration was 2.0 mg-Chl/m^3, 60% less than the base case. On the east shelf, the average chlorophyll concentration was 5.7 mg-Chl/m^3, 50% less than the base case.

3. The Effect of River Diversion

a. Hypoxic Area

The all MR, base and 1/3 MR cases were the same in total river flow. The all MR case assumed that the Mississippi River discharge was 100% of the total flow. The 1/3 MR case assumed that the Mississippi River discharge was 33.3% of the total flow. In actuality, the Mississippi River discharges about 66.7% of the total flow, which was the base case setting. The hypoxic* area of the base case was the smallest of all, following the all MR case. The 1/3 MR case had the largest hypoxic* area. The maximum hypoxic* area in the base case was 13,000 km^2, about 12.7% smaller

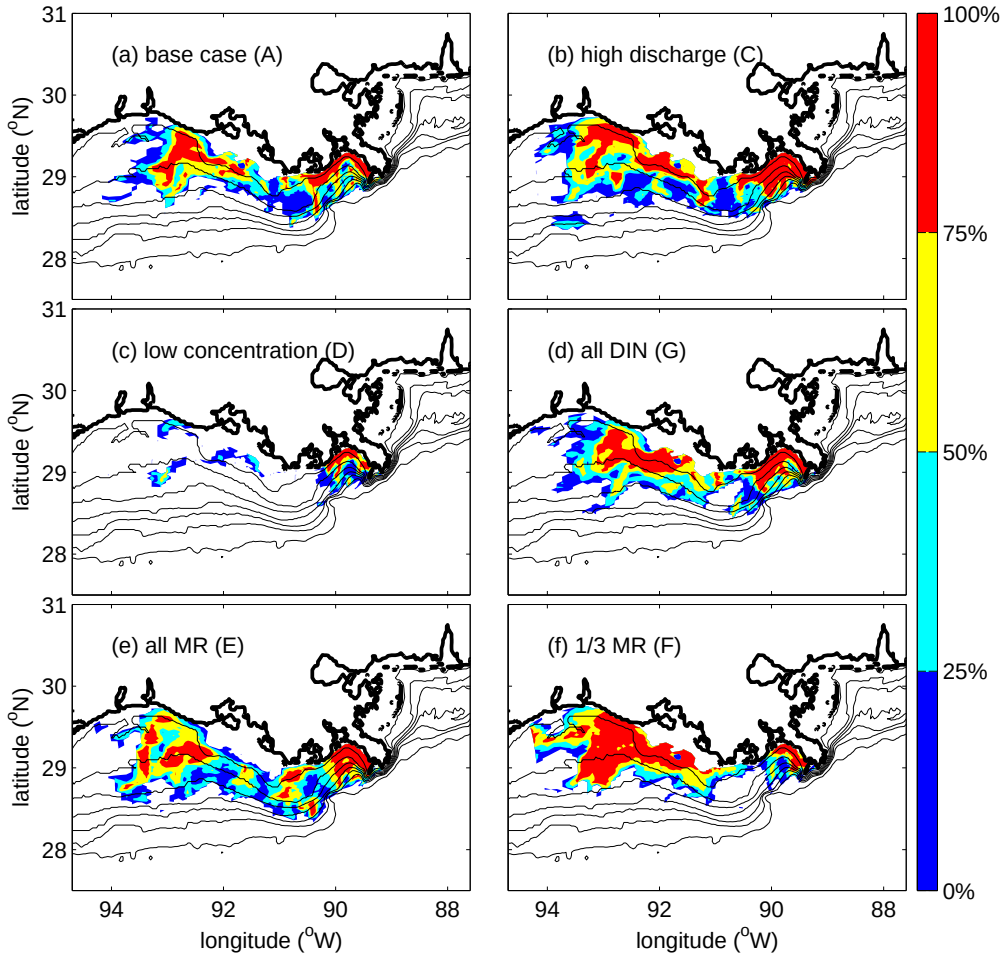

Fig. 38: The frequency of hypoxia* during late summer (14 July–12 August) of scenarios A (a, base), C (b, high discharge), D (c, low concentration), E (d, all MR), F (e, 1/3 MR) and G (f, all DIN). The scenario descriptions are in Table IX. The depth contours are 10, 20, 30, 40, 50, 60, and 100 m isobaths.

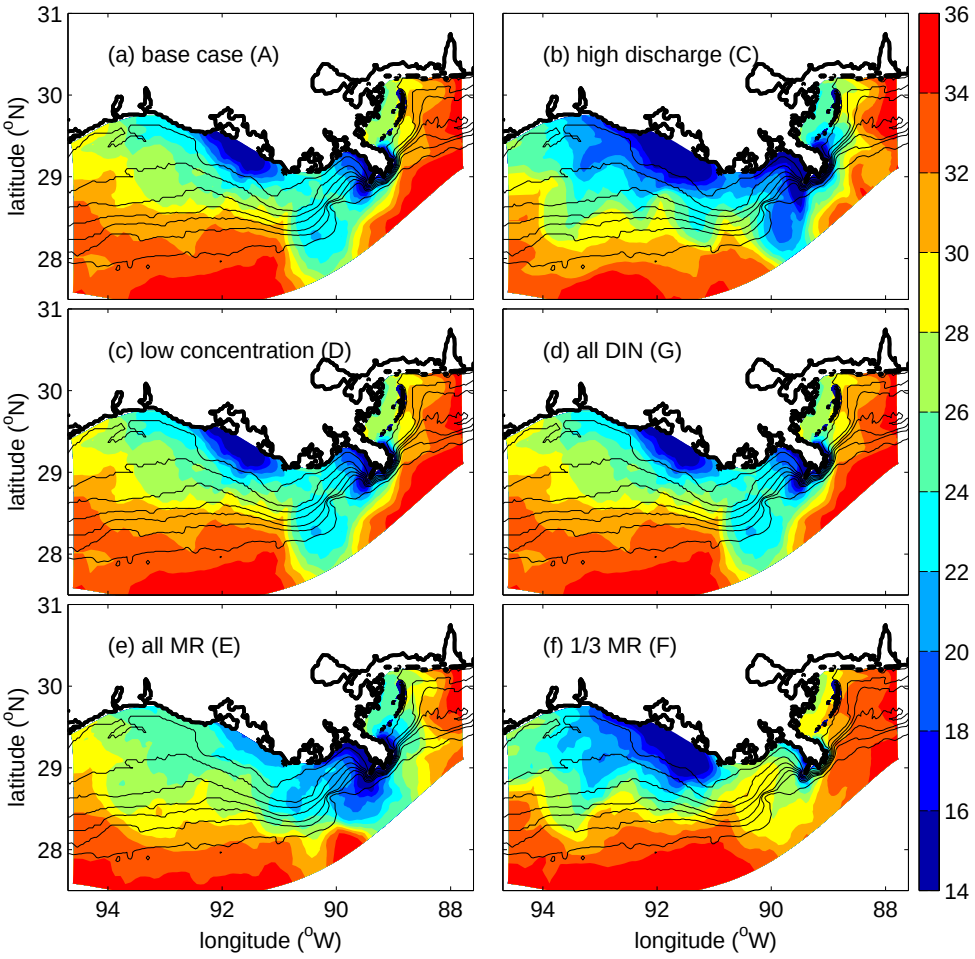

Fig. 39: The average surface salinity during late summer (14 July–12 August) for the scenarios A (a, base), C (b, high discharge), D (c, low concentration), E (d, all MR), F (e, 1/3 MR) and G (f, all DIN). The scenario descriptions are in Table IX. The depth contours are 10, 20, 30, 40, 50, 60, and 100 m isobaths.

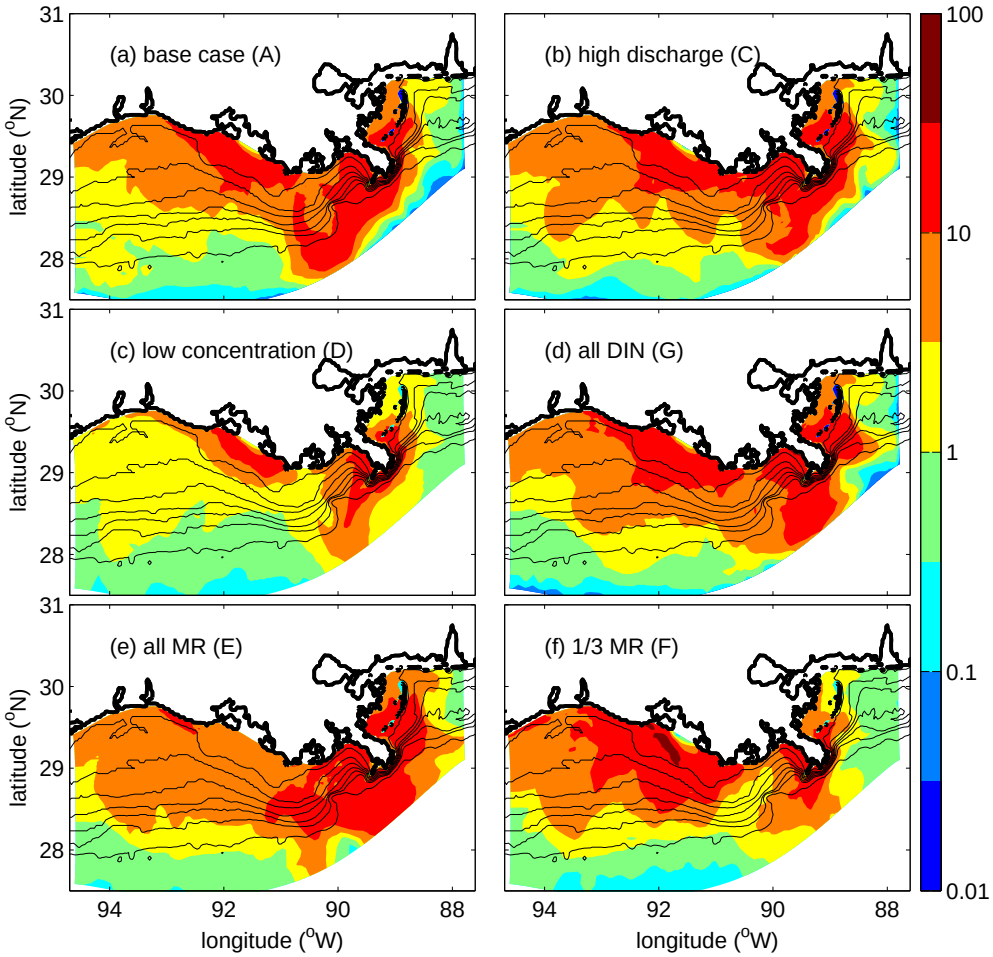

Fig. 40: The average surface chlorophyll concentration (mg-chl/m^3) during the late summer (14 July–12 August) for the scenario A (a, base), C (b, high discharge), D (c, low concentration), E (d, all MR), F (e, 1/3 MR) and G (f, all DIN). The scenario descriptions are in Table IX. The depth contours are 10, 20, 30, 40, 50, 60, and 100 m isobaths.

than that of the all MR case (14,900 km^2) and 29.7% smaller than the 1/3 MR case (18,500 km^2, Fig. 41). Note that the 18,500 km^2 for 1/3 MR case was estimated using the current model domain. The westward extension of the hypoxic area reached the western boundary of the model, indicating a potentially larger area in the 1/3 MR case. The hypoxic area could conceivably extend to Texas if the model domain were expanded.

The large change of hypoxia* in the 1/3 MR case could also be found from the frequency of hypoxia* figure (Fig. 42). Unlike the all MR and base cases, the hypoxic region was not continuous on the Louisiana shelf in 1/3 MR case. There was almost no hypoxia in the region south of Terrebonne Bay, between 90°W to 91°W. In addition, the period of hypoxia on the west shelf increased considerably in the 1/3 MR case. For a large area on the west shelf, hypoxia* lasted more than three weeks (frequency $> 75\%$), which was about one week longer than the base and all MR cases (frequency $> 50\%$).

Although the hypoxic period was relatively short in the all MR case, the southward extension of the hypoxic region on the west shelf was the largest. The hypoxic region was over the 30 m isobath. In comparison, the hypoxic area was shallower than the 20 m isobaths in the base and 1/3 MR cases. The period (also frequency) of hypoxia from the Mississippi River to Sabine showed a patchy pattern rather than a continuous one. For the all MR case, the hypoxia lasted two weeks or more across the shelf but was most persistent in the Louisiana Bight and between 92°W and 93.5°W.

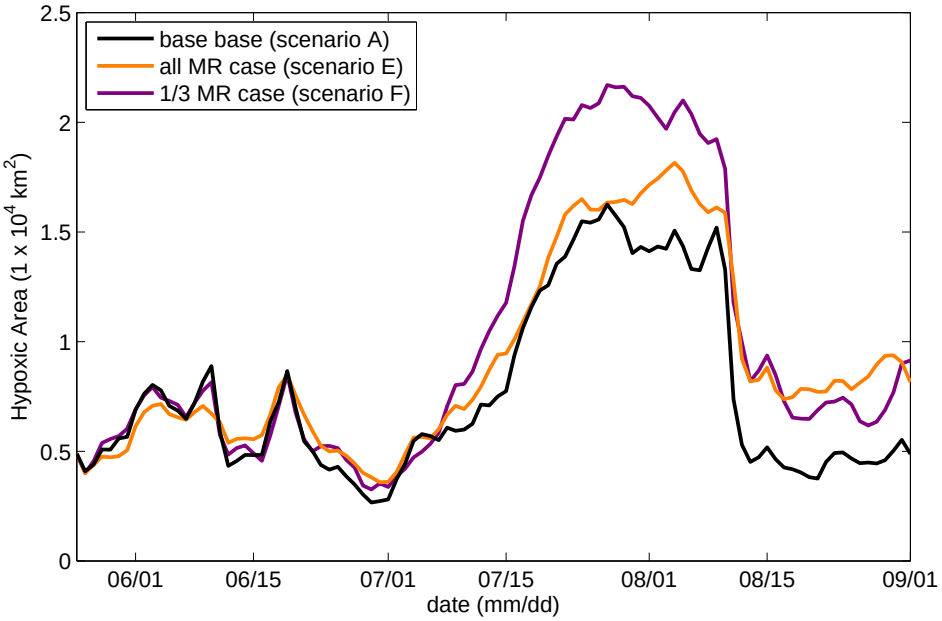

Fig. 41: The hypoxic* areas for the base (scenario A, black), all MR (scenario E, orange) and 1/3 MR (scenario D, magenta) cases through the season (Table IX).

b. Salinity and Chlorophyll Concentration

The westward and southward extents of low salinity waters were comparable for the all MR and base cases, which are different from the 1/3 MR case (Fig. 39). At the western boundary of the model domain, the salinity for the all MR and base cases was 28, but 2 lower in the 1/3 MR case. The 28 isohaline extended southward over the 30 m isobath for the all MR and base cases, and across the 50 m isobath for the 1/3 MR case. In addition, with more freshwater being discharged by the Atchafalaya River in the 1/3 MR case, the west shelf became fresher. The average salinity on the west shelf was 27 for both the base and all MR case, 25 for the 1/3 MR case.

Higher chlorophyll concentration results from more nutrient-laden fresh water being discharged onto the western shelf. (Fig. 40). The average chlorophyll concentration on the west shelf in the 1/3 MR case was 9.3 mg-Chl/m^3, over 48% larger

than in the base case (4.8 mg-Chl/m^3). Although there was no freshwater supply from the Atchafalaya River in the all MR cases, the average chlorophyll concentration on the west shelf was still 6.0 mg-Chl/m^3, 19% larger than the base case. The maximum chlorophyll concentrations near the mouth of the Atchafalaya Bay, however, are greatly diminished.

4. Effect of Nitrogen Form from the River

The all DIN case treated all organic N as if it were as inorganic N. The resulting hypoxic* area was smaller than that for the base case before July 20th, but larger afterwards (Fig. 42). The average hypoxic* area from July 16th to August 12th was 14,800 km^2, 13% larger than the base case. The hypoxic* region extended south and west with a gap around 90.8°W between 10–20 m (Fig. 38).

Because the physical forcing factors (wind and freshwater) were the same, there was no change from the base case in the salinity fields in the all DIN case (Fig. 39). However, enhanced chlorophyll concentrations extended further offshore along the shelf (Fig. 40). Compared to the the base case, the chlorophyll concentration increased about 32% in the all DIN case on the west shelf.

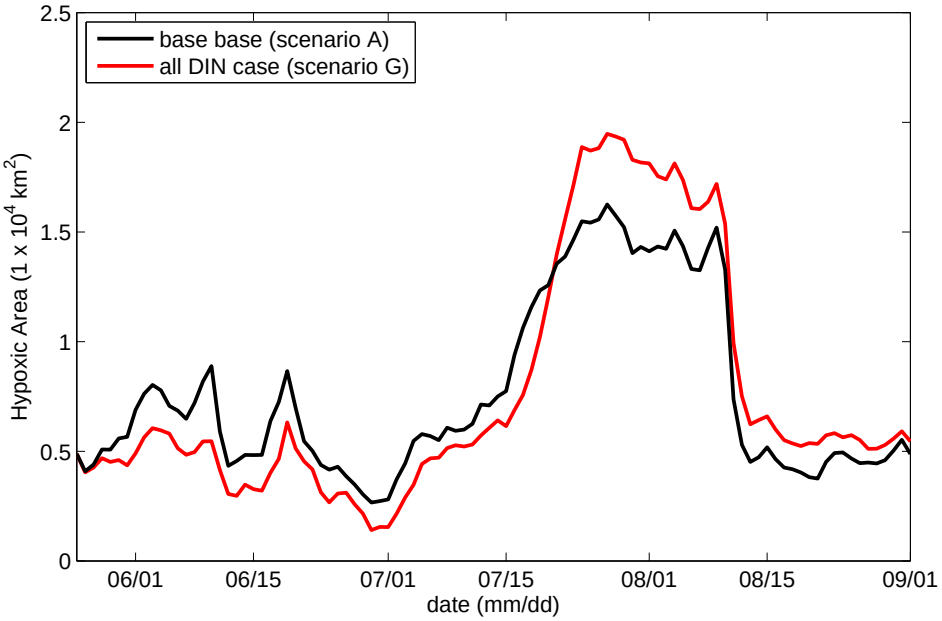

Fig. 42: The hypoxic* areas for the base (scenario A, black) and all DIN (scenario G, red) cases through the season (Table IX).

D. Discussion

1. The Response of the Hypoxic Area to the Upwelling Favorable (West) Wind

The simulated hypoxic* area is generally consistent with the observations (Fig. 43). A comparison of observations in 2002 and 2009 with the two scenarios using wind data from those years shows that the observations and the model results show the same extension of hypoxic area. In 2002, the simulated hypoxic* region was large and reached west to Calcasieu Lake. The observed hypoxic region extended even further west reaching Sabine Lake. For 2009, the simulated hypoxic area was limited to the region east and south of Atchafalaya Bay. The observed hypoxia occurred almost entirely in the region east of the Atchafalaya Bay.

In 2009, the May–June nitrogen loading was large (3.5×10^5 metric tons), but

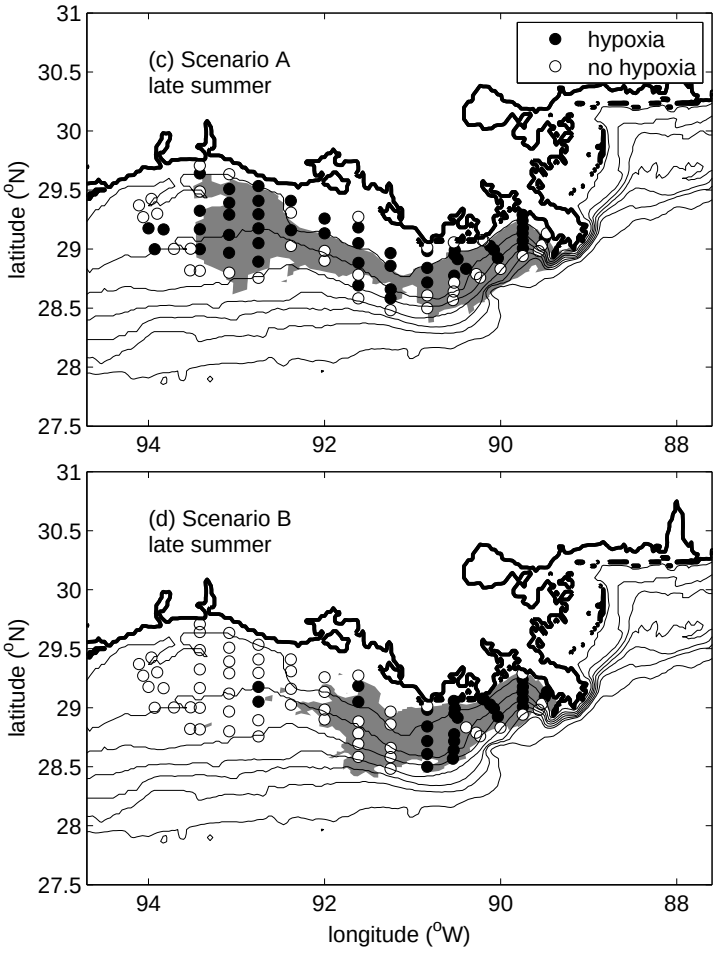

Fig. 43: The shelf-wide survey on hypoxia in 2002 (upper) and 2009 (lower), and the simulated hypoxic* region (where hypoxia* frequency ≥ 1, gray area) during the late summer period (14 July–12 August) in scenario A and scenario B. The stations where hypoxia was observed are shown in black dots, where it was not observed in white dots. In 2002, the cruise period was from 21 July – 26 July. In 2009, the cruise period was 18 July–23 July. Both scenario A and scenario B used the 2009 freshwater flux and nitrogen concentration. Scenario A was forced by 2002 winds, and scenario B was forced by 2009 winds.

the wind was atypical because of an usually long west wind duration (2 month in 2009 vs about 1 month normally). The simulation for 2009 showed that the hypoxic* area was large right after the wind switched from downwelling to upwelling favorable, but shrank as the upwelling wind continued. The sampling cruise was 18 July 2009–23 July 2009, well into the upwelling phase. This was a year with high nitrogen loading that created a large hypoxic area, but the cruise didn't capture it because of its timing.

As mentioned before, the observed 2009 hypoxic area was 8,000 km^2. The *Turner et al.* (2006) model predicted that the 2009 hypoxic area would be 25,000 km^2. The *Scavia et al.* (2003) model predicted that it would be 19,000 km^2 (17,100 - 22,000 km^2 for 95% percentile interval). Their simulations were 140–210% larger than the observation. My simulation predicted that the average hypoxic* area during the cruise would be 9,860 km^2, only 23% larger than the observation.

The traditional predictive models do not account for changes in the wind fields. However, as the base case showed, the hypoxic area can increase dramatically a few days after the wind changes from downwelling to upwelling favorable. If the hypoxic area measurements were taken shortly after the wind turns in the base, both *Turner et al.*'s and *Scavia et al.*'s prediction would have been closer to the observations.

The hypoxic area can vary greatly over the course of a summer in response to changes in wind and river flow. With a downwelling favorable wind, freshwater is confined close to shore and flows down west to the Texas coast. Vertical isohalines are a sign that vertical mixing is high and limiting the development of hypoxia. However, with an upwelling wind, freshwater is transported offshore. The stratification on the Louisiana shelf is reduced because the offshore-moving freshwater lies on top of the onshore-moving seawater. In addition, nutrients are carried away by the freshwater. With more freshwater occupying the Louisiana shelf, more nutrients stay on the shelf

and support a high primary production. The flux of organic matter to the bottom increases as primary production increases. When combined with reduced vertical mixing, the result is that the oxygen concentrations that are drawn down rapidly and a larger area of hypoxia is found on the Louisiana shelf.

Generally speaking, the Mississippi–Atchafalaya River discharge has a characteristic annual cycle. It floods in spring and flow then decreases, becoming lowest in the fall. The decrease in river discharge after the spring flood is one reason why the hypoxic area decreased in the late summer of 2009. As mentioned above, the upwelling favorable winds started early (June 1) and persisted (August 1) through most of the summer of 2009. When the upwelling favorable winds started, the freshwater on the west shelf moved east and offshore and stayed on the Louisiana shelf. However, as the upwelling favorable winds continued, the freshwater continued to move offshore and eastward. Because the river flow decreased, no freshwater replenished the west Louisiana shelf. As a result, the low oxygen bottom water on the west shelf was ventilated. In addition, the nutrients moved with the freshwater, reducing the primary production as well as the fluxes of bottom organic matter on the west shelf. The reduced bottom organic matter flux, together with the increased vertical mixing, increased the oxygen concentration and reduced the hypoxic area on the west shelf.

Using observational data, *Wiseman et al.* (1997) found that the primary pycnocline, which was set up by the return flow under the condition of upwelling favorable wind, was necessary for the occurrence of hypoxia. They also found that a weak secondary pycnocline, which may be a thermocline, determined the shape of the hypoxic zone. My simulations showed that the wind strongly influences the spatial distribution and variability of the river plume. In addition, the simulations captured the oxygen reduction on the Louisiana shelf resulting from the river plume resides on the shelf, decreasing the vertical mixing and increasing the primary production

(high chlorophyll concentration). However, the model cannot fully simulate the development of the secondary pycnocline, one reason why the oxygen concentration in the simulations does not reach to 2 mg/L (62 μM). Simulating the fine density structure requires a better understanding of the formation of the secondary pycnocline. I have used hypoxia* instead of hypoxia to compensate for this deficiency in oxygen reduction when looking at areal effects.

2. The Response of the Hypoxic Area to River Discharge and Nitrogen Concentration

One important conclusion from the low concentration case (scenario D) is that the hypoxic area is highly sensitive to the total amount of nitrogen loading. When the total nitrogen loading was reduced by 50% by cutting the nitrogen concentration to one half of the original, the hypoxic area was reduced by 75%. However, the size of the hypoxic area created by a given amount of nitrogen loading was not fixed. Although the total nitrogen loading was the same, the hypoxic area of the scenario with high discharge (scenario C) was 42% larger than the area of the scenario with low discharge (scenario A).

The change in river discharge caused a series of changes in oceanic conditions, which changed the concentration of bottom dissolved oxygen. First, more freshwater was released to the Louisiana shelf, increasing density stratification and decreasing vertical mixing. The decreased vertical mixing reduced the exchange of oxygen across the pycnocline. Second, increased freshwater discharge enhanced the crossshore pressure gradient, which intensified the alongshore currents. The intensified current allowed more nutrients ($NH_4^+ + NO_3^-$) to reach the west shelf and offshore regions, therefore, enhancing primary production there. The two effects tend to decrease the benthic oxygen concentration.

The non-linear interaction between the hypoxic area and nitrogen loading has also been studied using other models. *Justic et al.* (2003a,b, 2005) simulated the hypoxia frequency from 1955 to 2000 at the C6X station from a two box model. The results showed that a 30% decrease in the nitrate concentration resulted in a 37% decrease in the frequency of hypoxia. A 20% increase in the river discharge resulted in the same percentage increase in frequency of hypoxia. The difference in relative response results because an increase in river discharge intensifies density stratification, slowing vertical oxygen exchange. Note that their model had only one dimension and cannot predict the area extent of hypoxia.

Greene et al. (2009) used a multiple regression model to assess the effect of nutrient concentration (including both nitrate and TP) and river discharge on the hypoxic area. In their calculation, a 20% increase in river discharge resulted in the same hypoxic area increase as a 20% increase in nutrient concentration. A 45% decrease in nitrate concentration with no change in flow resulted in the same hypoxic area increase as a 54% decrease in nitrate concentration and a 20% increase in flow. That is, when the nutrient loading (concentration $\times$ flow) was constant, the area was too. The difference between *Greene et al.*'s and my results may be because the statistical model does not include non-linear physical oceanographic conditions (stratification and flow) caused by the river-induced buoyancy change.

Over the years, the Environmental Protection Agency has aimed to reduce the extent of the hypoxic area in the Gulf of Mexico to 5000 km^2. The main effort was through voluntary reduction by farmers of the amount of nutrients released to the Mississippi River, including reducing the use of nitrogen and phosphorous containing fertilizers along the Mississippi River Basin, and improving the management of animal manure in livestock-raising areas (*Mississippi River/Gulf of Mexico Watershed Nutrient Task Force*, 2001, 2008). Our results support the conclusion that the

hypoxic area is highly sensitive to nitrogen loading. With over 50% nitrogen concentration reduction, the hypoxic area can be reduced by 75%. Such results conflict with the previous, simple 1-D model studies, which suggested that considering the role of physical processes, a 40% – 70% reduction of nitrogen was necessary (*Scavia et al.*, 2003; *Scavia and Donnelly*, 2007; *Donner and Scavia*, 2007; *Liu et al.*, 2010).

As mentioned above, the physical conditions on the Louisiana shelf are controlled by a complex interaction of wind and river discharge. In the 1-D model, all the physical processes on the Louisiana shelf were integrated into only one parameter. Forecasting the physical environmental variation from the 1-D model was not very reliable. We need a 3-D hydrodynamic coupled model with realistic topography and forced by realistic wind and river fluxes. The relationship between forcings and current fields have been studied dynamically. The prediction results from the 3-D model are therefore more trustworthy.

Our experiments suggest that decreasing nitrogen-containing fertilizer use may by a large percentage not be necessary under certain conditions. However, our result from the one experiment in our study has a limitation. We forced our model with 2002 winds and 2009 nitrogen loading and river discharge. The 2002 wind regime was distinct from those of other years because of the short duration of upwelling favorable wind in summer. The 2009 nitrogen loading comes from a relatively high nitrogen concentration and river discharge. To get a stronger result about how much the hypoxic area can be reduced by cutting nitrogen release to the river, there need to be larger numbers of simulation with different forcing conditions.

3. The Response of the Hypoxic Area to the Ratio of Mississippi and Atchafalaya River Flows

One of the most important conclusions from the river diversion experiments is the two sources of fresh river water, the Mississippi and the Atchafalaya, have great impacts on where hypoxia occurs on the Louisiana shelf. The Atchafalaya River plays an important role in delivering the fresh river water to the west Louisiana shelf. Although the effect was not apparent when the Atchafalaya had 33.3% of the total flow, it was clear when the Atchafalaya had 66.7% of the total flow. Large amount of the Atchafalaya river water brought large amount of nutrients to the west shelf, intensifying the stratification at the same time. As a result, both the area of hypoxia and its frequency on the west Louisiana shelf increased. The western extension of the hypoxic zone for the 1/3 MR case reached the western boundary of our current model domain setting at Texas border. The hypoxic area could extend to Texas coast if the model domain were larger. In contrast, as the river flow of the Mississippi was reduced, both the area of hypoxia and its frequency decreased on the east Louisiana shelf.

The consequences of shifting flow from the Mississippi River to the Atchafalaya River showed that although the total nitrogen loading and freshwater discharge were the same, the case with 1/3 of river flow from the Mississippi River had a larger hypoxic area than either the base case with 2/3 flow or the case when 3/3 river flows come from the Mississippi River. The hypoxic area in the 2/3 river flow from the Mississippi River case was the smallest. A possible reason for the relatively small hypoxic area in the 2/3 MR case was the change of bathymetry along the Louisiana coast. There is a large shallow area next to the Atchafalaya Bay. As a result, the bottom stress on the flow is strong. A small flow diversion to the Atchafalaya could

not overcome the strong bottom stress. Therefore, the freshwater stayed attached to the bottom and confined to a narrow nearshore band west of the discharge. Because the nearshore freshwater contacted the bottom, the stratification in the nearshore band was weak. As a result, the hypoxic area in the base case was the smallest. As the diversion of flow to the Atchafalaya increased, the freshwater overcame the bottom stress and floated on top of the seawater, resulting in stratification on the west shelf being more intense, creating the condition that favors the formation of hypoxia.

Another interesting feather on the frequency of hypoxia on the Louisiana shelf in the all MR case was that the frequency of hypoxia was distributed patchily rather than continuously. In addition to the area next to the Mississippi River mouth on the east Louisiana shelf, there was a frequent hypoxic region (frequency $> 75\%$) on the west shelf. The patchy pattern was created by the combined river and wind effects. The river discharge was from high to low during our selected period (July 14th – August 02). The fresh river water from the Mississippi was able to flush to the west Louisiana shelf during the high discharge period. As the river flow decreases through time, the freshwater layer on the west shelf become thinner. The west shelf was then easier disrupt with the wind, making the frequency of hypoxia more variable there. In contrast, the Mississippi River discharge was on the east Louisiana shelf. A thick freshwater layer could be maintained even when the river discharge was low in the all MR case. As a result, the region next to the Mississippi River on the east Louisiana shelf had a continuous frequent hypoxic zone in the all MR case.

Over the past 200 years, the relative discharge of the Atchafalaya River has increased (*Fisk*, 1952; *Day et al.*, 1995). *Krug* (2007) examined the implications of the river diversion. He argued that the large wetland loss during the diversion process released large amounts of nutrients to the Louisiana shelf, and thus increased

the hypoxic area. These results show that the circulation over the hypoxic region of the Louisiana shelf is highly influenced by shifting the river discharge. Although more nutrients are released to the Louisiana shelf from the Atchafalaya, how far west and south they reach depended on the strength and direction of the currents. The shift in the stratification also changed because the flow changed the freshwater distribution on the shelf. The alteration of the physical oceanic conditions intensified the effect of nutrient addition from wetland loss.

Krug's studies recommended that an integrated assessment on the effect of the Atchafalaya's partial capture of the Mississippi River should be conducted to improve the current Gulf hypoxia management strategy. The present study suggests that in addition to the nutrient addition effect caused shifting discharge, the change in the physical oceanic conditions, including the stratification and circulation, needs to be included in any evaluation. Such an evaluation could be conducted through the present three dimensional, coupled-biogeochemical model.

4. The Response of the Hypoxic Area to the Different Nitrogen Form from the River

Although the total nitrogen loadings were the same, the hypoxic* areas of the scenario with all nitrogen in DIN (NO_3^- + NH_4^+) form was 13% larger than that of the base case.

In my biogeochemical model, the organic matter was added by the river as small detritus. The small detritus aggregated with the phytoplankton to form large detritus, which was the dominant form of nitrogen being decomposed and remineralized in the sediment. However, the DIN had to go through the phytoplankton, zooplankton and small detritus stages before becoming large detritus and sinking. As a result, DIN stayed in the water longer and moved further with the flow, resulting in a slightly

larger hypoxic* area.

Very few hypoxia mechanistic models consider the importance of nutrient form for oxygen depletion. The box model of *Justic et al.* (1996, 2002) assumed that the primary production of the C6X station is proportional to the NO_3^- load from the Mississippi River one month earlier. The model of *Scavia et al.* (2003) assumed that the oxygen-consuming material in July is proportional to the total nitrogen loading (DIN + PON) of the Mississippi and Atchafalaya in May–June. The 1–2 month delays in nutrient conversion are based on statistical analysis. Nutrient-supported primary production is a necessary condition for hypoxia formation, but describing the pathway of nutrient into oxygen-consuming material is also important for developing the predictive hypoxia model.

The combined DON and PON is over 40% of total nitrogen loading, a fact important for the formation and development of the hypoxic region in the Gulf of Mexico (*Bianchi et al.*, 2010; *Dale et al.*, 2010; *Dagg et al.*, 2004). My current model simplifies the pathway of PON after it reaches the bottom. Including a new model to describe the biophysical dynamics of the sediment is the next step in my model development. A better understanding of the fate of PON in the sediment is required for improving the model configuration on the sediment part. *Xu* (2011) have begun an effort to couple a sediment component to the coupled physical-biogeochemcial model described here.

E. Conclusions

In this chapter, I presented the coupled physical-biogeochemical model introduced in the previous chapter to study the sensitivity of the Gulf hypoxic area to different wind, river and nutrient conditions. The most important findings are:

1. The upwelling-favorable wind facilitates the development of the hypoxic area. However, a long duration of upwelling-favorable wind decreases the area. Since the hypoxic area is highly variable during summer, measuring the area more than once is important to capture the "largest" hypoxic area of the year.

2. The hypoxic area in the Gulf of Mexico is highly sensitive to the total nitrogen loading. A 50% nitrogen concentration reduction can reduce the hypoxic area by 75% under certain wind and river forcings. To reduce the hypoxic area to 5000 km^2, reducing nitrogen-contained fertilizer use by a large percentage may not be necessary. However, the relationship between the hypoxic area and total nitrogen loading is highly non-linear. With the same total nitrogen loading, increasing the river discharge by 50% and decreasing the nitrogen concentration by 33.3% may increase the hypoxic area by 42%. The above numbers are reached by comparing 2002 wind foricng (short duration of upwelling favorable wind) and 2009 river forcing. To get a more general idea about how much the hypoxic area will decrease as nitrogen flux is reduced, ensemble runs under different forcing conditions are suggested.

3. The present diversion of water from the Mississippi to the Atchafalya River does not change the physical (freshwater) and biological (chlorophyll) fields compared with the case with no diversion. However, increasing the diversion to two thirds of the total discharge could increase the hypoxic area greatly. High flow diversion to the Atchafalaya River could also cause the most intense hypoxic region to move from the east to the west Louisiana shelf.

4. With the same total nitrogen loading, the scenario with all nitrogen in DIN form created a slightly larger hypoxic area than the scenario with nitrogen in both DIN and PON forms. One deficiency of the current model is that nutrient

recycling at the sediments was not well described. A future effort in developing the model is to refine the sediment contributions to the oxygen dynamics.

CHAPTER V

CONCLUSIONS

Seasonal hypoxia has been observed in the northern Gulf of Mexico for more than 25 years. It has been generally believed that the variation in the areal extent of hypoxia is determined by variations in nutrient addition from the Mississippi River. Management strategies have focused on controlling the use of nitrogen-containing fertilizer to improve the coastal water quality. However, the nitrogen – area relationship is influenced by many other factors, such as the wind field, the freshwater discharge, and the apportioning of flows between the Mississippi and Atchafalaya river discharge.

In this research, I use both statistical and numerical models to study the influence of those factors on the oxygen dynamics and variability of the hypoxic area in the northern Gulf of Mexico. The single and multiple linear regression analyses identified statistically significant relationships between hypoxic area and multiple factors, including duration of westerly wind (i.e. upwelling favorable), 11-month averaged Mississippi River flow, May NO_3^- loading from the Mississippi River and May-June NO_3^- loading from the Mississippi River. The numerical model provides insight into the mechanisms that drive these relationships. The model is the coupled physical-biogeochemical model (ROMS-Fennel with the oxygen component). This is the first time a three-dimensional, nitrogen-based model has been used to study hypoxia in the Gulf of Mexico. The model includes a full hydrological model, giving a unique advantage to investigate the role of physical processes on the area variability when compared to most previous models. In addition, the model has a continuous spatial and temporal coverage, allowing us to gain a better understanding of the hypoxic area variability.

In this research, I first assessed the model performance by comparing the sim-

ulated oxygen field with available observations. Next, I examined the ability of the model to estimate the hypoxic area. I performed EOF analyses on the model results to identify typical spatial and temporal patterns of hypoxia. Finally, I conducted seven hypothetical scenario experiments to study the sensitivity of the hypoxic area to naturally-induced physical forcing variability and anthropogenic nitrogen load. The main findings are:

1. An additional variable, the duration of west wind, is significantly correlated with the hypoxic area. The wind duration explains 55% of the variance of the hypoxic area since 1993. A multilinear regression using both wind duration and nitrogen loading as predictors explains more than 70% of the variance in hypoxic area; using wind duration and river discharge explains more than 85% of the variance. A bootstrap analysis shows that the correlations are statistically robust.

2. Four skill metrics have been used to assess the performance of the coupled ROMS-Fennel model in reproducing the oxygen concentration at one fixed station and two cross-shelf transects. The model captures the seasonal variation in concentration of DO, but it underestimates the concentration of DO at the surface, and overestimates the concentration of DO at the bottom. At the bottom grid point of the model at the fixed station (18.23 m), the bias is 38 μM, RMS is 71 μM; MEF is as low as 0.18, but r is as high as 0.68. For the two cross-shore transects, the model skill is better nearshore than offshore.

3. The model reproduces the spatial pattern of the DO concentration at the bottom. However, the observed oxygen concentration is lower than that simulated by the model. The mean bias is 23 μM. The areas associated with different DO concentrations at the bottom were compared to observations. The best model

skills were obtained when the areas with DO less than 3 mg/L were used to calculate the low oxygen areas (r = 0.71, MEF = 0.35, RMS = 4,600 km^2 and bias = 1,020 km^2). A DO concentration less than 3 mg/L (just 1 mg/L, or 31 μM more than the common used definition of 2 mg/L) in the model is defined here as hypoxia*.

4. The best fit for oxygen concentration changed during the 25-year period. Before 1991, the simulated values fit the observations using values of 2 mg/L to calculate the hypoxic area. After 1991 areas using simulated values of less than 3 mg/L fit the observations better. The existence of the "jump" is consistent with previous finding that the reported hypoxia area went through an abrupt shift in the early 1990s (*Turner et al.*, 2008; *Greene et al.*, 2009; *Liu et al.*, 2010).

5. An EOF analysis of the frequency of hypoxia* for monthly intervals over 25 years explains much of the variabillity. The first-three EOF modes, all of which have strong seasonal cycles, explain 62%, 8.1% and 4.9% of the variability, respectively. They documented the evolution of hypoxia* events in a year. The first mode showed strong hypoxia* events from May-September over the mid-Louisiana shelf. The second mode showed strong hypoxia* events from March-July near the coast.

6. Cross-correlations were calculated between the PC-time series of different modes and important physical and biogeochemical variables. The first EOF mode was highly correlated ($r > 0.5$) with the wind power density at 0–1 month lag, the duration of southwest wind at 0–1 month lag, the combined Mississippi-Atchafalaya River flow at 2–4 month lag, the Mississippi River DIN concentrations at 1–3 month lag and the Atchafalaya River DIN concentrations at 0–2

month lag. The second EOF mode was positively correlated ($r > 0.25$) with the duration of southeast wind, the combined river flow, and the Mississippi and Atchafalaya river DIN concentrations at 0–2 month lag. The EOF analysis showed the dynamic relationship between the hypoxic area, wind duration, river discharge, and nutrient concentrations. The above cross-correlation results were consistent with the regression model results.

7. The hypoxic area was highly influenced by the duration of upwelling (southwest) winds during summer. With the same nitrogen loading, early upwelling favorable wind years (such as in 2009) caused a large hypoxic area in the early summer. However, as the upwelling wind continued and river flow decreased, the hypoxic area decreased. In contrast, the upwelling favorable wind which occurred later in the season (such as 2002) caused a large hypoxic area in the late summer. The shelf-wide cruise to document the size of the hypoxic zone has been conducted during late summer for 25 years. Whether the cruise data described the "largest" hypoxic area of the year or not depends on whether or not the cruise started right after the upwelling favorable wind.

8. The hypoxic area was highly sensitive to the total nitrogen loading. However, the relationship between the hypoxic area and nitrogen loading was non-linear. In our selected wind (2002 wind, short upwelling favorable wind duration) and river (2009 river discharge, high flow and high nitrogen loading) cases, increasing the river discharge by 50% and decreasing the nutrient concentration by 33% can increase the hypoxic area by 42%. With the same river discharge, reducing the nitrogen loading 50% by reducing the nitrogen concentration 50% can decrease the hypoxic area by 75%.

9. With the nitrogen loading fixed, the hypoxic area that results from the scenario

with all the flows coming from the Mississippi River is comparable to the situation where 2/3 of the flow was from the Mississippi River. However, if the flow was cut to 1/3 from the Mississippi River, the hypoxic area increased by 30%.

10. Although our model describes the water column processes, the processes occurring in the bottom boundary layer, which are simply configured in our model, dominate hypoxia formation. The model performance may be improved in the future by properly formulating the biogeochemical processes in the sediments.

REFERENCES

Aller, R. C. (1998), Mobile deltaic and continental shelf muds as suboxic, fluidized bed reactors, *Mar. Chem.*, *61*(3-4), 143 – 155, doi:10.1016/S0304-4203(98)00024-3.

Baden, S. P., L. O. Loo, L. Pihl, and R. Rosenberg (1990), Effects of eutrophication on benthic communities including fish: Swedish west coast., *Ambio. Stockholm.*, *19*(3), 113–122.

Baird, D., R. Christian, C. Peterson, and G. Johnson (2004), Consequences of hypoxia on estuarine ecosystem function: Energy diversion from consumers to microbes, *Ecol. Appl.*, *14*(3), 805–822, doi:10.1890/02-5094.

Belabbassi, L. (2006), Examination of the relationship of river water to occurrences of bottom water with reduced oxygen concentrations in the northern Gulf of Mexico, Ph.D. dissertation, Texas. A&M University, College Station.

Bianchi, T. S., and M. A. Allison (2009), Large-river delta-front estuaries as natural recorders of global environmental change, *Proc. Natl. Acad. Sci. (USA)*, *106*(20), 8085–8092, doi:10.1073/pnas.0812878106.

Bianchi, T. S., S. F. DiMarco, R. W. Smith, and K. M. Schreiner (2009), A gradient of dissolved organic carbon and lignin from Terrebonne-Timbalier Bay estuary to the Louisiana shelf (USA), *Mar. Chem.*, *117*(1-4), 32 – 41, doi:10.1016/j.marchem.2009.07.010.

Bianchi, T. S., S. F. DiMarco, J. H. Cowan Jr., R. D. Hetland, P. Chapman, J. W. Day, and M. A. Allison (2010), The science of hypoxia in the northern Gulf of Mexico: A review, *Sci. Total Environ.*, *408*, 1471–1484, doi:10.1016/j.scitotenv.2009.11.047.

Bierman, V. J., S. C. Hinz, D. W. Zhu, W. J. Wiseman, N. N. Rabalais, and R. E. Turner (1994), A preliminary mass-balance model of primary productivity and dissolved-oxygen in the Mississippi River plume inner Gulf shelf region, *Estuaries*, *17*, 886–899.

Breed, G. A., G. A. Jackson, and T. L. Richardson (2004), Sedimentation, carbon export and food web structure in the Mississippi River plume described by inverse analysis, *Mar. Ecol. Prog. Ser.*, *278*, 35–51.

Breitburg, D. L., D. W. Hondorp, L. A. Davias, and R. J. Diaz (2009), Hypoxia, nitrogen, and fisheries: Integrating effects across local and global landscapes, *Annu. Rev. Mar. Sci.*, *1*(1), 329–349, doi:10.1146/annurev.marine.010908.163754.

Caddy, J. F. (1993), Toward a comparative evaluation of human impacts on fishery ecosystems of enclosed and semi-enclosed seas, *Rev. Fish. Sci.*, *1*(1), 57–95, doi: 10.1080/10641269309388535.

Chen, C. C., G. C. Gong, and F. K. Shiah (2007), Hypoxia in the East China Sea: One of the largest coastal low-oxygen areas in the world, *Mar. Environ. Res.*, *64*, 399–408.

Chen, C. S., D. A. Wiesenburg, and L. S. Xie (1997), Influences of river discharge on biological production in the inner shelf: A coupled biological and physical model of the Louisiana-Texas shelf, *J. Mar. Res.*, *55*, 293–320.

Cheng, W., C.-H. Liu, J.-P. Hsu, and J.-C. Chen (2002), Effect of hypoxia on the immune response of giant freshwater prawn macrobrachium rosenbergii and its susceptibility to pathogen enterococcus, *Fish. Shellfish. Immun.*, *13*(5), 351 – 365, doi:10.1006/fsim.2001.0411.

Cho, K., R. O. Reid, and W. D. Nowlin Jr. (1998), Objectively mapped stream function fields on the Texas-Louisiana shelf based on 32 months of moored current meter data, *J. Geophys. Res.*, *103*(C5), 10,377 – 10,390, doi:10.1029/98JC00099.

Cochrane, J. D., and F. J. Kelly (1986), Low-frequency circulation on the Texas-Louisiana continental-shelf, *J. Geophys. Res.*, *91*, 645–659, doi:10.1029/JC091iC09p10645.

Conley, D. J., H. W. Paerl, R. W. Howarth, D. F. Boesch, S. P. Seitzinger, K. E. Havens, C. Lancelot, and G. E. Likens (2009), Controlling eutrophication: Nitrogen and phosphorus, *Science*, *323*, 1014–1015, doi:10.1126/science.1167755.

Corbett, D. R., B. McKee, and D. Duncan (2004), An evaluation of mobile mud dynamics in the Mississippi River deltaic region, *Mar. Geol.*, *209*, 91–112.

da Silva, A. M., C. C. Young-Molling, and S. Levitus (1994a), Atlas of surface marine data 1994 vol. 3: Anomalies of fluxes of heat and momentum, *Tech. Rep. 8*, NOAA Atlas NESDIS, U.S. Gov. Printing Office, Washington, D.C.

da Silva, A. M., C. C. Young-Molling, and S. Levitus (1994b), Atlas of surface marine data 1994 vol. 4: Anomalies of fresh water fluxes, *Tech. Rep. 9*, NOAA Atlas NESDIS, U.S. Gov. Printing Office, Washington, D.C.

Dagg, M. J., and G. A. Breed (2003), Biological effects of Mississippi River nitrogen on the northern Gulf of Mexico–a review and synthesis, *J. Mar. Sys.*, *43*(3-4), 133 – 152, doi:10.1016/j.jmarsys.2003.09.002.

Dagg, M. J., R. Benner, S. Lohrenz, and D. Lawrence (2004), Transformation of dissolved and particulate materials on continental shelves influenced by large rivers: Plume processes, *Cont. Shelf Res.*, *24*, 833–858.

Dale, V. H., C. L. Kling, J. L. Meyer, J. Sanders, H. Stallworth, T. Armitage, D. Wangsness, T. S. Bianchi, A. Blumberg, W. Boynton, D. J. Conley, W. Crumpton, M. B. David, D. Gilbert, R. W. Howarth, R. Lowrance, K. Mankin, J. Opaluch, H. Paerl, K. Reckhow, A. N. Sharpley, T. W. Simpson, C. S. Snyder, and D. Wright (Eds.) (2010), *Hypoxia in the northern Gulf of Mexico*, Springer, New York.

Day, J., D. Pont, P. Hensel, and C. Ibanez (1995), Impacts of sea-level rise on deltas in the Gulf of Mexico and the mediterranean: The importance of pulsing events to sustainability, *Estuaries and Coasts*, *18*, 636–647, 10.2307/1352382.

Diaz, R. J. (2001), Overview of hypoxia around the world, *J. Environ. Qual.*, *30*(2), 275–281.

Diaz, R. J., and R. Rosenberg (1995), Marine benthic hypoxia: A review of its ecological effects and the behavioural responses of benthic macrofauna, *Oceanogr. Mar. Biol. Ann. Rev.*, *33*, 245–303.

Diaz, R. J., and R. Rosenberg (2008), Spreading dead zones and consequences for marine ecosystems, *Science*, *321*, 926–929.

Diaz, R. J., A. Solow, and NOAA Coastal Ocean Program (U.S.) (1999), *Ecological and economic consequences of hypoxia: Topic 2, report for the integrated assessment on hypoxia in the Gulf of Mexico*, 46 pp., U.S. Dept. of Commerce, National Oceanic and Atmospheric Administration, National Ocean Service, National Centers for Coastal Ocean Science, Center for Sponsored Coastal Ocean Research–Coastal Ocean Program, Silver Spring, MD, USA.

DiMarco, S. F., and R. O. Reid (1998), Characterization of the principal tidal current constituents on the Texas-Louisiana shelf, *J. Geophys. Res.*, *103(C2)*, 3093?109, doi:10.1029/97JC03289.

DiMarco, S. F., P. Chapman, N. Walker, and R. D. Hetland (2010), Does local topography control hypoxia on the eastern Texas-Louisiana shelf?, *J. Mar. Sys.*, *80*(1-2), 25 – 35, doi:10.1016/j.jmarsys.2009.08.005.

Dinnel, S. P., and W. J. Wiseman (1986), Fresh-water on the Louisiana and Texas shelf, *Cont. Shelf Res.*, *6*, 765–784, doi:10.1016/0278-4343(86)90036-1.

Donner, S., and D. Scavia (2007), How climate controls the flux of nitrogen by the Mississippi River and the development of hypoxia in the Gulf of Mexico, *Limnol. Oceanogr.*, *52*(2), 856–861, doi:10.4319/lo.2007.52.2.0856.

Eby, L. A., and L. B. Crowder (2002), Hypoxia-based habitat compression in the Neuse River Estuary: Context-dependent shifts in behavioral avoidance thresholds, *Can. J. Fish. Aquat. Sci.*, *59*(6), 952–965, doi:10.1139/f02-067.

Fasham, M. J. R., H. W. Ducklow, and S. M. McKelvie (1990), A nitrogen-based model of plankton dynamics in the oceanic mixed layer, *J. Mar. Res.*, *48*, 591–639.

Fennel, K., J. Wilkin, J. Levin, J. Moisan, J. O'Reilly, and D. Haidvogel (2006), Nitrogen cycling in the Mid Atlantic Bight and implications for the North Atlantic nitrogen budget: Results from a three-dimensional model, *Global Biogeochem. Cy*, *20*, GB3007, doi:10.1029/2005GB002456.

Fennel, K., J. Wilkin, M. Previd, and R. Najjar (2008), Denitrification effects on air-sea co2 flux in the coastal ocean: Simulations for the northwest north atlantic, *Geophys. Res. Lett.*, *35*, L24,608, doi:10.1029/2008GL036147.

Fennel, K., R. Hetland, Y. Feng, and S. DiMarco (2011), A coupled physical-biological model of the northern Gulf of Mexico shelf: Model description, validation and

analysis of phytoplankton variability, *Biogeosciences*, *8*(7), 1881–1899, doi:10.5194/bg-8-1881-2011.

Fisk, H. N. (Ed.) (1952), *Geologic Investigation of the Atchafalaya Basin and the Problem of Mississippi River Diversion*, U.S. Army Corps of Engineers, Vicksburg, MS, USA.

Flather, R. A. (1976), A tidal model of the north-west European continental shelf, *Mem. Soc. R. Sci. Liege*, *10*(6), 141–164.

Fuenzalida, R., W. Schneider, J. Garcs-Vargas, L. Bravo, and C. Lange (2009), Vertical and horizontal extension of the oxygen minimum zone in the eastern South Pacific Ocean, *Deep-sea Res. Pt. II*, *56*(16), 992 – 1003, doi:10.1016/j.dsr2.2008.11.001.

Garcia, H. E., and L. I. Gordon (1992), Oxygen solubility in seawater - better fitting equations, *Limnol. Oceanogr.*, *37*, 1307–1312.

Geyer, W. R., P. S. Hill, and G. C. Kineke (2004), The transport, transformation and dispersal of sediment by buoyant coastal flows, *Cont. Shelf Res.*, *24*(7-8), 927 – 949, doi:10.1016/j.csr.2004.02.006.

Goolsby, D. A., W. A. Battaglin, B. T. Aulenbach, and R. P. Hooper (2001), Nitrogen input to the Gulf of Mexico, *J. Environ. Qual.*, *30*(2), 329–336, doi:10.2134/jeq2001.302329x.

Grantham, B. A., F. Chan, K. J. Nielsen, D. S. Fox, J. A. Barth, A. Huyer, J. Lubchenco, and B. A. Menge (2004), Upwelling-driven nearshore hypoxia signals ecosystem and oceanographic changes in the northeast pacific, *Nature*, *429*, 749–754.

Gray, J. S., R. S. S. Wu, and Y. Y. Or (2002), Effects of hypoxia and organic enrichment on the coastal marine environment, *Mar. Ecol. Prog. Ser.*, *238*, 249–279.

Green, R. E., T. S. Bianchi, M. J. Dagg, N. D. Walker, and G. A. Breed (2006), An organic carbon budget for the Mississippi River turbidity plume and plume contributions to air-sea co2 fluxes and bottom water hypoxia, *Estuar. Coast*, *29*, 579–597.

Green, R. E., G. A. Breed, M. J. Dagg, and S. E. Lohrenz (2008), Modeling the response of primary production and sedimentation to variable nitrate loading in the Mississippi River plume, *Cont. Shelf Res.*, *28*, 1451–1465.

Greene, R. M., J. C. Lehrter, and J. D. Hagy III (2009), Multiple regression models for hindcasting and forecasting midsummer hypoxia in the Gulf of Mexico, *Ecol. Appl.*, *19*(5), 1161–1175, doi:10.1890/08-0035.1.

Haidvogel, D., H. Arango, W. Budgell, B. Cornuelle, E. Curchitser, E. D. Lorenzo, K. Fennel, W. Geyer, A. Hermann, L. Lanerolle, J. Levin, J. McWilliams, A. Miller, A. Moore, T. Powell, A. Shchepetkin, C. Sherwood, R. Signell, J. Warner, and J. Wilkin (2008), Ocean forecasting in terrain-following coordinates: Formulation and skill assessment of the Regional Ocean Modeling System, *Journal of Computational Physics*, *227*(7), 3595 – 3624, doi:10.1016/j.jcp.2007.06.016.

Helly, J. J., and L. A. Levin (2004), Global distribution of naturally occurring marine hypoxia on continental margins, *Deep-sea Res. Pt. I*, *51*(9), 1159 – 1168, doi:10.1016/j.dsr.2004.03.009.

Hetland, R. D., and S. F. DiMarco (2008), How does the character of oxygen demand control the structure of hypoxia on the Texas-Louisiana continental shelf?, *J. Mar. Sys.*, *70*, 49–62, doi:10.1016/j.jmarsys.2007.03.002.

Ichiye, T. (1960), On the hydrography near Mississippi Delta, *Oceanogr. Mag.*, *11*(2), 65–78.

Jamil, M., S. Parsa, and M. Majidi (1995), Wind power statistics and an evaluation of wind energy density, *Renewable Energy*, *6*(5-6), 623 – 628, doi:10.1016/0960-1481(95)00041-H.

Jochens, A., S. DiMarco, W. D. Nowlin Jr., R. Reid, and M. Kennicutt II (2002), Northeastern Gulf of Mexico chemical oceanography and hydrography study, synthesis report., *OCS Study MMS 2002*, US Department of the Interior, Minerals Management Service, Gulf of Mexico OCS Region, New Orleans, LA.

Justic, D. (1988), Trend in the transparency of the northern Adriatic Sea 1911-1982, *Mar. Pollut. Bull.*, *19*(1), 32 – 35, doi:10.1016/0025-326X(88)90751-5.

Justic, D., N. N. Rabalais, and R. E. Turner (1996), Effects of climate change on hypoxia in coastal waters: A doubled co2 scenario for the northern Gulf of Mexico, *Limnol. Oceanogr.*, *41*, 992–1003.

Justic, D., N. N. Rabalais, and R. E. Turner (2002), Modeling the impacts of decadal changes in riverine nutrient fluxes on coastal eutrophication near the Mississippi River delta, *Ecol. Model.*, *152*, 33–46.

Justic, D., R. E. Turner, and N. N. Rabalais (2003a), Climatic influences on riverine nitrate flux: implications for coastal marine eutrophication and hypoxia, *Estuar. Coast*, *26*, 1–11, doi:10.1007/BF02691688.

Justic, D., N. N. Rabalais, and R. E. Turner (2003b), Simulated responses of the Gulf of Mexico hypoxia to variations in climate and anthropogenic nutrient loading, *J. Mar. Sys.*, *42*(3-4), 115 – 126, doi:10.1016/S0924-7963(03)00070-8.

Justic, D., N. N. Rabalais, and R. E. Turner (2005), Coupling between climate variability and coastal eutrophication: Evidence and outlook for the northern Gulf of Mexico, *J. Sea Res.*, *54*(1), 25 – 35, doi:10.1016/j.seares.2005.02.008.

Justic, D., V. Bierman, D. Scavia, and R. Hetland (2007), Forecasting gulfs hypoxia: The next 50 years?, *Estuar. Coast*, *30*, 791–801, 10.1007/BF02841334.

Kamykowski, D., and S.-J. Zentara (1990), Hypoxia in the world ocean as recorded in the historical data set, *Deep-sea Res. Pt. I*, *37*(12), 1861 – 1874, doi:10.1016/0198-0149(90)90082-7.

Karlson, K., R. Rosenberg, and E. Bonsdorff (2002), Temporal and spatial large-scale effects of eutrophication and oxygen deficiency on benthic fauna in Scandinavian and Baltic waters - a review, *Oceanogr. Mar. Biol.*, *40*, 427–489.

Karstensen, J., L. Stramma, and M. Visbeck (2008), Oxygen minimum zones in the eastern tropical Atlantic and Pacific oceans, *Prog. Oceanogr.*, *77*(4), 331 – 350, doi:10.1016/j.pocean.2007.05.009.

Kodama, K., I. Aoki, M. Shimizu, and T. Taniuchi (2002), Long-term changes in the assemblage of demersal fishes and invertebrates in relation to environmental variations in Tokyo Bay, Japan, *Fisheries Manag. Ecol.*, *9*(5), 303–313, doi:10.1046/j.1365-2400.2002.00313.x.

Krug, E. C. (2007), Coastal change and hypoxia in the northern Gulf of Mexico: Part i, *Hydrol. Earth Syst. Sci.*, *11*(1), 180–190, doi:10.5194/hess-11-180-2007.

Krug, E. C., and K. Merrifield (2007), Marine modification of terrestrial influences on Gulf hypoxia: Part ii, *Hydrol. Earth Syst. Sci.*, *11*(1), 191–209, doi:10.5194/hess-11-191-2007.

Liu, Y., M. A. Evans, and D. Scavia (2010), Gulf of Mexico hypoxia: Exploring increasing sensitivity to nitrogen loads, *Environ. Sci. Technol.*, *44*(15), 5836–5841, doi:10.1021/es903521n.

Marchesiello, P., J. C. McWilliams, and A. F. Shchepetkin (2001), Open boundary conditions for long-term integration of regional ocean models, *Ocean Model.*, *3*, 1–20.

McKee, B. A., R. C. Aller, M. A. Allison, T. S. Bianchi, and G. C. Kineke (2004), Transport and transformation of dissolved and particulate materials on continental margins influenced by major rivers: Benthic boundary layer and seabed processes, *Cont. Shelf Res.*, *24*(7-8), 899 – 926, doi:10.1016/j.csr.2004.02.009.

Mellor, G. L., and T. Yamada (1982), Development of a turbulence closure model for geophysical fluid problems, *Rev. Geophys. Space Phys*, *20*, 851–875.

Milliman, J. D., and R. H. Meade (1983), World-wide delivery of river sediment to the oceans, *J. Geol.*, *91*(1), 121.

Mississippi River/Gulf of Mexico Watershed Nutrient Task Force (2001), Action plan for reducing, mitigating and controlling hypoxia in the northern Gulf of Mexico, Office of Wetlands, Oceans, and Watersheds, Washington, DC.

Mississippi River/Gulf of Mexico Watershed Nutrient Task Force (2008), Gulf hypoxia action plan 2008 for reducing, mitigating and controlling hypoxia in the northern Gulf of Mexico and improving water quality in the Mississippi River basin, Office of Wetlands, Oceans, and Watersheds, Washington, DC.

Mitsch, W. J., J. W. Day, J. W. Gilliam, P. M. Groffman, D. L. Hey, G. W. Randall, and N. M. Wang (2001), Reducing nitrogen loading to the Gulf of Mexico from

the Mississippi River basin: Strategies to counter a persistent ecological problem, *Bioscience*, *51*, 373–388.

Nelsen, T., P. Blackwelder, T. Hood, B. McKee, N. Romer, C. Alvarez-Zarikian, and S. Metz (1994), Time-based correlation of biogenic, lithogenic and authigenic sediment components with anthropogenic inputs in the Gulf of Mexico NECOP study area, *Estuar. Coast*, *17*, 873–885, 10.2307/1352755.

Newcombe, C. L., and W. A. Horne (1938), Oxygen-poor waters of the Chesapeake Bay, *Science*, *88*, 80–81, doi:10.1126/science.88.2273.80.

Nissling, A., and L. Vallin (1996), The ability of Baltic cod eggs to maintain neutral buoyancy and the opportunity for survival in fluctuating conditions in the Baltic Sea, *J. Fish. Biol.*, *48*(2), 217–227, doi:10.1111/j.1095-8649.1996.tb01114.x.

Nixon, S. W. (1995), Coastal marine eutrophication: A definition, social causes, and future concerns, *Ophelia*, *41*, 199–219.

Nowlin, W. D., A. E. Jochens, R. O. Reid, and S. F. DiMarco (1998), Texas-Louisiana shelf circulation and transport processes study - synthesis report.vol.i and ii., *OCS Study MMS 98-0035 and MMS 98-0036*, US Department of the Interior, Minerals Management Service, Gulf of Mexico OCS Regional Office, New Orleans, LA.

Nowlin, W. D., A. E. Jochens, S. F. DiMarco, R. O. Reid, and M. K. Howard (2005), Low-frequency circulation over the Texas-Louisiana continental shelf', circulation in the Gulf of Mexico: Observations and models (Wilton Sturges and Alexis Lugo-Fernandez, eds.), *AGU Geophysical Monograph*, *161*, 219–240.

Osterman, L. (2003), Benthic foraminifers from the continental shelf and slope of

the Gulf of Mexico: an indicator of shelf hypoxia, *Estuar. Coast. Shelf. S.*, *58*(1), 17–35, doi:{10.1016/S0272-7714(02)00352-9}.

Osterman, L., R. Poore, P. Swarzenski, and R. Turner (2005), Reconstructing a 180 yr record of natural and anthropogenic induced low-oxygen conditions from Louisiana continental shelf sediments, *Geology*, *33*(4), 329–332, doi:{10.1130/G21341.1}.

Osterman, L. E., R. Z. Poore, P. W. Swarzenski, D. B. Senn, and S. F. DiMarco (2009), The 20th-century development and expansion of Louisiana shelf hypoxia, Gulf of Mexico, *Geo-Mar. lett.*, *29*(6), 405–414, doi:{10.1007/s00367-009-0158-2}.

Paulmier, A., and D. Ruiz-Pino (2009), Oxygen minimum zones (OMZs) in the modern ocean, *Prog. Oceanogr.*, *80*(3-4), 113 – 128, doi:10.1016/j.pocean.2008.08.001.

Rabalais, N. N., and R. E. Turner (2001), *Coastal Hypoxia: Consequences for Living Resources and Ecosystems*, Coastal Estuarine Studies 58, American Geophysical Union, Washington, D. C.

Rabalais, N. N., W. J. Wiseman, R. E. Turner, B. K. SenGupta, and Q. Dortch (1996), Nutrient changes in the Mississippi River and system responses on the adjacent continental shelf, *Estuaries*, *19*, 386–407.

Rabalais, N. N., R. E. Turner, D. Justic, Q. Dortch, and W. J. W. Jr (1999), Characterization of hypoxia: Topic 1 report for the integrated assessment of hypoxia in the Gulf of Mexico, *Tech. Rep. NOAA Coastal Ocean Program Decision Analysis Series No. 15.*, NOAA Coastal Ocean Programs, Silver Spring, MD, USA

Rabalais, N. N., R. E. Turner, and W. J. Wiseman (2001), Hypoxia in the Gulf of Mexico, *J. Environ. Qual.*, *30*, 320–329.

Rabalais, N. N., R. E. Turner, and W. Wiseman (2002a), Gulf of Mexico hypoxia, aka "The dead zone", *Annu. Rev. Ecol. Syst.*, *33*, 235–263, doi:10.1146/annurev.ecolsys.33.010802.150513.

Rabalais, N. N., R. E. Turner, and D. Scavia (2002b), Beyond science into policy: Gulf of Mexico hypoxia and the Mississippi River, *BioScience*, *52*(2), 129–142, doi:10.1641/0006-3568(2002)052[0129:BSIPGO]2.0.CO;2.

Rabalais, N. N., R. E. Turner, B. K. S. Gupta, E. Platon, and M. L. Parsons (2007a), Sediments tell the history of eutrophication and hypoxia in the northern Gulf of Mexico, *Ecol. Applic. Spec. Issue Nutrient Enrichment and Estuarine Eutrophication and Coastal Marine Environments*, *17*(5), S129–S143.

Rabalais, N. N., R. E. Turner, B. K. Sen Gupta, D. F. Boesch, P. Chapman, and M. C. Murrell (2007b), Hypoxia in the northern Gulf of Mexico: Does the science support the plan to reduce, mitigate, and control hypoxia?, *Estuar. Coast*, *30*, 753–772, doi:10.1007/BF02841332.

Renaud, M. L. (1986), Hypoxia in Louisiana coastal waters during 1983: Implications for fisheries, *Fish. Bull.*, *84*(1), 19–26.

Rowe, G. T. (2001), Seasonal hypoxia in the bottom water off the Mississippi River delta, *J. Environ. Qual.*, *30*, 281–290.

Scavia, D., and K. A. Donnelly (2007), Reassessing hypoxia forecasts for the Gulf of Mexico, *Environ. Sci. Technol.*, *41*(23), 8111–8117, doi:10.1021/es0714235.

Scavia, D., N. N. Rabalais, R. E. Turner, D. Justic, and W. J. Wiseman Jr. (2003), Predicting the response of Gulf of Mexico hypoxia to variations in Mississippi River nitrogen load, *Limnol. Oceanogr.*, *48*, 951–956.

Scully, M. E. (2010a), The importance of climate variability to wind-driven modulation of hypoxia in Chesapeake Bay, *J. Phys. Oceanogr.*, *40*(6), 1435–1440, doi: 10.1175/2010JPO4321.1.

Scully, M. E. (2010b), Wind modulation of dissolved oxygen in Chesapeake Bay, *Estuaries and Coasts*, *33*, 1164–1175, doi:10.1007/s12237-010-9319-9.

Seitzinger, S., and A. Giblin (1996), Estimating denitrification in north Atlantic continental shelf sediments, *Biogeochemistry*, *35*, 235–260.

SenGupta, B., R. Turner, and N. Rabalais (1996), Seasonal oxygen depletion in continental-shell waters of Louisiana:Historical record of benthic foraminifers, *Geology*, *24*(3), 227–230, doi:{10.1130/0091-7613(1996)024⟨0227:SODICS⟩2.3.CO;2}.

Shchepetkin, A. F., and J. C. McWilliams (2003), A method for computing horizontal pressure-gradient force in an oceanic model with a nonaligned vertical coordinate, *J. Geophys. Res.*, *108(C3)*, 3090, doi:10.1029/2001JC001047.

Shchepetkin, A. F., and J. C. McWilliams (2005), The regional ocean modeling system: A split-explicit, free-surface, topography following coordinates ocean model, *Ocean Model.*, *9*, 347–404.

Stow, C. A., S. S. Qian, and J. K. Craig (2005), Declining threshold for hypoxia in the Gulf of Mexico, *Environ. Sci. Technol.*, *39*(3), 716–723, doi:10.1021/es049412o.

Stow, C. A., J. Jolliff, D. J. M. Jr., S. C. Doney, J. I. Allen, M. A. Friedrichs, K. A. Rose, and P. Wallhead (2009), Skill assessment for coupled biological/physical models of marine systems, *J. Mar. Sys.*, *76*(1-2), 4 – 15, doi:10.1016/j.jmarsys.2008.03.011.

Turner, R. E., and N. N. Rabalais (1991), Changes in Mississippi River water-quality this century, *Bioscience*, *41*, 140–147.

Turner, R. E., and N. N. Rabalais (1994), Coastal eutrophication near the Mississippi River delta, *Nature*, *368*, 619–621.

Turner, R. E., and N. N. Rabalais (2003), Linking landscape and water quality in the Mississippi River Basin for 200 years, *Bioscience*, *53*(6), 563–572.

Turner, R. E., N. N. Rabalais, E. M. Swenson, M. Kasprzak, and T. Romaire (2005), Summer hypoxia in the northern Gulf of Mexico and its prediction from 1978 to 1995, *Mar. Environ. Res.*, *59*, 65–77, doi:10.1016/j.marenvres.2003.09.002.

Turner, R. E., N. N. Rabalais, and D. Justic (2006), Predicting summer hypoxia in the northern Gulf of Mexico: Riverine N, P, and Si loading, *Mar. Pollut. Bull.*, *52*, 139–148, doi:10.1016/j.marpolbul.2005.08.012.

Turner, R. E., N. N. Rabalais, and D. Justic (2008), Gulf of Mexico hypoxia: Alternate states and a legacy, *Environ. Sci. Technol.*, *42*(7), 2323–2327, doi: 10.1021/es071617k, pMID: 18504960.

Tyson, R. V., and T. H. Pearson (1991), Modern and ancient continental shelf anoxia: An overview, *Geological Society, London, Special Publications*, *58*(1), 1–24, doi: 10.1144/GSL.SP.1991.058.01.01.

Ulloa, O., and S. Pantoja (2009), The oxygen minimum zone of the eastern South Pacific, *Deep-sea Res. Pt. II*, *56*(16), 987 – 991, doi:10.1016/j.dsr2.2008.12.004.

U.S. Enviromental Protection Agency (1998), *National Strategy for the Development of Regional Nutrient Criteria*, United States Environmental Protection Agency, Office of Water, Washington, D.C., USA.

U.S. Enviromental Protection Agency (2004), *Evaluation of the Role of Nitrogen and Phosphorus in Causing or Contributing to Hypoxia in the Northern Gulf*, United States Environmental Protection Agency Region 4, 61 Forsyth Street SW Atlanta, GA.

U.S. Enviromental Protection Agency (2007), *Hypoxia in the Northern Gulf of Mexico An Update by the EPA Science Advisory Board*, United States Environmental Protection Agency, Office of Water, Washington, D.C., USA.

Wanninkhof, R. (1992), Relationship between wind-speed and gas-exchange over the ocean, *J. Geophys. Res.*, *97(C5)*, 7373, doi:10.1029/92JC00188.

Ward, C. H., M. Bender, and D. Reish (1979), *The Offshore Ecology Investigation: Effects of Oil Drilling and Production in A Coastal Environment*, Rice University Studies, 65, 1 - 589. Houston, TX

Watson, D., and G. Philip (1984), Triangle based interpolation, *Math. Geol.*, *16*, 779–795, 10.1007/BF01036704.

Wei, H., Y. He, Y. Li, Z. Liu, and H.Wang (2006), Summer hypoxia adjacent to the changjiang estuary, *J. Mar. Sys.*, *6*(1).

Wilson, R. E., R. L. Swanson, and H. A. Crowley (2008), Perspectives on long-term variations in hypoxic conditions in western Long Island Sound, *J. Geophys. Res.*, *113*, C12,011, 10.1029/2007JC004693.

Wiseman, W. J., N. N. Rabalais, R. E. Turner, S. P. Dinnel, and A. MacNaughton (1997), Seasonal and interannual variability within the Louisiana coastal current: Stratification and hypoxia, *J. Mar. Sys.*, *12*, 237–248, doi:10.1016/S0924-7963(96)00100-5.

Wu, R. S. S., B. S. Zhou, D. J. Randall, N. Y. S. Woo, and P. K. S. Lam (2003), Aquatic hypoxia is an endocrine disruptor and impairs fish reproduction, *Environ. Sci. Technol.*, *37*, 1137–1141.

Xu, K. H., C. K. Harris., R. D. Hetland, J. M. Kaihatu (2011), Dispersal of Mississippi and Atchafalaya sediment on the Texas-Louisiana shelf: Model estimates for the year 1993, *Cont. Shelf Res.*, *31*(12), 15581575, doi:10.1016/j.csr.2011.05.008.

Zaitsev, Y. P. (1992), Recent changes in the trophic structure of the Black Sea, *Fish. Oceanogr.*, *1*(2), 180–189, doi:10.1111/j.1365-2419.1992.tb00036.x.

Zhang, X., S. F. DiMarco, D. C. Smith, M. K. Howard, A. E. Jochens, and R. D. Hetland (2009), Near-resonant ocean response to sea breeze on a stratified continental shelf, *J. Phys. Oceanogr.*, *39*(9), 2137–2155, doi:10.1175/2009JPO4054.1.

Zhang, X., D. C. Smith, S. F. DiMarco, and R. D. Hetland (2010), A numerical study of sea-breeze-driven ocean Poincare wave propagation and mixing near the critical latitude, *J. Phys. Oceanogr.*, *40*(1), 48–66, doi:10.1175/2009JPO4216.1.

VITA

Yang Feng received both her Bachelor of Science and Master of Science degrees in oceanography from Ocean University of China. She entered the Department of Oceanography at Texas A&M University in fall 2006 and received her Ph.D. in May 2012.

Yang Feng may be reached at the Department of Oceanography, 3146 TAMU, College Station, Texas, 77843-3146. Her email is cathyyangfeng@tamu.edu.